The role of H-bonds on the structure and dynamics of very concentrated polymer solutions

by

Guido Goracci

Thesis supervisors:

Arantxa Arbe

Angel Alegría Loinaz

Ph.D. Thesis

2015

CONTENTS

ABSTRACT

El propósito de la presente tesis doctoral es determinar como la presencia de moléculas de disolventes afecta las dinámicas de un polímero en diferentes escalas temporales y espaciales y como la dinámica del disolvente está influenciada por las interacciones con el polímero. En particular, es de fundamental interés entender cual es la función de los enlaces hidrógeno en esta interacción reciproca. Además, con el objetivo de conseguir una visión completa del asunto, es muy importante investigar también los aspectos estructurales de las mezclas. Con este fin, ha sido necesario un estudio comparativo con disolventes caracterizados por distintas interacciones con los polímeros. Los sistemas elegidos han sido poli(dimetiloaminoetilo metacrilato) (PDMAEMA) en soluciones con tetrahidrofurano (THF) y agua con distintas concentraciones. El THF como el agua son buenos disolventes para el polímero investigado. Sin embargo, mientras que en las soluciones con agua los enlaces hidrógeno dominan las interacciones polímero/disolvente, el THF no interacciona con el polímero por esta forma. La información sobre las propriedades estructurales de los sistemas ha sido adquirida por la combinación de difracción de rayos-X y difracción de neutrones. El uso conjunto de espectroscopia dieléctrica (DS) y espectroscopia de difusión de neutrones (NS) cuasi-elástica y inelástica ha sido una herramienta muy útil para la investigación de las dinámicas en las mezclas. De hecho, la primera técnica permite explorar un rango de frecuencia muy amplio y puede ser selectiva si una de las componentes tiene un momento de dipolo mucho mayor que las otras. La segunda concede la posibilidad de seleccionar una dada componente a través de las etiquetas isotópicas (H/D). Primero, han sido investigados a fondo las propriedades estructurales y dinámicas del polímero seco y de las mezclas con THF y agua en una concentración representativa (c=30 wt%). Luego, las propriedades dinámicas de las mezclas en función de la concentración de disolvente han sido estudiadas por DS y calorimetría diferencial de barrido (DSC).
La estructura del PDMAEMA seco ha sido caracterizada por difracción de rayos-X (SAXS y WAXS) y difracción de neutrones (DNS). Han sido identificados cuatro picos en el "pattern" de difracción. A través de una comparación con estudios sobre polímeros similares (caracterizados por grupos laterales voluminosos) estas contribuciones han sido asociadas a las distintas correlaciones entre los grupos moleculares

del PDMAEMA. El pico alrededor de ~ 2.2 Å^{-1} ha sido asociado a las correlaciones intra-cadena. El pico principal, alrededor de ~ 1.2 Å^{-1}, ha sido relacionado a las correlaciones entre átomos de los grupos laterales de distintos monómeros. Alrededor de ~ 0.8 Å^{-1} se ha encontrado un pico poco definido. En polímeros parecidos, ese rango en Q está relacionado con las correlaciones que implican los "backbone" atomos. Finalmente, un pre-pico ha sido encontrado alrededor de ~ 0.5 Å^{-1}. Su presencia ha sido asociada a un tipo de segregación de "nano-phase" entre los grupos laterales y los "backbones" que lleva a la existencia de nano-dominios ricos de "polymeric subspecies". Este pico reflejaría entonces las correlaciones entre-dominios incluyendo las distancias entre-cadenas principales. En PDMAEMA/THF 30 wt% hemos encontrado que la presencia de moléculas de THF afecta principalmente las distancias entre los grupos laterales. El pre-pico está ligeramente afectado por el disolvente sugiriendo que las estructuras de los nano-dominios asociadas a este pico son esencialmente las mismas encontradas en el polímero seco. Ademas hemos visto que en esta mezcla las moléculas de disolvente parecen estar distribuidas de forma homogénea en la muestra ya que no hay indicio de "cluster" de THF en nuestros resultados. Al contrario, los experimentos de rayos-X y difracción de neutrones sobre la muestra PDMAEMA/H_2O 30 wt% han mostrado la presencia de "clusters" de agua. Estos agregados llevan a una distribución no uniforme de la hidratación del polímero como sugerido por la heterogeneidad encontrada en la S(Q) en el rango de Q entre 0.6 y 1.0 Å^{-1}. Además, las distancias ente los nano-dominios son mas grandes que las encontradas en el polímero seco y en la mezcla PDMAEMA/THF. Finalmente, la dependencia con la temperatura de las contribuciones observadas en el rango de Q $\sim$1–2 Å^{-1} es parecida a la reportada para el agua confinada en otros sistemas, implicando un cambio de las interacciones agua-agua y una efecto de "extra finite size" dado por la "vidrificacion" del polímero.

En relación con las propriedades dinámicas, ha sido abordada la cuestión de como los plastificantes afectan las dinámicas del PDMAEMA combinando las técnicas de espectroscopia dieléctrica y de difusión de neutrones. Desafortunadamente, DS no nos permite sacar información sobre la componente del polímero en las mezcla acuosa por el aplastante señal del agua. A pesar de eso, ha sido posible sacar conclusiones interesantes gracias a las téncicas de NS y DSC. La relajación-"α" del polímero está drásticamente afectada por la presencia de los disolventes. Las medidas de DSC nos muestran un fuerte desplazamiento de la temperatura de transición vidria. En las mezclas con THF, ese desplazamiento aumenta en función de la cantidad de disolvente y se observa un comportamiento "más fuerte" de la relajación-"α", también en la muestra con la concentración menor (15 wt%). En las mezclas acuosas, se ha observado por DSC un comportamiento "bimodal" lo cual sugiere una distribución no homogénea de las moléculas de agua en las muestras. Ademas, las medidas de DSC nos han mostrado un marcado "broadening" de la transición vidria en las regiones hydratadas. En el otro extremo, las dinámicas de los grupos metilos no parecen afectadas por la presencia de disolvente. La análisis combinada de los resultados de DS y QENS del polímero seco y de las mezcla con THF nos ha permitido identificar dos tipologias de movimientos moleculares del grupo lateral –una lenta y una rápida– que contribuyen al proceso-β del polímero seco. Basándonos en la información espacial provista por QENS, ha sido propuesto un modelo para la geometría de los movimientos involucrados en el proceso rápido. Añadiendo el disolvente, este proceso permanece esencialmente inalterado, mientras que la población involucrada en

el movimiento lento se reduce. Esta reducción es completa, dentro la incertidumbre experimental, en las mezclas con THF y solo parcial en el sistema acuoso. Ademas, se ha encontrado por DS una energía de activación del proceso-β bastante mas baja en todas las mezclas con THF. Este resultado sugiere que, ya con c=15 wt%, la componente lenta de la relajación-β del PDMAEMA observada en su estado seco esta altamente dificultada. El marcado "broadening" de la región de transición vidria como la menor influencia de la presencia de agua sobre los movimientos del grupo lateral del polímero, comparada con la del THF, podría atribuirse a la existencia de "clusters" de moléculas de agua distribuidas de forma heterogénea en la matriz polimerica y consiguientemente unos segmentos del polímero no estarían afectados por el agua. Esta podría sera la diferencia introducida por la capacidad de las moléculas de agua de formar enlaces hidrógeno a diferencia de las moléculas de THF.
La combinación de DS y NS aplicada a una muestra "etiquetada" ha permitido la caracterización de las dinámicas de las moléculas de THF en la mezcla con PDMAEMA con c=30 wt%. Ademas, las propriedades dinámicas del disolvente in función de la concentración ha sido investigada por DS y DSC. Con respecto a la distribución de las moléculas de THF en las muestras, se ha observado una cristalización parcial en el enfriar la muestra con la mayor concentración de THF (c=48 wt%) evidencia la presencia de segregación de las moléculas de THF que lleva a una distribución no uniforme de las moléculas de disolvente en la mezcla. Este comportamiento está confirmado por el estudio de espectroscopia dieléctrica de las dinámica del polímero como del THF en esta concentración. La mezcla con c=30 wt%, que corresponde a una molécula de THF por monomero, está caracterizada por la distribución más uniforme de disolvente comparada con las otras concentraciones investigadas. Esto esta sugerido por la "saturación" de T_g in función de la cantidad de disolvente encontrada en las medidas de DSC. Sobre las propriedades dinámicas de disolvente, dos procesos independientes del THF han sido identificados. El 'rápido' ha sido asociado a los movimientos internos del anillo del THF que llevan a un desplazamiento del hidrógeno de aproximadamente 3 Å. Las energías de activación de este movimiento están ampliamente distribuidas alrededor de un valor pro medio de 104 meV (10.03 kJ/mol). El proceso 'lento' está caracterizado por una dependencia de los tiempos de relajación con la temperatura de tipo Arrhenius. Esta dependencia persiste en todo el rango estudiado, hasta temperaturas muy altas, donde los tiempos alcanzan el rango de los nanosegundos. Los resultados de QENS evidencian la naturaleza confinada de este proceso, determinando un tamaño de aproximadamente 8 Å de la región dentro la cual los movimientos de los hidrógeno del THF están limitados. Podemos provisionalmente asignar este proceso a la relajación-α de las moléculas de THF confinadas por la más lenta y más rígida matriz del polímero. En todas las mezclas de THF y en todo el rango de temperaturas investigadas por DS, no hay marca de "crossover" hacia un carácter cooperativo de la dinámica 'lenta' del THF. Los experimentos de difusión nos han dado una información importante sobre las propriedades estructurales de la mezcla PDMAEMA/THF 30 wt%. Como comentado anteriormente, las moléculas de THF en esta concentración están bien dispersadas entre los nano-dominios de la matriz del polímero y entonces aisladas entre ellas. Consecuentemente, sienten un ambiente rico de grupos laterales del polímero. La dispersión de THF junta a la alta movilidad local de los grupos laterales podría impedir que los efectos cooperativos

entre las moléculas de THF puedan desarrollar una relajación estructural del disolvente, previniendo de esa forma una transición hacia un comportamiento de tipo Vogel-Fulcher a altas temperaturas. Podemos entonces interpretar el proceso-'lento' del THF como una proceso que implica una colectividad con otras pocas unidades moleculares –principalmente los grupos laterales del PDMAEMA– dentro los nanodominios de la matriz del polímero.
En relación con el estudio de los sistemas acuosos en función de la concentración de agua, la muestra PDMAEMA/H_2O 20 wt% investigada por DSC ha mostrado un comportamiento "bimodal" indicando la presencia de dos distintas T_g. Este comportamiento sugiere una distribución no uniforme de las moléculas de agua debida a la mas favorable interacción agua-agua. Esto llevaría a la existencia de partes de la muestra donde el polímero está poco hidratado. Sin embargo, también en las muestras con una concentración más alta de agua es posible identificar una ligera marca de este comportamiento "bimodal". A baja temperatura, los tiempos de relajación del proceso del agua presenta una dependencia de temperatura de tipo Arrhenius. La energía de activación como el pre-factor no depende considerablemente de la concentración de agua. Contrariamente, los tiempos de relajación de la muestra con c=20 wt% son mas grandes de los de la muestra PDMAEMA/H_2O 30 wt% de casi un orden de magnitud, mientras que los tiempos de relajación obtenidos para c=40 wt% son ligeramente más pequeños que los de la mezcla con c=30 wt%. La distribución ancha de los tiempos de relajación de PDMAEMA/H_2O 20 wt% a baja temperatura sugiere un ambiente bastante "inhomogéneo", mientras que la distribución de moléculas de agua se vuelve más uniforme al subir la concentración de agua. Ademas, se ha encontrado un fuerte incremento de la $\Delta\epsilon$ en las concentraciones mayores que c=20 wt%. Estos resultados nos indican una fuerte interacción de las moléculas de agua con el PDMAEMA a baja concentración la cual limita la re-orientación del momento de dipolo. Al contrario, al subir la concentración, las moléculas de agua tienden a juntarse en cuanto las interacciones agua-agua son mas favorables que las con el polímero. Al subir la temperatura, se ha encontrado un "crossover" de los tiempos característicos de la dinámica del agua desde un dependencia con la temperatura Arrhenius a non-Arrhenius. Sin embargo, la temperatura a la que esta transición ocurre parece depender de la cantidad de agua. De hecho, en las muestras con 30 and 40 wt% de agua este cambio se verifica donde se observa la transición vidria, mientras que en la muestra con la cantidad más baja de agua (c=20 wt%) el "crossover" ocurre a una temperatura más baja. De acuerdo con las medidas de DSC, la distribución de los tiempos de relajación y la fuerza dieléctrica obtenidas por DS, y tambien de acuerdo con estudios anteriores sobre las dinámicas del agua en solución con polímeros, hemos sugerido el siguiente escenario: a alta concentración un acoplamiento de la relajación del agua con la relajación-α del polímero desestabiliza los "clusters" de agua permitiendo una transición desde una dinámica de tipo local hacia una dinámica de tipo cooperativa al subir la temperatura. Al contrario, a bajas concentraciones, los "clusters" de agua deberían ser mas pequeños por las interacciones más fuertes con el polímero y la contribución térmica podría ser suficiente para disturbar las agregaciones de agua y, entonces, para observar el "crossover" desde una dependencia con la temperatura Arrhenius hacia una dependencia non-Arrhenius.

CHAPTER

1

INTRODUCTION

1.1 Polymers

Polymers are macromolecules composed of many repeated structural subunits linked by covalent bonds. Normally, the subunits are derived from smaller molecules (monomers) that react to form the polymer chain. Due to their broad range of properties, nowadays polymers play a central role in our daily life. We can identify two main categories: the natural and the synthetic polymeric materials. Natural polymers have been used for centuries (i.e. natural rubber, silk, wool) and are simply fundamental for our living being (i.e. DNA, proteins, bio-macromolecules in general). Otherwise, synthetic polymeric systems have been very important in development of new industry products affecting directly our modern society (i.e. plastics, synthetic fibres, etc...). The simplest example of polymers are homopolymers, that is polymers consisting of identical repeated units, while polymers comprising two or more types of chemical units are referred to as copolymers.

In a polymeric system chains of different sizes are usually found. Therefore, molecular weight distribution functions are used to describe this situation. The number-average molecular weight M_n and the weight-average molecular weight M_w are respectively defined as

$$M_n = \frac{\sum_i N_i M_i}{\sum_i N_i} \tag{1.1}$$

$$M_w = \frac{\sum_i N_i M_i^2}{\sum_i N_i M_i} \tag{1.2}$$

with N_i the number of molecules of molecular weight M_i. The polydispersity index is defined as the ratio M_w/M_n and provides a characterization of the width of the molecular weight distribution. Same polymers with different average molecular weights and/or polydispersity can exhibit very different properties related to chain

structure and dynamics. However, these are not the only characteristics affecting the polymeric features. In fact, polymers can exist in various conformations, that is the spatial arrangement of the molecular groups of the polymer chain established by rotations about single bonds (i.e. planar zigzag, folded chain and random coils), and in different configurations, that is the organization of the atoms along the chain. There are also many different architectures in which polymers can be found. The most basic polymer architecture is a linear chain, but polymers can present more complex structures, for example closed ring, chain branching, or a set of polymers can be connected by bonds to form a polymer network. All these characteristics influence the mechanical and dynamical properties of each specific system, mainly at high temperature –i.e. in the rubbery state.

However, at low temperature –i.e. approaching the glass transition temperature– the dynamics associated to the polymer chain become too slow. In this temperature range, only motions with characteristic length-scale of the order of inter- and intramolecular distances control the main properties of the polymer. At these relatively small length scales, the atomic disorder is the key factor and the dynamical and structural features of the polymers are those typical of glass-forming systems in general.

1.2 The Glass Transition

1.2.1 The Vitrification Phenomenon

When a glass-forming system is cooled down from the melt to a given temperature, its viscosity increases affecting the structural rearrangements necessary to find the equilibrium for that temperature (the so called α-relaxations). When during a continuous cooling these rearrangements cannot follow the cooling rate, the system falls out of equilibrium and a glass is formed. The structure of this material is "frozen" within the experimental observation time. The glass transition temperature, T_g, can be defined from a thermodynamic point of view by the temperature at which changes in the temperature dependence of the volume or enthalpy take place [1]. The glass transition temperature depends on the cooling rate: the smaller is the cooling rate, the larger is the time given to the system to reach its equilibrium. However, the dependence on cooling rate is relatively weak. An order of magnitude change in cooling rate may change T_g by only 3-5 K. Below T_g the glassy state is unstable with respect to the supercooled liquid states and the crystalline solid state. A glass is continuously relaxing toward a more stable state. Nevertheless, from an experimental point of view, the molecular motions involved in the structural relaxations in a glass some ten degrees below the T_g are too slow compared to the laboratory time-scale and its physical properties do not appreciably change over time scales of several years. Hence, the glassy system is mechanically stable for practical purposes, even though is thermodynamically unstable [2].

Regarding the structure, glass-forming systems are amorphous solids. The structure of amorphous systems does not have any long-range order. Nevertheless, elastic scattering experiments such as X-ray or neutron diffraction on glass-forming systems reveal a broad peak in the structure factor, also called amorphous halo, related to correlations between structural units (short-range order). In particular, in polymers such a peak is mainly due to the correlations between pairs of atoms located in

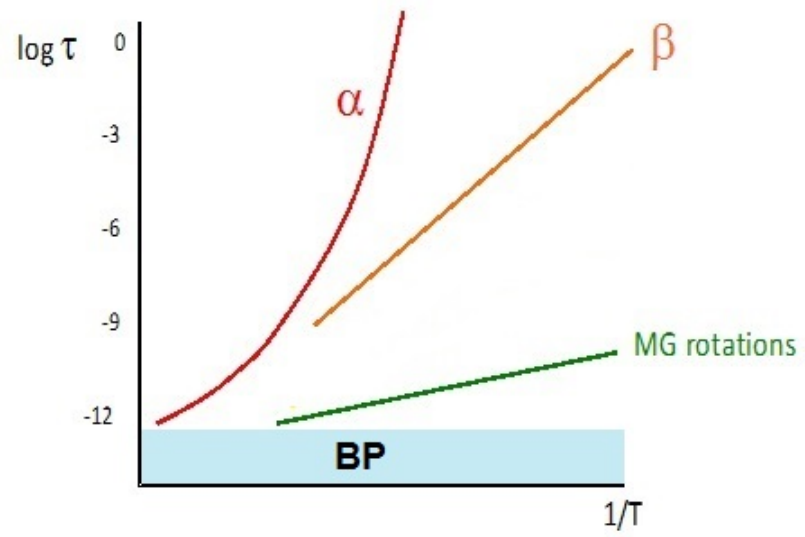

Figure 1.1: Representative scheme of relaxation map illustrating the temperature dependence of characteristic times corresponding to the different dynamics involved in glass-forming polymers.

neighbouring chains, though it usually also contains correlations relating repeating units along the axial direction of a single chain. In addition, polymers are characterized by the presence of a second peak at higher Q-values that can be interpreted in terms of intra-chain correlations between covalently bonded atoms.

1.2.2 Molecular dynamics in glass-forming systems

The main macroscopic properties of materials are strongly related to the dynamical processes occurring at molecular level. The molecular motions are accessible by means of different experimental approaches as the relaxation techniques and quasi-elastic and inelastic scattering. The dynamics of glass-forming systems are very complex and the microscopic mechanisms involved are still poorly understood. Normally, several relaxation processes are observed in such systems. The characteristic lengths of the molecular motions involved vary from one process to another and, some of them, are highly sensitive to temperature and external pressure. Furthermore, the characteristic times span over many decades (from 10^{-13} s to 10^{5} s). Hence, it is necessary to combine different experimental techniques to cover the wide time region where the dynamics occur. At sub-picosecond level, the vibrational dynamics are observed, in particular the so-called Boson peak, a feature typical for glasses. At lower frequencies, short-range motions as rotations –i.e., methyl group rotations– and other rather local motions giving rise to the so-called secondary relaxations. Above T_g the primary relaxation (α-relaxation) becomes active allowing thermodynamic equilibration of the system. Finally, in polymers whole chain motions are required for the system to flow. A representative scheme is shown in Fig. 1.1). In the following, a brief description of the general features of the processes occurring in typical glass-forming systems is given.

α-relaxation

The α-relaxation, or primary relaxation, is the process associated to structural rearrangements and cooperative processes directly related to the glass transition. As mentioned previously, the molecular motions involved in the α-relaxation strongly depend on temperature: approaching T_g from the melt, they drastically slow down and the system finally appears "frozen". The temperature dependence of the characteristic relaxation time τ_α associated to the primary relaxation is non-Arrhenius and it can usually be described by a Vogel-Fulcher-Tamann function:

$$\tau_\alpha \;=\; \tau_\alpha^o \exp\!\left(\frac{B}{T - T_o}\right) \tag{1.3}$$

where τ_α^o and B are temperature independent parameters, while the Vogel temperature T_o represents the singularity at which the characteristic relaxation time would diverge. This empirical temperature dependence of the structural relaxation times can be justified by two main phenomenological theoretical approaches: the *free volume theory* developed by Doolittle [3] and Cohen [4, 5] , and the *Adam-Gibbs theory* [6] . The first theory is based on the assumption of a local volume V attributed to molecules –i.e. low molecular weight glass-formers or liquids– or segments of the polymer chain. Defining the free volume V_f as $V_f = V - V_c$ where V_c is a critical volume and assuming that the mechanism of the molecular transport is a jump over a distance, the relaxation can occur only if $V_f > V^*$ where V^* is the minimal free volume required for the jump. In this framework, T_0 in the VFT equation is the temperature at which the free volume vanishes. The latter theory, is based on the cooperativity approach to the glass transition. Adam and Gibbs introduced the concept of cooperatively rearranging region (CRR) defined as a subsystem which, upon a sufficient thermal fluctuation, can rearrange into another configuration independently of its environments. In this scenario, the Vogel temperature T_0 corresponds to a divergence of the size of the CRR.

It is possible to find some peculiar and universal features of the α-relaxations occurring in all glass-forming systems. The first is related to the non-Arrhenius behaviour of the temperature dependence of the primary relaxation above mentioned. In connection to this feature, the fragility parameter m defined as

$$m \;=\; \frac{\mathrm{d}\log\tau}{\mathrm{d}\left(\frac{T_g}{T}\right)}\,\Bigg|\, T_g = T \tag{1.4}$$

allow us to classify the system as *fragile* or *strong* according to the well-known Angell's criterium [7] . According to the way the characteristic relaxation time τ_α approaches the glass-transition temperature, systems showing a prominent non-Arrhenius behaviour are called fragile, while those manifesting an Arrhenius-like dependence on temperature are classified as strong. In this classification, glass-forming polymers are usually fragile.

Another feature of glass forming systems is the *non-exponential* nature of the response of the system to various perturbations. This particular behaviour can be explained taking into account two different scenarios. One is supposing a heterogeneous set of environments in the system. Each environment is characterized by its own exponential relaxation and the relaxation time varies among them. Therefore, the non-exponential relaxation is due to the superposition of exponential functions

with different relaxation times. Alternatively, a homogeneous scenario has been proposed where all the environments relax almost identically in an intrinsically non-exponential way. Generally, it is accepted that heterogeneities are an important key in the dynamics of glass-forming systems, although the question whether the relaxation function is intrinsically exponential is still a subject of debate. Usually, a stretched exponential function, or Kohlrausch-Williams-Watts (KWW), is used to characterize response functions in the time domain:

$$\phi_{KWW}(t) = \mathrm{e}^{-\left(\frac{t}{\tau_w}\right)^{\beta}} \tag{1.5}$$

with τ_w setting the time scale and $\beta < 1$ determining the stretching of the decay. From a mathematical point of view, the KWW function can be expressed as a superposition of exponential functions:

$$\phi_{KWW}(t) = \int g(\tau)\mathrm{e}^{-\left(\frac{t}{\tau}\right)}\mathrm{d}\tau \tag{1.6}$$

with $g(\tau)$ distribution function of the relaxation time. This would correspond to the physical picture of the heterogeneous scenario above mentioned. We note that distributions of relaxation times are commonly found behind the broad features of the relaxations in the glassy state. Usually, these distributions are symmetric and can be attributed to heterogeneous environments in the glassy materials.

Before describing the phenomenological features of other dynamic processes in glass-formers, it is worth mentioning the *mode coupling theory* (MCT) that represents a microscopic approach to the structural glass transition. MCT considers the density fluctuations as the most important low-frequency process and describes the glass transition as an essentially dynamic phenomenon [8]. The main physical interpretation behind the structural arrest, that would occurs at a critical temperature T_c, is the so-called 'cage effect'. The particles are constrained in their motion in a cage formed by their neighbours. As the system gets denser structural arrest occurs because particles can no longer leave their cage at finite time. Exhaustive review on MCT can be found in Refs. [9, 10, 11, 12, 13].

Relaxations in the Glassy State

Below the glass transition temperature, only short-range processes can take place. In general, these local motions are called secondary relaxations in order to distinguish them from the structural relaxation above T_g. Such dynamics can be of different nature depending on the glass-forming material. In polymers, secondary relaxations are often associated to local motions of molecular groups in the main chain or in the side group –i.e. methyl group rotations, twisting motions or motions of the side group about the bonds linking them to the main chain–. In low molecular weight glass formers, such relaxations may involve the motions of essentially all parts of the basic structural unit [14] . However, some secondary relaxations may not involve just intra-molecular motions. In fact, Johari and Goldstein [15] showed the presence of these relaxations even in glass formers composed of completely rigid molecules originated from some motion of the entire molecule.

The temperature dependence of the relaxation times associated to relaxations in the glassy state is that expected for the thermally activated processes, that is the

Arrhenius law:

$$\tau = \tau_o \exp\left(\frac{E_a}{k_B T}\right) \tag{1.7}$$

where E_a represents the activation energy of the process, k_B is the Boltzmann's constant and τ_o is a parameter that represents the relaxation time at $T \to \infty$. Finally, as commented above, such relaxations are characterized by a distribution of the relaxation times.

Vibrational Dynamics

In the sub-picosecond region, the dynamics is dominated by vibrational motions occurring along all the temperature range, above and below the T_g. The atoms that compose the polymer are not 'quiet', but vibrate around their equilibrium positions giving rise to a vibrational spectrum. A characteristic and universal vibrational feature of glass-forming systems is the so-called Boson peak. Such a process is detectable by different scattering techniques – i.e. neutron scattering and Raman inelastic scattering spectroscopy– in the energy range of 1.5-4 meV and is resolved well below the T_g. It has been observed in different glass-forming systems as biomacromolecules (i.e. proteins), polymers, low molecular weight glass formers like glycerol and ionic glasses although showing relevant changes regarding the position of the maximum and the intensity. Several investigations carried out on various amorphous polymers and inorganic glasses allowed to associate the Boson peak to an excess in the density of the vibrational states $G(\omega)$. Nonetheless, the origin of the Boson peak is still a subject of debate. A variety of explanations of the Boson peak has been proposed, e.g. in terms of the soft potential model [16, 17], phonon localization models [18, 19], or a model of coupled harmonic oscillators with a distribution of force constants [20]. The Boson peak was also modelled within the MCT [21]. However, even if these models can describe some experimental results, none can elucidate satisfactory the origin of the Boson peak.

1.3 Liquid, supercooled and glassy water

1.3.1 Basic Features and Anomalies

Water, despite of its very simple chemical composition, is one of the most important liquids on earth. Its unique properties result to be fundamental for life. In fact, it has unique hydration properties for biological macromolecules: for example, it is involved in the functional dynamics of proteins, as folding and unfolding, plays a key relevant role on the three-dimensional structure of enzymes that is necessary for the metabolism of nutrients and is involved in the temperature regulations and resistance against dehydration. Moreover, water is essential in many industrial processes as a solvent (it is commonly referred to as the universal solvent), as a reactant or as an impurity. A water molecule is composed by two hydrogen atoms covalently bonded to an oxygen atom. The atoms are arranged with the two OH bonds at an angle of about 104.5° in the gas phase. This V-shape structure and the fact that the oxygen electronegativity is higher than that of the hydrogen atoms give rise to a strong dipole moment that has significant implications. In fact, the attraction between an oxygen and a hydrogen of different water molecules leads to the formation of a

hydrogen bond, stronger than van der Waals but weaker than a covalent or ionic bond. Many of the above mentioned properties of water are due to the hydrogen bonds between adjacent molecules. Each water molecule can participate in four hydrogen bonds giving rise to the formation of a network. The structure of bulk water is still a matter of debate, although is commonly accepted the idea that water molecules tend to form a tetrahedral hydrogen bonded structure [22], these hydrogen bonds having very short lifetimes (in order of picoseconds at room temperature [23]). Such peculiar properties allow the water molecules to arrange in a defined structure below 273 K (at atmospheric pressure), the ordinary hexagonal ice (Ih). In addition, the ice structure of water strongly depends on pressure. In fact, besides the ordinary hexagonal ice, water has 13 polymorphs in the crystalline state. Among them, nine are stable over a certain range of temperature and pressure (ices II, III, V, VI, VII, VIII, X, XI, Ih) and four metastable (IV, XI, XII and cubic ice Ic). Not only its properties, but also its anomalies make water a very interesting liquid. It's well known that the water density reaches its maximum at 277 K in contrast with other liquids which contract upon cooling. Moreover, different response functions of liquid water as a function of temperature show a unique behaviour. *i)* The isothermal compressibility, defined as

$$K_T = -\frac{1}{V}\left(\frac{\partial V}{\partial P}\right)_T = \frac{<(\Delta V)^2>}{k_B T V} \tag{1.8}$$

measures the volume fluctuations $<(\Delta V)^2>$ and should decrease upon decreasing the temperature. In the case of water, instead, it increases and seems to diverge with a power of law. *ii)* The coefficient of thermal expansion defined as

$$\alpha_P = \frac{1}{V}\left(\frac{\partial V}{\partial T}\right)_P = \frac{P}{k_B^2 T} < \Delta V \Delta S > \tag{1.9}$$

is the measure of cross fluctuations of volume and entropy $< \Delta V \Delta S >$ and is positive for normal liquids, while for water it becomes negative below 277 K and diverges at low temperatures. *iii)* The specific heat read as

$$C_p = T\left(\frac{\mathrm{d}H}{\mathrm{d}T}\right)_P = T\left(\frac{\partial S}{\partial T}\right)_P = \frac{<(\Delta S)^2>}{k_B} \tag{1.10}$$

is a measure of the enthalpy fluctuations, therefore it would decrease as the temperature is decreased. Contrastingly, C_p increases sharply in water as the temperature is decreased below 330 K.

1.3.2 Liquid to Glassy Water

The glass transition temperature of bulk water is still a strong debated argument and currently a hot investigated topic. For many years it has been accepted that $T_g = 136\ K$ even though it has been recently suggested to be located around 165 K. Unfortunately, this temperature is in the region usually called no man's land between 150 K and 235 K (see Fig. 1.2), that means comprised between the homogeneous nucleation temperature and the spontaneous crystallization to cubic ice. As a consequence, it is not possible to observe experimentally bulk water in the no man's land. In order to overcome this problem, it is possible to study water in confinement or in

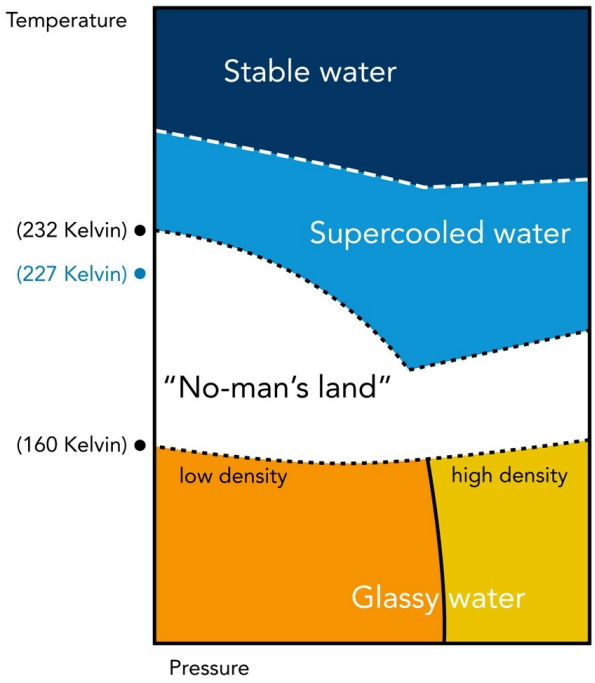

Figure 1.2: Diagram of the rough boundaries of 'no mans land', a temperature region where supercooled water is difficult to study because of rapid ice formation [24]

mixtures. In fact, in a confined environment or in interaction with macromolecules (e.g. polymers), water molecules change their orientation with respect to the adjacent molecules affecting the probability of forming the network structure necessary for crystallization.

1.3.3 Water Dynamics in Confined Environments

The dynamics of water in confined geometry and in supercooled regime is a subject of a very active research. Its study is strongly stimulated not only due to the decisive role played by water dynamics in biological processes, but also to understand its anomalies in the "no man's land". It has been investigated by several different experimental techniques (such as neutron scattering, dielectric spectroscopy, NMR) and in different environments (in solutions of polymers, small organic molecules, biomolecules and in geometrical confinement) [25, 26, 27, 28]. In particular, dielectric spectroscopy often revealed two processes. The slower one usually shows a VFT temperature dependence of the characteristic relaxation times. This behaviour is similar to that exhibited by the α-relaxation process observed in supercooled systems above the glass transition temperature. According to the results obtained by the studies on supercooled systems, the slow process of water in solution or in confined environment was related to the cooperative rearrangement of the whole system, i.e. water plus solute. On the other hand, the fast process shows a peculiar behaviour. In fact, in contrast with normal liquids in confinement (i.e. propylene glycol in Na-vermiculite clay [29]), the water fast process is strongly affected by the interactions with the host material and a crossover from an Arrhenius to a VFT dependence on temperature of the relaxation times on cooling down the system

is observed. Depending on the size and the geometry of the confinement and the interaction of water molecules with the solute or host material, the temperature at which this phenomenon is observed is comprised between 180-250K. It was suggested that the origin of such a crossover is related to a fragile to strong transition [30] and ascribed to a change from high-density liquid to low-density upon cooling [31]. However, the behaviour of the fast process of water is strongly debated. Such a fast dynamics has been associated with the reorientation of water molecules in solutions [26, 32, 33]. Moreover, it has been noticed that the crossover takes place in the temperature range where differential scanning calorimetry measurements show a global glass transition process [25]. Therefore, the crossover has been related to a confinement effect due to the glass transition of the system. That is, at high temperature, above the T_g, the water molecule reorientation is coupled to the cooperative motions involved in the global relaxation process of the system. Cooling down the system above the glass transition temperature, the global dynamics becomes too slow and water molecules are trapped in a frozen matrix. Therefore, the fast process at low temperature shows a behaviour typical of the secondary process in glass-forming system. Moreover, comparing the Arrhenius temperature dependence of water fast dynamics in the glassy state for several systems (in solution with biopolymers [34, 35], low molecular weight glass formers [26, 25] and polymers [25, 36]) a very similar activation energy of $\sim$0.54 eV has been found and a master curve for the temperature dependence of water dynamics below the crossover temperature could be obtained. However, in some systems no calorimetric glass transition can be observed [37, 38, 39]. Thus, it has also been proposed that the apparent strong to fragile transition is due to a merging from the observed β-like water relaxation with a non-observable α-relaxation [28].

1.4 Dynamics in Polymer/Solvent Mixtures

Dynamics in glass-forming materials constitute a complex problem. These systems displays a variety of dynamical processes, as it has been previously shown. Such complexity becomes obviously even more intricate if mixtures are considered. However, mixtures are ubiquitous both in industry as well in nature. In fact, at present, is quite difficult to commercialize new pure polymers. In practical use, many polymeric materials contain low molecular weight additives (plasticizers) to tailor their physical properties to particular technical needs. Moreover, from a biological point of view, the presence of water molecules is simply fundamental for the functional properties of the biomolecules. For these reasons, it is of utmost interest to understand how the presence of solvent molecules affects the properties of the macromolecules and vice versa. In particular, it appears necessary to elucidate the role of solvent/polymer interactions on their mutual effects on the dynamics.

Among the glass-forming mixtures, a specially interesting situation has been found for those with large difference in the glass transition temperatures of the neat components, and in particular for high concentrations of the slower component. This kind of situation is provided by mixtures of polymers and solvent molecules, for high polymer concentrations. In these systems, confinement effects on the fast component have been observed upon the vitrification of the slower component [40, 41, 42]. This fact has been exploited particularly in the case of aqueous solutions where water crystallization is avoided and it is possible to study the dynamics of the water

molecules in the so-called 'no-man's land'. However, this kind of studies constitute a challenge from an experimental point of view, since covering a large dynamic range and selectivity to the different components are required. For this purpose, the combination of broadband dielectric spectroscopy and neutron scattering techniques is a suitable tool. The former allows exploring a very wide range in frequency and might be selective for one of the components if it has a much stronger dipole moment than the other, while the latter offers selectivity to a given component through isotopic (H/D) labelling. Such synergetic investigation has been repeatedly carried out on some concentrated mixtures [43, 44, 41, 42].

These studies and other works performed over many years applying only dielectric spectroscopy and/or more conventional techniques like e.g. calorimetry or nuclear magnetic resonance (NMR) have allowed establishing a series of phenomenological facts on these systems. Regarding the polymer dynamics, it turns out that the presence of small molecules affects principally the slow processes and the chain dynamics. The presence of plasticizers leads to a shift toward lower temperature of the T_g (plasticization effect) and so a change on the time-scale of the structural rearrangements (α-relaxations) of the polymer is found. Moreover, in neutron scattering experiments [42, 45, 46, 47] an additional stretching of the scattering functions with respect to that of the bulk component and strong deviations from Gaussian behaviour in the whole Q-range explored were found. Below T_g, the effects of plasticizers on the dynamics are not as dramatic as those found for the α-process. However, they might be also affected. For example, suppression of local motions related to the β-relaxations has been found in some plasticized polymers [44, 48] . Moreover, the dynamical changes strongly depend on the character of the solvent. For example, *Bistac et al.* studied cast films of poly(methyl methacrylate) in different solutions [49]. They found that different acid-base character of the solvents implies different effects on polymer dynamics: the presence of chloroform increases the polymer mobility and the polymer β-relaxation appears faster in solution; on the contrary, solutions with tetrahydrofuran, acetone and toluene are characterized by slower secondary relaxations in comparison with the bulk system.

Many polymers are characterized by the presence of methyl groups in their monomer. In the glassy state it has been found that the presence of other surrounding faster component – in these cases another polymer– does not appreciably affect the methyl group dynamics of the polymer, at least in systems exhibiting a weak intermolecular coupling –i.e. poly(vinyl acetate)/poly(ethylene oxide) (PVAc/PEO) [50] and poly(methyl methacrylate)/poly(ethylene oxide) (PMMA/PEO) [51]. Such behaviour has been related to the rather localized character of the motions involved. Concerning the vibrational properties of polymers in the glassy state, hydrated samples show a shift of the Boson peak position toward higher energies of ∼1-2 meV and a decrease of its intensity. Such an effect has been observed for proteins [52, 53, 54] and for polymers in water solution as PVME [42] investigated by neutron scattering experiments. It has been proposed that the presence of hydration water affects the protein energy landscape making it more rugged and the protein state is trapped in a local minimum causing the characteristic Boson peak frequency to shift to higher values [55]. However, this does not explain the decrease of the peak intensity. Therefore a comparative study focused on the effect of the hydrogen bonds on the Boson peak intensity and energy were performed on different hydrogen-bonded molecular glasses by *Yamamuro et al.*[56]. In that work, it was

found that the peak intensity decreases and the peak energy increases as the number of hydrogen bonds increase.
On the other hand, polymer/solvent interactions also affect the solvent dynamics. Aqueous concentrated solutions are the most investigated systems due to the enormous interest in the water dynamics in the 'no-man's land'. In these systems there is a general agreement about the existence of a crossover from low-temperature Arrhenius to high-temperature non-Arrhenius behaviour of the characteristic times obtained from dielectric spectroscopy and quasi-elastic neutron scattering experiments –i.e. poly(vinyl methylether) (PVME) [42] , poly(vinyl pyrrolidone) (PVP) [57] , and polyamide (PA) [41] in aqueous solutions–. Interestingly, such a crossover recently has been also reported for methyl-tetraydrofuran (MTHF) as minority component in mixture with polystyrene [58] . Moreover, in these concentrated solutions, a stretching of the scattering functions and a non-Gaussian behaviour of the water component investigated by QENS have been found [42] . These effects – also observed in the polymer component as previously mentioned– were explained invoking on the one hand a distribution of mobilities for water and polymer components, related to the structural heterogeneities present in the systems, and, on the other hand, the formation of H-bonds that could slow down the dynamics of polymer molecular groups adding heterogeneities to the system. Concerning mixtures with solvents different from water, an NMR investigation on poly(methyl methacrylate)/tri-m-cresyl phosphate (PMMA/TCP) revealed a strong difference between the dynamics of the pure plasticizer (TCP) and the plasticizer in the mixture [59] . In fact, the TCP relaxations changes from a stretched exponential decay to a quasi-logarithmic decay in presence of polymer. This effect has been related to a broadening of the distribution of the relaxation times due to the polymer matrix.
It is reasonable to attribute to the polymer/solvent interactions a key role in the dynamical features of the mixtures with high polymer concentrations mentioned above. In presence of water, the formation of H-bonds plays a crucial part. Considering pairs of components interacting via weaker interactions, like Van der Waals, removes such an important ingredient and might shed light on the general problem of dynamics in concentrated polymer mixtures.

1.5 Objectives

The aim of this Ph.D. thesis is to determine how the presence of solvent molecules affects the dynamics of a polymer at different levels and how the solvent dynamics is influenced by the interactions with the polymer. In particular, it is of fundamental interest to understand which is the role of hydrogen bonds in this mutual interplay. For this purpose, a comparative investigation with solvents interacting differently with the polymers is necessary. Moreover, in order to have a complete scenario, it is fundamental to investigate the structural aspects of the mixtures as well. The chosen system in this work was poly(2-(dimethylamino)ethyl methacrylate) (PDMAEMA) in concentrated mixtures with either tetrahydrofuran (THF) or water (30 wt%). Regarding the polymer, PDMAEMA is commonly investigated for the development of materials with antibacterial properties [60]. PDMAEMA is rich in tertiary amino groups(see scheme in Fig. 1.3) which can be converted to positively charged quaternary ammonium groups with bactericidal properties. Moreover it has been investigated to build gene deliveries in the gene therapy field

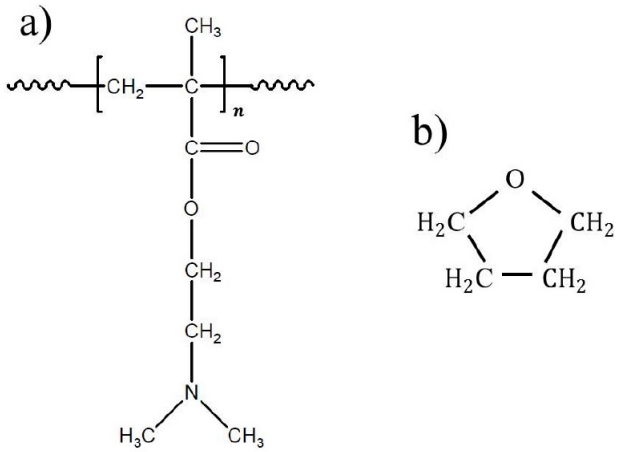

Figure 1.3: Chemical formulae of PDMAEMA (a) and THF molecule (b).

[61]. So far, viral vectors are the most used gene carriers. However, due to safety issues associated with them, i.e. immune responses or gene mutations, it has been necessary to develop non-viral gene carrier. Among them, polycationic polymers, as PDMAEMA, are now widely used in gene therapy for their chemical properties [62]. Both, THF and water are good solvents for this polymer and are available in their deuterated forms. However, while in aqueous solutions the hydrogen bonds dominate the solvent/polymer interactions, THF does not interact via H-bonds. Dielectric spectroscopy and neutron scattering have been combined to determine both polymer and solvent dynamics. X-ray and neutron diffraction experiments have also been performed to study the structural properties of the mixtures. The dry polymer has been also investigated as reference. As a representative concentration, 70 wt% in polymer (1 THF molecule per monomer and 4 H_2O molecules per monomer respectively) was chosen. In addition, a calorimetric and dielectric spectroscopy study as function of the solvent concentration has been carried out on both THF and water mixtures.

CHAPTER

2

EXPERIMENTAL TECHNIQUES AND DATA ANALYSIS

2.1 Neutron Scattering

2.1.1 Basic properties of neutrons

Neutrons are an extremely versatile probe to investigate condensed matter due to their unique properties:

1. Neutrons are neutral particles. They are thus highly penetrating, probing the bulk properties of the sample.

2. Due to the range of wavelengths, neutrons can provide spatial information in the range from the pico-meter to the 100 μm range, i.e, covering inter-atomic spacing as well as typical sizes of macromolecules.

3. Neutrons interact with the sample via nuclear forces, hence the interaction cross section depends on the internal structure of the nuclei and not on the mass or electric charge of the whole atom. As a consequence, neutrons are very sensitive to light atoms like hydrogen, which is difficult to detect by X-rays since hydrogen bonded with other heavier atoms has often less than one surrounding electron. On the other hand, they allow isotopic labelling, in particular by H/D substitution.

4. Neutrons have a magnetic moment ($\mu = -1.913\ \mu_N$) due to the nuclear spin, hence they are sensitive to the magnetic properties of the sample e.g. magnetic structures, excitations in solids, etc. ...

Neutrons are in particular useful because their energy and wavelength corresponds very well with the inter-atomic distances and the typical excitations in con-

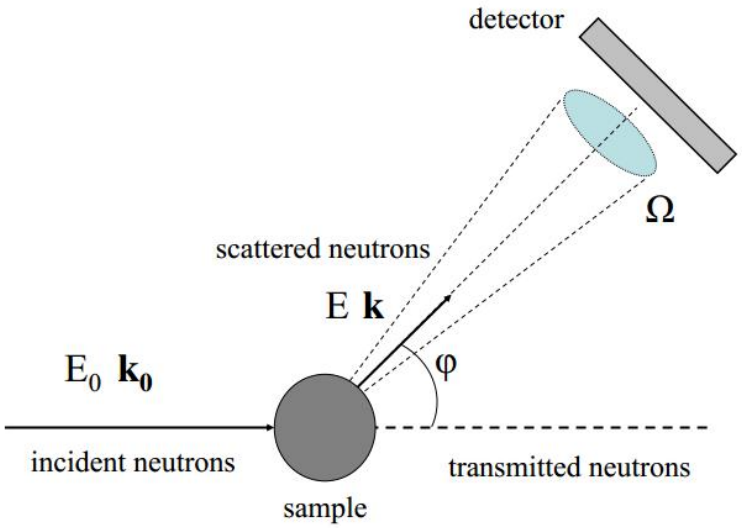

Figure 2.1: Geometry of a neutron scattering experiment

densed matter [63, 64, 65, 66, 67] . In fact the kinetic energy of a free neutron is

$$\begin{aligned} E_{kin} &= \frac{1}{2} m_N v^2 \\ &= \frac{p^2}{2m_N} \\ &= \frac{h^2}{2m_N \lambda^2} \end{aligned} \tag{2.1}$$

The neutron mass is $m_N = 1.675 \times 10^{-27}$ Kg and for $\lambda = 1$ Å the corresponding energy results $E_N = 81.8$ meV while the equivalent energy for X-ray would be $E_x = 12.5$ KeV. The basic physical magnitudes which give information about the neutron scattering process are the energy transferred $\hbar\omega$ and the momentum transfer $\mathbf{Q}$.

$$\hbar\omega = E - E_0 = \frac{\hbar^2}{2m}(k^2 - k_0^2) \tag{2.2}$$

$$\mathbf{Q} = \mathbf{k} - \mathbf{k}_0 \tag{2.3}$$

In figure 2.1 the scheme of a neutron scattering experiment is shown. The neutron beam, characterized by an initial energy E_0 and initial wavelength $\mathbf{k}_0$, is incident on the sample. The neutrons scattered by the sample in the solid angle Ω are characterized by a final energy E and wave-vector $\mathbf{k}$. The scattered neutrons will be counted by the detectors spanning such solid angle. If the neutron is scattered without exchanging energy with the nuclei of the sample, that is $E_0 = E$, the scattering process is defined as *elastic*. This kind of experiment allows to study the structure of the system under investigation. Otherwise, if the neutron is scattered exchanging energy and momentum transfer with the sample due to processes occurring with discrete energy steps (vibrational modes, stretching modes, ...), the process is called *inelastic*

scattering. Finally, if neutrons exchange a small amount of energy with the sample ($\hbar\omega \approx \mu eV$), less than the minimal energy amount necessary for an excitation, such exchange is observed as a broadening of the elastic peak and the scattering process is called *quasi-elastic*. The study of this process is very adequate to probe rotations of small molecular units, local motions, and structural relaxations.

2.1.2 Differential cross-section

The magnitude measured in a neutron scattering experiment is proportional to the double differential cross section that gives the probability that a neutron, with incident energy E_0, leaves the sample in the solid angle element $d\Omega$ around Ω and with energy exchange comprised between $\hbar\omega = E - E_0$ and $\hbar(\omega + d\omega)$ and is defined by the equation:

$$\frac{\partial^2\sigma}{\partial\Omega\partial\omega} = \frac{C}{\eta\Phi N\Delta\Omega\Delta\omega} \tag{2.4}$$

where Φ is the flux of incident neutrons, C is the count rate in the detector with efficiency η and N is the number of atoms in the sample. Measuring the double differential cross section for all the energy transfers E we obtain *the differential cross section*:

$$\frac{\partial\sigma}{\partial\Omega} = \int dE \frac{\partial^2\sigma}{\partial\Omega\partial E} \tag{2.5}$$

Considering neutrons scattered by a sample undergoing a change from a state λ_0 to a state λ while the state of the neutron changes from $(\mathbf{k}_0, \sigma_0)$ to $(\mathbf{k}, \sigma)$, the corresponding differential scattering cross section is given by:

$$\frac{\partial\sigma}{\partial\Omega} = \frac{1}{N\Phi d\Omega} W_{\mathbf{k}_0,\sigma_0,\lambda_0\to\mathbf{k},\sigma,\lambda} \tag{2.6}$$

where $W_{\mathbf{k}_0,\sigma_0,\lambda_0\to\mathbf{k},\sigma,\lambda}$ is the number of transitions per second from the state $\mathbf{k}_0, \sigma_0, \lambda_0$ to the state $\mathbf{k}, \sigma, \lambda$.

The right-hand side of the above equation is evaluated by using the Fermi's golden rule:

$$W_{\mathbf{k}_0,\sigma_0,\lambda_0\to\mathbf{k}_1,\sigma_1,\lambda_1} = \frac{2\pi}{\hbar}\left|\langle\mathbf{k}_1,\sigma_1,\lambda_1|V|\mathbf{k}_0,\sigma_0,\lambda_0\rangle\right|^2 \rho_{\mathbf{k}_1,\sigma_1(E_1)} \tag{2.7}$$

where V is the interaction potential between the incident neutron and the target sample that causes the transition, and $\rho_{\mathbf{k}_1}$ is the density of the final scattering states per unit energy range. To evaluate the latter, we consider a large box of volume L^3 and the initial and final state of the neutrons expressed by

$$\psi_{\mathbf{k}_0}(\mathbf{r}) = \frac{1}{L^{3/2}} \mathrm{e}^{(i\mathbf{k_0}\cdot\mathbf{r})} \tag{2.8}$$

and

$$\psi_{\mathbf{k}}(\mathbf{r}) = \frac{1}{L^{3/2}} \mathrm{e}^{(i\mathbf{k}\cdot\mathbf{r})} \tag{2.9}$$

In order to keep the solutions in the form of plane waves, periodic boundary conditions have to be applied, namely

$$\psi_{\mathbf{k}}(\mathbf{r}+\mathbf{L}_\alpha) \;=\; \psi_{\mathbf{k}}(\mathbf{r}) \tag{2.10}$$

where $\mathbf{L}_\alpha$ is any of the edge vectors of the cubic box. This leads to the expression of the wave-vector as

$$\mathbf{k} \;=\; \frac{2\pi}{L^2}(m\mathbf{L}_x + n\mathbf{L}_y + p\mathbf{L}_z) \tag{2.11}$$

with m,n,p integers. In the momentum space $\mathrm{d}\mathbf{k} \;=\; k^2\mathrm{d}\mathbf{\Omega}\mathrm{d}k$, thus it follows from (2.11) that each extremity of a moment vector occupies in the reciprocal space a volume equal to $(2\pi/L)^3$ and the density of final states is such that

$$\rho(\mathbf{k})\mathrm{d}\mathbf{k} \;=\; \left(\frac{L}{2\pi}\right)^3 k^2\mathrm{d}\mathbf{\Omega}\mathrm{d}k \tag{2.12}$$

Changing to energy space, considering $E = \hbar^2k^2/2m$, we obtain

$$\rho(E)\mathrm{d}E \;=\; \left(\frac{L}{2\pi}\right)^3 \frac{mk^2}{\hbar^2}\mathrm{d}\mathbf{\Omega}\mathrm{d}E \tag{2.13}$$

It follows, integrating over the energy, the equation for the density of the final scattering states per unit energy range:

$$\rho(E) \;=\; \left(\frac{L}{2\pi}\right)^3 \frac{mk^2}{\hbar^2}\mathrm{d}\mathbf{\Omega} \tag{2.14}$$

To obtain the cross-section we have now only to determine the incident flux of neutrons Φ that, with the aid of De Broglie relation, $p = \hbar k$, can be written as:

$$\Phi \;=\; \frac{v}{L^3} \;=\; \frac{1}{L^3}\frac{\hbar k_0}{m} \tag{2.15}$$

Hence, from (2.7) (2.14) (2.15) :

$$\frac{\partial\sigma}{\partial\Omega} \;=\; \frac{1}{N}\frac{k}{k_0}\left(\frac{m}{2\pi\hbar}\right)^2 \left|\langle\mathbf{k}\lambda\sigma|V|\mathbf{k}_0\lambda_0\sigma_0\rangle\right|^2 \tag{2.16}$$

Finally we obtain the double differential cross section from (2.16) incorporating the energy conservation $\hbar\omega \;=\; E - E_0$:

$$\frac{\partial\sigma}{\partial\Omega\partial E} \;=\; \frac{1}{N}\frac{k}{k_0}\left(\frac{m}{2\pi\hbar}\right)^2 \left|\langle\mathbf{k}\lambda\sigma|V|\mathbf{k}_0\lambda_0\sigma_0\rangle\right|^2 \partial(\hbar\omega + E - E_0) \tag{2.17}$$

From experimental results we know that the nucleus-neutron interaction has a very short range of the order of 10^{-13} cm therefore much smaller than the wavelength of low energy neutrons. Moreover the nuclear radius is only about an order of magnitude larger than the neutron one. It follows that the neutron-nucleus scattering is isotropic and can be characterized by a single parameter b called the scattering length. Therefore, the interaction potential between the neutrons and the sample can be described by the so-called Fermi pseudopotential:

$$V(\mathbf{r}) \;=\; \frac{2\pi\hbar}{m}\sum_i b_i\delta(\mathbf{r} - \mathbf{R}_i) \tag{2.18}$$

with $\mathbf{R}_i$ and $\mathrm{b_i}$ respectively the vector position and the scattering length of the i-th nucleus. Thus

$$\begin{aligned}\langle \mathbf{k}|V|\mathbf{k}_0\rangle &= \sum_i b_i \int d\mathbf{r}\exp(-i\mathbf{k}\cdot\mathbf{r})\delta(\mathbf{r}-\mathbf{R}_i)\exp(-i\mathbf{k_0}\cdot\mathbf{r}) \\ &= \sum_i b_i \exp(i\mathbf{Q}\cdot\mathbf{R}_i)\end{aligned} \tag{2.19}$$

with $\mathbf{Q} = \mathbf{k} - \mathbf{k_0}$. Substituting (2.18) and (2.19) in (2.17) and considering, for simplicity, an unpolarized neutron scattering experiment, the master formula results:

$$\frac{\partial\sigma}{\partial\Omega\partial E} = \frac{1}{N}\frac{k}{k_0}\sum_{\lambda_0} p_{\lambda_0}\sum_{\lambda}\left|\langle\lambda|\sum_i b_i e^{-i\mathbf{Q}\mathbf{R}_i}|\lambda_0\rangle\right|^2 \partial(\hbar\omega + E - E_0) \tag{2.20}$$

where p_{λ_0} is the probability to find the sample in the initial state λ_0.

In a real experiment, the intensity measured is not the double differential cross-section for a process in which the sample goes from a specific state to another, therefore it is necessary to sum over all the final states λ, keeping λ_0 fixed, and then average over all the initial states. To carry out this task the Heisenberg operators and a representation of the delta Dirac function by an integral over time are used. The final expression is called real-time representation of the double differential cross section

$$\frac{\partial\sigma}{\partial\Omega\partial E} = \frac{1}{N}\frac{k}{k_0}\int_{-\infty}^{\infty} \mathrm{e}^{-i\omega t}dt\sum_{i,j} b_i^* b_j \langle \mathrm{e}^{i\mathbf{Q}(\mathbf{R}_i(t)-\mathbf{R}_j(0))}\rangle \tag{2.21}$$

2.1.3 Coherent and Incoherent Scattering

In order to derive Eq. 2.21 we assumed a system of N chemically identical particles, but even in a monoisotopic system there may be variance of scattering lengths due to the disorder of the nuclear spin orientation, since the scattering length also depends on the combined spin state of the scattered neutron and the scattering nucleus. Let now assume that the nuclear spins and the isotopes are randomly distributed in any atomic configuration and let $\bar{b}_i$ denote the average scattering length for a given atomic species. We can explicitly split the terms in the sum in (1.18) into the average values and the deviations from the average:

$$\begin{aligned}\sum_{i,j} b_i^* b_j \mathrm{e}^{i\mathbf{Q}[\mathbf{R}_i(t)-\mathbf{R}_j(0)]} &= \sum_{i,j}(\bar{b}_i^*\bar{b}_j + b_i^* b_j - \bar{b}_i^*\bar{b}_j)\mathrm{e}^{i\mathbf{Q}[\mathbf{R}_i(t)-\mathbf{R}_j(0)]} \\ &= \sum_{i,j}\bar{b}_i^*\bar{b}_j\mathrm{e}^{i\mathbf{Q}[\mathbf{R}_i(t)-\mathbf{R}_j(0)]} + \sum_{i,j}(b_i^* b_j - \bar{b}_i^*\bar{b}_j)\mathrm{e}^{i\mathbf{Q}[\mathbf{R}_i(t)-\mathbf{R}_j(0)]}\end{aligned} \tag{2.22}$$

We can consider the sample to be as an ensemble of a large number of independent 'subsamples' and so the cross-section will be an average over all these 'subsamples'. The first sum on the right side of (2.22) is the same for all the subsamples, and it is

called "coherent" scattering. Since under ordinary conditions isotopes and nuclear spins are fully randomly distributed in the sample, there is no correlation between the occupation i and j. Therefore, if $i \neq j$

$$\langle b_i^* b_j - \bar{b}_i^* \bar{b}_j \rangle \;=\; \langle b_i^* \rangle \langle b_j \rangle \;-\; \bar{b}_i^* \bar{b}_j \equiv 0 \tag{2.23}$$

while for $i = j$

$$\langle b_i^* b_j - \bar{b}_i^* \bar{b}_i \rangle \;=\; \langle b_i^* \rangle \langle b_i \rangle \;-\; \bar{b}_i^* \bar{b}_i = \; (b_i^{inc})^2 \tag{2.24}$$

with

$$b_i^{inc} \;=\; \sqrt{\langle b_i^2 \rangle - \bar{b}_i^2} \tag{2.25}$$

called incoherent scattering length. Substituting (2.23) (2.24) in (2.22):

$$\begin{aligned} \frac{\partial \sigma}{\partial \Omega \delta E} \;&=\; \frac{1}{N} \frac{k}{k_0} \int \mathrm{e}^{-i\omega t} dt \Bigg(\sum_{i,j} \langle \bar{b}_i^* \bar{b}_j \rangle \mathrm{e}^{i\mathbf{Q}[\mathbf{R}_i(0) - \mathbf{R}_j(t)]} + \\ &+ \sum_{i,j} \langle (b_i^* b_j - \bar{b}_i^* \bar{b}_j) \rangle \mathrm{e}^{i\mathbf{Q}[\mathbf{R}_i(0) - \mathbf{R}_j(t)]} \Bigg) \\ &= \; \frac{1}{N} \frac{k}{k_0} \int \mathrm{e}^{-i\omega t} dt \Bigg(\sum \langle \bar{b}_i^* \bar{b}_j \rangle \mathrm{e}^{i\mathbf{Q}[\mathbf{R}_i(0) - \mathbf{R}_j(t)]} + \sum_i \langle (b_i^{inc})^2 \rangle \mathrm{e}^{i\mathbf{Q}[\mathbf{R}_i(0) - \mathbf{R}_i(t)]} \Bigg) \end{aligned} \tag{2.26}$$

In Eq. 2.26 the first sum in the right side represents the *coherent* double differential cross section and depends on the correlation between the position of the atom i at time 0 with an atom j (which can be different from i or also i) at time t, while the second sum represents the *incoherent* double differential cross-section which depends on the correlation between the position of the same atom i at different times. Defining the *coherent dynamic structure factor* and the *incoherent dynamic structure factor* as:

$$S(\mathbf{Q}, \omega) \;=\; \sum \int \mathrm{e}^{-i\omega t} dt \, \mathrm{e}^{i\mathbf{Q}[\mathbf{R}_i(0) - \mathbf{R}_j(t)]} \tag{2.27}$$

$$S_{inc}(\mathbf{Q}, \omega) \;=\; \sum_i \int \mathrm{e}^{-i\omega t} dt \, \mathrm{e}^{i\mathbf{Q}[\mathbf{R}_i(0) - \mathbf{R}_i(t)]} \tag{2.28}$$

and the *coherent cross-section* and the *incoherent cross-section* as:

$$\begin{aligned} \sigma_{coh} \;&=\; 4\pi \langle b \rangle^2 \\ \sigma_{inc} \;&=\; 4\pi (\langle b^2 \rangle - \langle b \rangle^2) \end{aligned} \tag{2.29}$$

we can finally write the double differential cross section as combination of a coherent and incoherent part as shown in the equation:

$$\frac{\partial \sigma}{\partial \Omega \partial E} \;=\; \left(\frac{\partial \sigma}{\partial \Omega \partial E} \right)_{coh} + \left(\frac{\partial \sigma}{\partial \Omega \partial E} \right)_{inc} \tag{2.30}$$

with

$$\begin{aligned}\left(\frac{\partial\sigma}{\partial\Omega\partial E}\right)_{coh} &= \frac{1}{N}\frac{k}{k_0}\frac{\sigma_{coh}}{4\pi}S(\mathbf{Q},\omega)\\ \left(\frac{\partial\sigma}{\partial\Omega\partial E}\right)_{inc} &= \frac{1}{N}\frac{k}{k_0}\frac{\sigma_{inc}}{4\pi}S_{inc}(\mathbf{Q},\omega)\end{aligned} \tag{2.31}$$

The cross-sections in Eq. 2.31 are factorized in three independent components: (i) the ratio of the wave numbers k and k_0 characterizing the scattering process, (ii) the total scattering cross-section σ depending on the composition of the sample and (iii) the *dynamic structure factor* $S(\mathbf{Q},\omega)$ and the incoherent scattering function $S_{inc}(\mathbf{Q},\omega)$. The structural and dynamical properties of the scattering sample are fully described by $S(\mathbf{Q},\omega)$, while $S_{inc}(\mathbf{Q},\omega)$ provides information on self-atomic motions (and no structural information).

2.1.4 Correlation Functions

We can define the dynamic structure factor $S(\mathbf{Q},\omega)$ as the time-Fourier transform of the *intermediate scattering function* $I(\mathbf{Q},t)$

$$\begin{aligned}S(\mathbf{Q},\omega) &= \frac{1}{2\pi}\int_{-\infty}^{\infty} I(\mathbf{Q},t)\,\mathrm{e}^{-i\omega t}dt\\ S_{inc}(\mathbf{Q},\omega) &= \frac{1}{2\pi}\int_{-\infty}^{\infty} I_{inc}(\mathbf{Q},t)\,\mathrm{e}^{-i\omega t}dt\end{aligned} \tag{2.32}$$

with

$$\begin{aligned}I(\mathbf{Q},t) &= \frac{1}{N}\sum_{i,j}\langle\exp(i\mathbf{Q}\cdot\mathbf{R}_i(t))\exp(-i\mathbf{Q}\cdot\mathbf{R}_j(0))\rangle\\ I_{inc}(\mathbf{Q},t) &= \frac{1}{N}\sum_{i}\langle\exp(i\mathbf{Q}\cdot\mathbf{R}_i(t))\exp(-i\mathbf{Q}\cdot\mathbf{R}_i(0))\rangle\end{aligned} \tag{2.33}$$

We can also obtain the *space-time correlation function* and the *self space-time correlation function*, also called *Van Hove correlation functions* by the Fourier transform in space of (2.33) :

$$\begin{aligned}G(\mathbf{r},t) &= \frac{1}{(2\pi)^3}\int \mathrm{d}\mathbf{Q}\,\mathrm{e}^{-i\mathbf{Q}\cdot\mathbf{r}}I(\mathbf{Q},t)\\ G_s(\mathbf{r},t) &= \frac{1}{(2\pi)^3}\int \mathrm{d}\mathbf{Q}\,\mathrm{e}^{-i\mathbf{Q}\cdot\mathbf{r}}I_{inc}(\mathbf{Q},t)\end{aligned} \tag{2.34}$$

Introducing the definition of intermediate scattering function (1.30) in (1.31) we can write the Van Hove correlation function under the form of a pair-correlation function:

$$G(\mathbf{r},t) = \frac{1}{N}\sum_{i,j}\int\langle\delta(\mathbf{r}-\mathbf{r}'+\mathbf{R}_i(0))\delta(\mathbf{r}'-\mathbf{R}_j(t))\rangle\mathrm{d}\mathbf{r}' \tag{2.35}$$

Now, if we define the microscopic particle density operator

$$\rho(\mathbf{r},t) \;=\; \sum_i \delta(\mathbf{r}-\mathbf{R}_i(t)) \tag{2.36}$$

it follows that (1.32) can be written as:

$$G(\mathbf{r},t) \;=\; \frac{1}{N}\int \langle \rho(\mathbf{r}'-\mathbf{r},0)\rho(\mathbf{r}',t)\rangle \mathrm{d}\mathbf{r} \tag{2.37}$$

with the condition of normalization

$$\int G(\mathbf{r},t)\mathrm{d}\mathbf{r} \;=\; N \tag{2.38}$$

Introducing the Fourier components $\rho_{\mathbf{k}}(t)$ of the particle density

$$\rho(r,t) \;=\; \frac{1}{(2\pi)^3}\int \rho_{\mathbf{k}}(t)\exp(i\mathbf{K}\cdot\mathbf{r})\mathrm{d}\mathbf{K} \tag{2.39}$$

it follows that:

$$I(\mathbf{Q},t) = \frac{1}{N}\langle \rho_{\mathbf{Q}}(0)\rho_{-\mathbf{Q}}(t)\rangle \tag{2.40}$$

The intermediate scattering function, and thus $S(\mathbf{Q},\omega)$, are now expressed in terms of the density-density correlation function: the interaction potential couples the neutron to the density of the target system and $S(\mathbf{Q},\omega)$ is thus determined by spontaneous density fluctuations in the sample, giving information on its structure and its dynamics. Moreover, under the classical approximation ($|\hbar\omega| \ll k_B T$) we can express the space-time correlation functions as:

$$\begin{aligned} G^{cl}(\mathbf{r},t) \;&=\; \frac{1}{N}\sum_{i,j}\langle \delta(\mathbf{r}-\mathbf{R}_j(t)+\mathbf{R}_i(0))\rangle \\ G_s^{cl}(\mathbf{r},t) \;&=\; \frac{1}{N}\sum_{i}\langle \delta(\mathbf{r}-\mathbf{R}_i(t)+\mathbf{R}_i(0))\rangle \end{aligned} \tag{2.41}$$

Thus, $G^{cl}(\mathbf{r},t)\mathrm{d}\mathbf{r}$ and $G_s^{cl}(\mathbf{r},t)\mathrm{d}\mathbf{r}$ represent the probability that, given particle i in the origin at time $t=0$, any particle j, or only the same particle i in the self case, is in the volume $\mathrm{d}\mathbf{r}$ around position $\mathbf{r}$ at time t. There are two special cases of the Van Hove correlation functions that result to be of particular interest. At $t=0$ we have:

$$\begin{aligned} G(\mathbf{r},t=0) \;&=\; \delta(\mathbf{r}) \\ G_s(\mathbf{r},t=0) \;&=\; \delta(\mathbf{r}) + g(\mathbf{r}) \end{aligned} \tag{2.42}$$

where $g(\mathbf{r})$ is the instantaneous pair correlation function accessible through diffraction experiments. By using 2.42 we obtain

$$S(\mathbf{Q}) \;=\; 1+\int_{-\infty}^{\infty} S(\mathbf{Q},\omega)\mathrm{d}\omega \;=\; \int_{-\infty}^{\infty} g(\mathbf{r})\mathrm{e}^{i\mathbf{Q}\mathbf{r}}\mathrm{d}\mathbf{r} \;=\; I(\mathbf{Q},t=0) \tag{2.43}$$

2.1.5 The elastic incoherent structure factor

Another important case related to the correlation functions is how they behave at very long times. Considering an atom diffusing in a space which is very large as compared to the inter-atomic distances, the self-correlation function $G_s(\mathbf{r},t)$ vanishes for $t \to \infty$, whereas if the atom is bound to a finite volume $G_s(\mathbf{r},\infty)$ approaches a finite value with $\mathbf{r}$ varying in the volume. Mathematically, the self-correlation function can be split in two parts: its asymptotic value in the infinite time limit and a time-dependent term $G_s^{'}(\mathbf{r},t)$:

$$S_{inc}(\mathbf{Q},\omega) \;=\; \frac{1}{2\pi}\int_{-\infty}^{+\infty}\int_{-\infty}^{+\infty} \mathrm{e}^{i(\mathbf{Q}\mathbf{r}-\omega t}[G_s(\mathbf{r},\infty)+G_s^{'}(\mathbf{r},t)]\mathrm{d}\mathbf{r}\mathrm{d}t \tag{2.44}$$

that gives

$$S_{inc}(\mathbf{Q},\omega) \;=\; S_{inc}^{el}(\mathbf{Q})\delta(\omega)+S_{inc}^{in}(\mathbf{Q},\omega) \tag{2.45}$$

Thus, the incoherent scattering function has been decomposed into a purely elastic line, $S_{inc}^{el}(\mathbf{Q})\delta(\omega)$, and an inelastic component, $S_{inc}^{in}(\mathbf{Q},\omega)$. The concept of the *elastic incoherent structure factor* (EISF) provides a method that permits to extract geometrical information on localized single-particle motions by the determination of the elastic fraction of the measured spectra intensity. Moreover, selecting the appropriate instrumental energy resolution and under the condition that the motion is sufficiently well separated on the energy-scale from slower motions of the same atom, it is possible to isolate the EISF of a specific component.

2.1.6 Separation of coherent and incoherent scattering by using polarization analysis

In order to simplify our presentation of the double differential cross section, an unpolarized neutron beam has been assumed. However, in many cases it is very important to separate the coherent and the incoherent contributions to the scattered intensity. This is possible by using a polarized neutrons beam. Neutron is characterized by spin 1/2 and its direction could change in the scattering process depending on the nuclear spin: coherent scattering is given by neutrons that do not change their spin direction while scattered. On the contrary neutrons changing the spin direction give an incoherent contribution. The scattering length b depends not only on the isotope type but also on its spin orientation. The dependence of nuclear scattering on neutron spin requires the definition of the scattering length operator $\hat{b}$ with eigenvalues b_+ and b_- corresponding to a parallel or anti-parallel, respectively, orientation of the neutron with the nuclear spin I. Mathematically:

$$\hat{b} \;=\; A + B\hat{\sigma}\hat{I} \tag{2.46}$$

where A and B are scalar values, $\hat{I}$ is the nuclear spin operator and $\hat{\sigma}$ is the neutron spin operator defined by Pauli matrix. Considering the z axis, in the case of a non-spin-flip (NSF), we obtain

$$\langle \pm \mid \hat{b} \mid \pm \rangle \;=\; \langle \pm \mid A + B\hat{\sigma}\hat{I} \mid \pm \rangle \;=\; \langle \pm \mid A + BI_z \mid \pm \rangle \tag{2.47}$$

while for a spin-flip (SF)

$$\langle \pm \mid \hat{b} \mid \mp \rangle \;=\; \langle \pm \mid A + B\hat{\sigma}\hat{I} \mid \mp \rangle \;=\; \langle \pm \mid B(I_x \pm I_y) \mid \mp \rangle \tag{2.48}$$

Table 2.1: Neutron scattering cross sections and scattering lengths for different isotopes

	b_{coh} (fm)	b_{inc} (fm)	σ_{coh} (barn)	σ_{inc} (barn)
H	-3.74	25.27	1.76	80.27
D	6.67	4.04	5.59	2.05
C	6.65	0	5.56	0
O	5.80	0	4.2	0
N	9.37	2	11.03	0.5

Considering a coherent scattering process, which probability is proportional to $|b|^2$, and isotopes with randomly oriented nuclear spin, $\langle I_x \rangle = \langle I_y \rangle = \langle I_z \rangle = 0$, eq. 2.47–2.48 result in:

$$NSF \rightarrow |b| = \langle A + BI_z \rangle = A + B\langle I_z \rangle =, A \tag{2.49}$$

$$SF \rightarrow |b| = \langle B(I_x \pm I_y) \rangle = 0 \tag{2.50}$$

therefore, just neutrons that do not flip when scattered can contribute to the coherent component. On the contrary, the incoherent scattering proportional to $[|b^2| - |b|^2]$, will have both NSF and SF contributions:

$$\begin{aligned} NSF \rightarrow [|b^2| - |b|^2] &= \langle A^2 + B^2 I_z^2 + 2ABI_z - A^2 \rangle \\ &= B^2 \langle I_z^2 \rangle = B^2 \frac{1}{3} I(I+1) \end{aligned} \tag{2.51}$$

$$SF \rightarrow [|b^2| - |b|^2] = \langle B^2(I_x^2 + I_y^2) \rangle = B^2 \frac{2}{3} I(I+1) \tag{2.52}$$

Hence, from calculations, the SF incoherent contribution results to be double than the NSF. Finally, analysing the polarization of the incident and scattered neutron beam, we can directly separate the incoherent and coherent contribution:

$$I_{inc} = \left(\frac{d\sigma}{d\Omega}\right)_{inc}^{NSF} + \left(\frac{d\sigma}{d\Omega}\right)_{inc}^{SF} = \frac{3}{2} I_{SF} \tag{2.53}$$

$$I_{NSF} = \left(\frac{d\sigma}{d\Omega}\right)_{coh}^{NSF} + \left(\frac{d\sigma}{d\Omega}\right)_{inc}^{NSF} = I_{coh} + \frac{1}{2} I_{SF} \tag{2.54}$$

2.1.7 QENS in soft matter

Quasi-elastic neutron scattering is a very suitable tool for the study of the dynamical processes in soft matter due to the neutron properties and to both time and spacial resolution of QENS instruments. In fact, quasi-elastic spectrometers cover time-scales in the range $\approx 10^{-13}$–10^{-9} s and length scales in the range $\approx$ 1-30 Å. That is, they allow us to study directly the typical dynamical processes occurring in soft matter systems, from the fast (i.e. vibrations, rotations and localized motions) to the slow motions (i.e segmental relaxations and diffusion). In a fully protonated sample, the signal is dominated by incoherent scattering from hydrogens (because of

the large value of σ_{inc})(see Table. 2.1). In these systems, we can obtain information on the self-motion of the hydrogen atoms of the sample. The cross-section of D is much smaller than that of hydrogen (see Table. 2.1). Therefore, substituting H by D the incoherent contribution is drastically reduced [68] . Thus, selective deuteration masks the contribution of the deuterated atoms and the signal is dominated by the incoherent scattering of the remaining hydrogens in the sample (Eq. 2.26). In soft matter systems, hydrogens are the most common atoms, therefore this feature has been greatly exploited. In fact, selective deuteration allows two kind of studies. In a partially deuterated sample, the incoherent scattering of the hydrogen atoms dominates in the high Q-range allowing us to study the self-motion of the hydrogens in a deuterated environment. This feature has been widely used in the studies of mixtures –i.e. polymer blends [43, 69, 51] and polymer solutions [42, 41] –. On the other hand, the major contribution to the scattering by H/D labelled sample in the low Q-range is given by the coherent scattering from the contrast between the labelled objects and the matrix. In this framework, it is possible to access the dynamic structure factor of isotopically labelled macromolecules and its static counterpart, that is the chain form factor. Diffraction experiments on these samples provided experimental evidences for the random coil conformation of macromolecules [70, 71] , while dynamic measurements gave fundamental contributions on the Rouse-like chain dynamics [8, 72] . Finally, the intensity scattered by fully deuterated samples is mainly coherent,allowing to investigate the collective dynamics of the system through the dynamic structure factor, where all atomic pairs contributions are equally weighted (Eq. 2.26).

We can find QENS investigations spanning from the simplest molecular liquids to complex biological systems, including liquid crystals, polymers, solutions, and gels (some examples have been already mentioned above). In glass-forming systems, QENS spectrometers have been successfully used to study the structural ($\alpha-$) relaxations in simple polymeric systems, like homopolymers [73, 74], and in more complex scenarios, line polymer blends [75, 76, 51] as well. Moreover, QENS experiments were performed on glassy system studies regarding local dynamical processes, i.e. methyl groups dynamics [77] and secondary relaxations [69, 78]. Remarkable investigations have been carried out on confinement effects on the dynamics in soft matter systems. Such spatial restriction can arise in conditions of high dynamic asymmetry, as in polymer blends and high polymer concentrations, or can be imposed under precisely determined geometries, like in thin films or pores. As mentioned in the Introduction, the case of confined water deserves special mention. Due to the fundamental role that water molecules play in biological systems, the study of its dynamics has raised an enormous interest.

2.1.8 Neutron scattering instruments

Time-of-flight spectrometers

A neutron time-of-flight spectrometer provides information on the neutron energy transfer $\hbar\omega$ by measuring both the time that a neutron needs to reach the sample from a known starting point and the time it needs to reach the detector after the scattering process. The monochromatization of the incoming neutron beam can either be done by Bragg reflection from a crystal or by a sequence of choppers which are phased in order to transmit a single wavelength only. The former principle

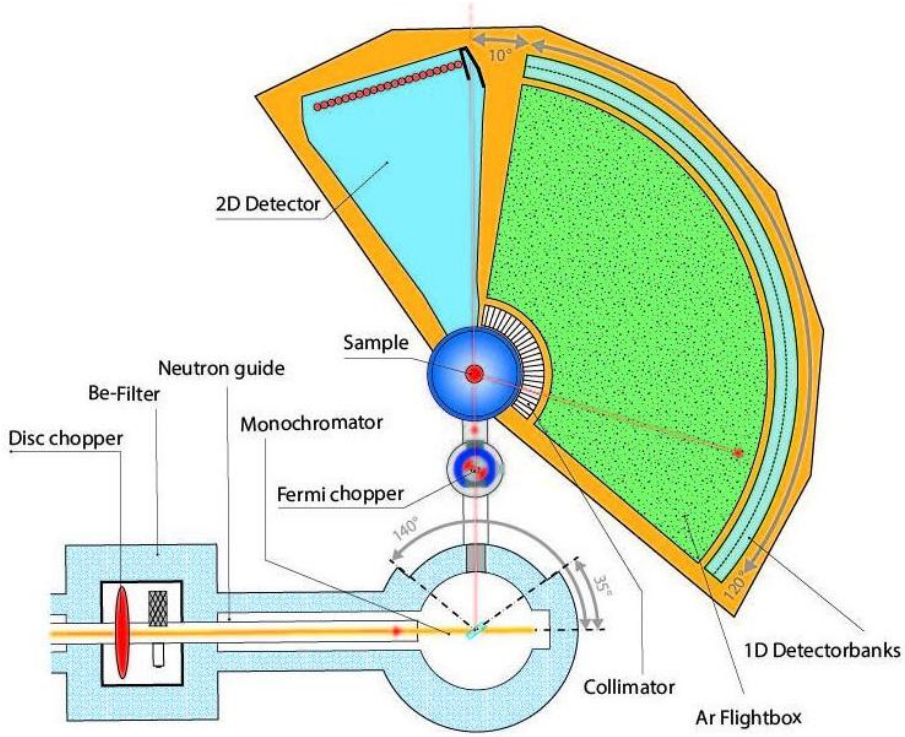

Figure 2.2: Geometry of the ToF spectrometer FOCUS,PSI,Villigen.

usually yields higher intensities while the latter is more flexible for the selection of the incident energy. Hence, a further chopper defines the start time of the neutrons. The electronic pulse from their registration in the detector gives the end of their flight through the spectrometer. From the time difference we obtain the velocity of the neutrons and so the energy transfer (2.55)

$$\hbar\omega = \left(\frac{l_1^2}{(l_0 - \sqrt{E/m_n}t_{flight})^2} - 1\right)E \tag{2.55}$$

with m_n the neutron mass, l_0 is the distance between the sample and the detector, l_1 is the distance between the chopper and the sample, t_{flight} is the time it takes a neutron to arrive to the detector and E is the incident energy. Depending on the desired incident wavelength, the instruments are constructed either using thermal neutrons (directly from the reactor moderator, $\lambda_{max} \approx 1.8$Å) or cold neutrons ($\lambda_{max} \approx 4$Å). Thermal neutrons make a larger Q range accessible while cold neutrons yield better energy resolution. A variant of the ToF spectrometer exists on spallation sources, the inverse time-of-flight spectrometer. The neutrons produced from spallation are pulsed, the start of the ToF clock is given directly by the creation time of the pulse and so, in principle, there is no need for a chopper. In this way all neutrons can be used in contrast to conventional ToF spectrometers which use only a few percent. In this work different time-of-flight spectrometers (FOCUS, TOFTOF, IRIS) were used to increase the accessible time-window range. FOCUS (Fig. 2.2 is a time and space focusing time of flight spectrometer for cold neutrons located at the end of the curved guide RNR 11 at the Paul Scherrer Institut (PSI)(Villigen, Switzerland). The white beam is reduced and then chopped by a pre-selector disc chopper. For incident wavelengths larger than 4 Å a Be-filter is used together with the first chopper to suppress higher order contamination. The distances neutron guide -

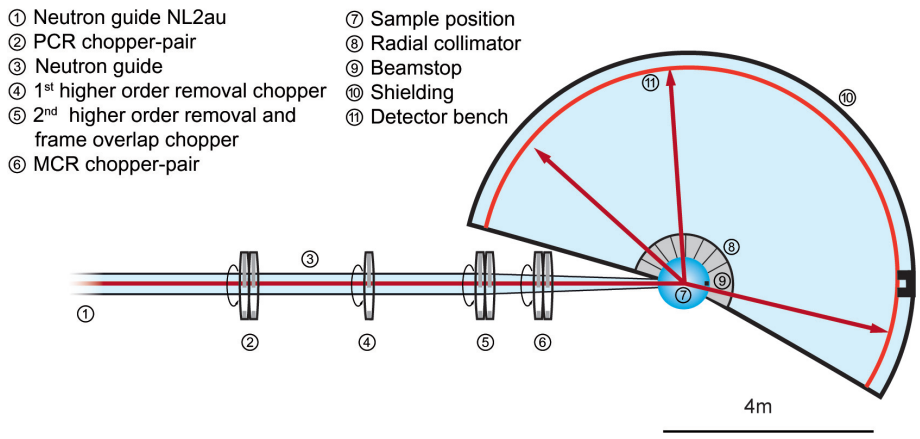

Figure 2.3: Geometry of the ToF spectrometer TOFTOF,MLZ,Garching.

monochromator and monochromator-sample are both variable such that the spectrometer can be operated either in time focusing or monochromatic focusing mode, hence being suited for quasi-elastic or inelastic scattering, respectively. TOFTOF (Fig. 2.3) is a direct geometry multi-chopper time-of-flight spectrometer operated with cold incident neutrons located at the Heinz Maier-Leibnitz Zentrum (MLZ) in Garching, Germany. Changing the chopper rotational frequency and adjusting the incident wavelength the resolution can be adapted to the needs of the experiment between 2 μeV and 3 meV. IRIS, situated at ISIS (Didcot, UK), is a time-of-flight inverted-geometry crystal analyser spectrometer (Fig. 2.4) designed for high resolution inelastic spectroscopy. Neutrons scattered from the sample are energy-analysed by means of Bragg reflection from one of two large single crystal arrays (pyrolytic graphite and muscovite mica) in close to backscattering geometry. The two analyser banks, which can operate simultaneously, afford high resolution over wide energy and momentum transfer ranges (see below, backscattering conditions). Moreover, in order to obtain data with large energy transfers, TOSCA spectrometer (ISIS, Didctot, UK) was used. TOSCA is a high resolution inverted-geometry inelastic spectrometer optimised for the study of molecular vibrations. It spans an energy-transfer range up to 500 meV. Scattered neutrons are Bragg reflected from a pyrolytic graphite analyzer and higher-order reflections beyond (002) are suppressed by a cooled Be filter defining a unique final energy of ∼4 meV. The incident neutron energy is determined from the measured total time of flight, t, through the following kinematic relation:

$$t = \frac{L_0}{v_0} + \frac{L_1}{v_1} \tag{2.56}$$

where L_0, L_1, v_0, v_1 are incident (0) and scattered (1) flight-path length and neutron velocities, respectively. The detector array is comprised of a total of ten banks each having thirteen 30 X 1 cm^2 ^3He tubes.

Backscattering spectrometers

Some relevant motions in soft matter are usually very slow and therefore difficult or impossible to be resolved by ToF, requiring pushing instrumental capabilities as much as possible to improve resolution. In a ToF experiment the energy resolution is limited by the selectivity of the monochromator crystal or the pulse lengths given

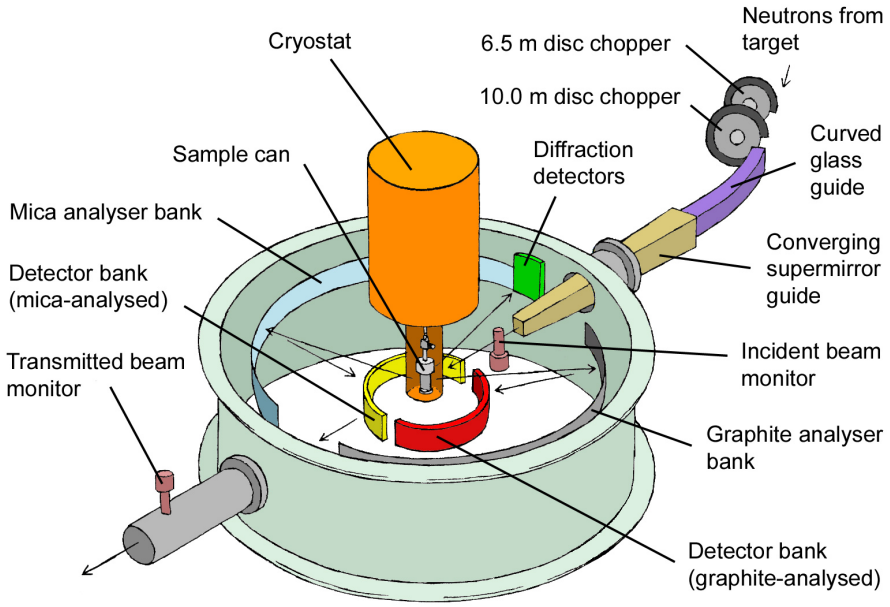

Figure 2.4: Geometry of the ToF spectrometer IRIS, ISIS, Oxford.

by the choppers that can be very small but at the expense of the intensity. If perfect crystals are used, the spread of the selected wavelength $\Delta\lambda/\lambda$ is determined by the angular divergence $\Delta\alpha$ of the reflected neutrons. Differentiating the Bragg conditions $\lambda = 2\sin\theta/d$ one obtains:

$$\Delta\lambda/\lambda \;=\; \cot\theta \cdot \Delta\theta \tag{2.57}$$

This expression becomes zero for $2\theta = 180°$ that means that the wavelength spread becomes minimal if the neutron beam is reflected by 180°. This is the principle of backscattering instruments that allows improving resolution in a very efficient way. Figure 2.5 shows schematically the instrument based on this principle. The first crystal in the beam is only a deflector with low wavelength selectivity. The actual monochromatization takes place upon the second reflection by the crystal in backscattering position. The monochromatized neutrons are then scattered by the sample which is surrounded by analyser crystals placed on the spherical surface. There they are scattered again under backscattering conditions. The reflected neutrons pass once more through the sample and finally reach the detector. This experimental setup yields two technical problems: *i*) the deflector must not accept all neutrons otherwise the monochromatized beam would be scattered back into the source, *ii*) the second passage of the neutrons through the sample causes additional multiple scattering. To investigate our system SPHERES (MLZ, Garching) has been used (Fig. 2.6). It is a third generation backscattering instrument with focussing optics and phase-space-transform chopper.

Diffraction with polarization analysis: DNS

DNS is a diffuse scattering cold neutron time-of-flight spectrometer with both longitudinal and vector polarization analysis. This allows the unambiguous separation

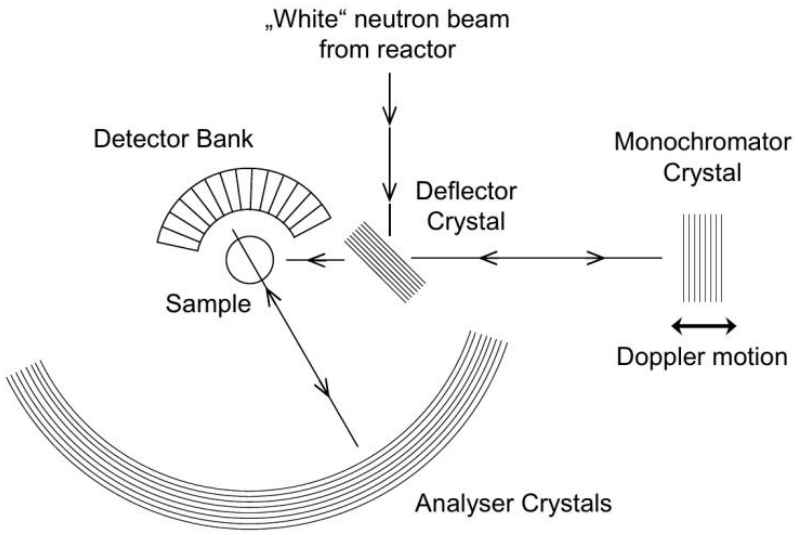

Figure 2.5: Schematic setup of a backscattering spectrometer

of nuclear coherent, spin incoherent and magnetic scattering contributions simultaneously over a large range of scattering vector Q and energy transfer E. It is equipped with a horizontally and vertically focusing monochromator, and a wide angular range around the sample is covered with detectors. A layout of the instrument is shown in Fig. 2.7. The monochromatic incident beam is polarized with a focusing supermirror bender, xyz-field coils allow for a change of the polarization at the sample, and the polarization analysis is performed with supermirror analysers in focusing arrangement in front of each detector.

2.2 Dielectric Spectroscopy

Dielectric spectroscopy is a suitable tool to study the dynamics of polymeric systems and soft materials in general. It involves the interactions of electromagnetic waves with matter in a frequency range comprised between 10^{-6} and 10^{12} Hz where molecular and collective dipolar fluctuations, charge transport, polarization effects occur [79] .

2.2.1 Dielectric Permittivity

Consider a pair of parallel plates of indefinite extent carrying equal but opposite charges of density $\sigma = q/A$. The Gauss law integration over a cylinder whose faces of area, A, enclose one of the plates gives:

$$DA = q \tag{2.58}$$

with D the *displacement field* and q the charge inside the area. In vacuum the displacement and the electric field are related by the dielectric permittivity of vacuum ϵ_0

$$\vec{D} = \epsilon_0 \vec{E} \tag{2.59}$$

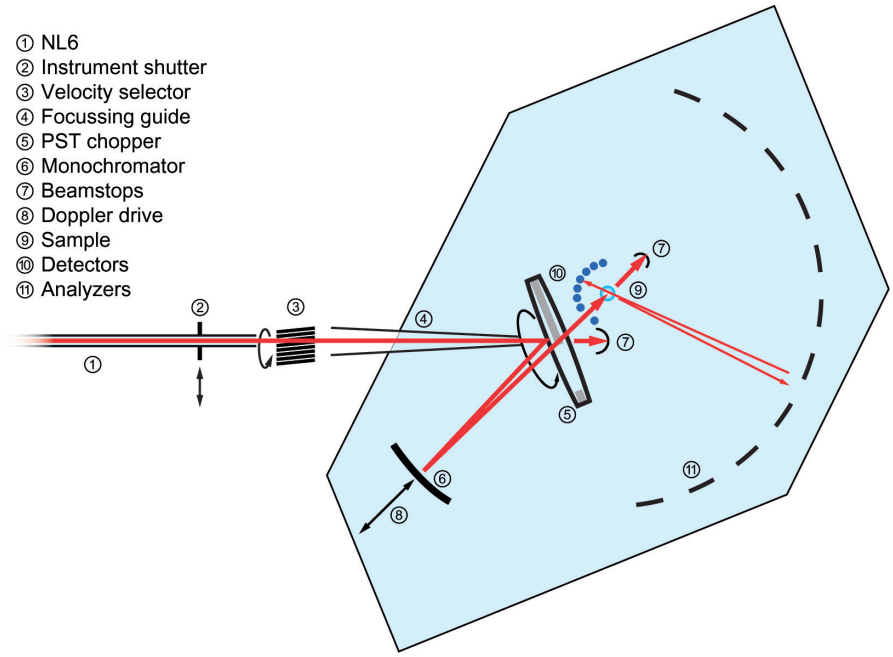

Figure 2.6: Geometry of the BS spectrometer SPHERES, MLZ, Garching.

Thus by (2.58) and (2.59) we obtain:

$$\begin{aligned} D &= \sigma \\ \epsilon_0 E &= \sigma \end{aligned} \tag{2.60}$$

Adding a dielectric material between the charged plates, the electric field will act on it polarizing the constituent matter. In the unpolarized state the centers of the negative charge clouds and positive nuclei coincide, while, in the presence of the field, they will be displaced yielding an excess charge of opposite sign on the plates.

This latter charge is denoted as σ' and the electric field becomes

$$\epsilon_0 E = \sigma - \sigma' \tag{2.61}$$

The induced surface charge density σ' is due to the molecular polarization $\vec{P}$. In a given point:

$$\vec{P} = \frac{1}{v} \sum \vec{\mu_i} \tag{2.62}$$

where v is the volume and $\vec{\mu_i}$ is the permanent dipole moment. Thus, in general:

$$\vec{D} = \epsilon_0 \vec{E} + \vec{P} \tag{2.63}$$

In homogeneous and isotropic materials the polarization is proportional to the applied electric field

$$\begin{aligned} P &= \chi \epsilon_0 E \\ D &= (1 + \chi) \epsilon_0 E \end{aligned} \tag{2.64}$$

where χ is called *susceptibility*. Finally we can define the *relative dielectric permittivity* as

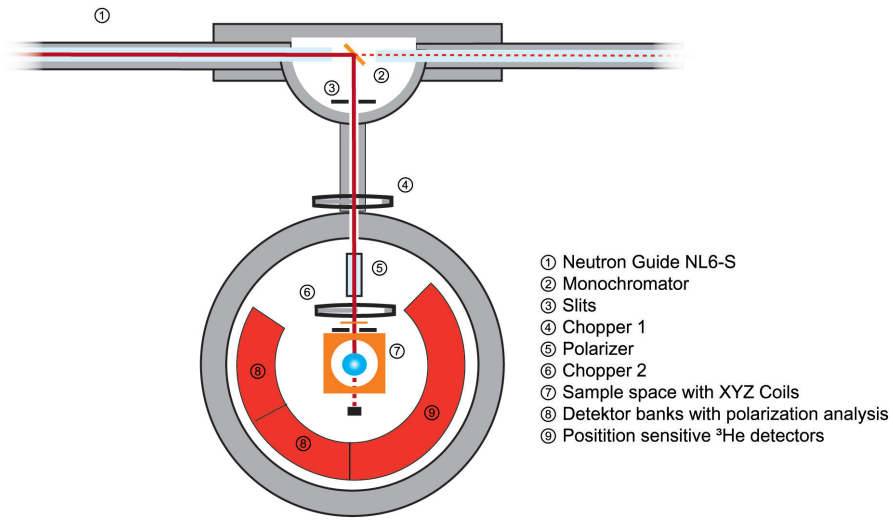

Figure 2.7: Geometry of the DNS spectrometer,JCNS,Garching.

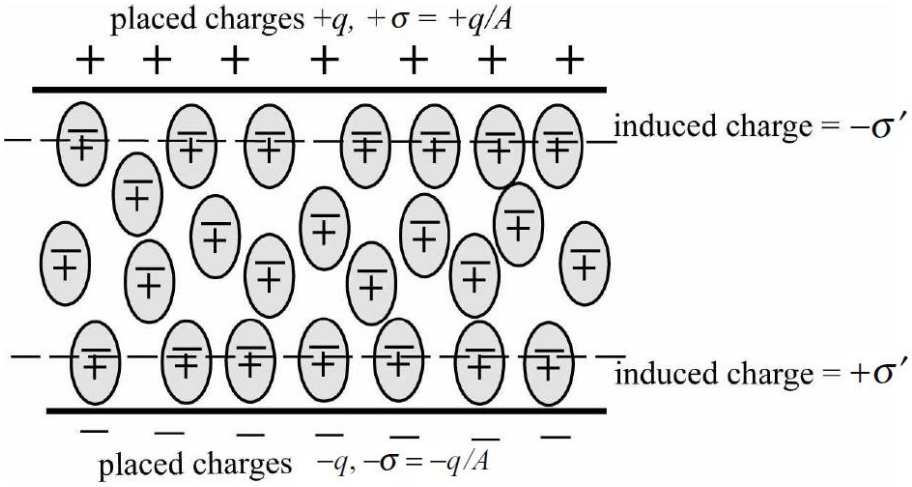

Figure 2.8: A collection of polarized atoms leads to an induced charge σ' collected on the plates

$$\begin{aligned} \epsilon &= 1 + \chi \\ D &= \epsilon\epsilon_0 E \end{aligned} \tag{2.65}$$

In general, a material cannot polarize instantaneously in response to an applied field (Fig. 2.9) making ϵ time (frequency) dependent. In polymeric systems the rotational fluctuations of molecular dipoles are very relevant. These fluctuations are related to characteristics parts of a molecule or to the whole chain. Hence, the investigation of such relaxation processes analysing the dielectric function gives us information about the molecular dynamics of the system. The electric field causes only a minor perturbation on the distribution of dipolar orientations, that means that the response is given by the same molecular motions that are taking place even in absence of the field. If the molecular motion is slow, the dipolar reorientation in the field will be slow, whereas rapid molecular motions lead to rapid dipolar reorientation.

2.2.2 Dielectric relaxation theory

Consider an outer disturbance $x(t)$ acting on a system and causing the response $y(t)$ and assume linearity and causality, therefore the response $y(t)$ can be described by the linear equation

$$y(t) \;=\; y_\infty + \int_{-\infty}^{t} \tilde{J}(t-t')\frac{\mathrm{d}x(t')}{\mathrm{d}t'}\mathrm{d}t' \tag{2.66}$$

$\tilde{J}(t)$ is the so-called memory function which can be consider as the time dependent response to a step-like disturbance. If we have a periodic disturbance $x(t) = x_0\exp(-i\omega t)$, in the stationary case one finds:

$$J^*(\omega) \;=\; J^{'}(\omega) - iJ^{''}(\omega) \;=\; J_\infty - \int_0^\infty \frac{\mathrm{d}\tilde{J}(\tau)}{\mathrm{d}\tau}\exp(-i\omega t)\mathrm{d}\tau \tag{2.67}$$

with $J^*(\omega)$ is the generalized complex susceptibility. Again partial integration leads to

$$J^*(\omega) \;=\; J^{'}(\omega) - iJ^{''}(\omega) \;=\; J_s - i\omega\int_0^\infty \tilde{J}(\tau)\exp(-i\omega t)\mathrm{d}\tau \tag{2.68}$$

The dielectric relaxation theory for a small electric field is a special case of linear response. Consider an isotropic system, the response $y(t)$ of a system following a disturbance $x(t)$ can be described by a linear equation. In dielectric spectroscopy the disturbance is the time dependent external electric field $x(t) = E(t)$ and the response is the polarization $y(t) = P(t)$. Therefore, in agreement with linear response theory:

$$P(t) \;=\; P_\infty + \epsilon_0\int_{-\infty}^{t}[\epsilon(t-t')-1]\frac{\mathrm{d}E(t')}{\mathrm{d}t'}\mathrm{d}t' \tag{2.69}$$

where $\epsilon(t)$ is the time dependent dielectric function and P_∞ covers all the fast contributions coming from induced polarization. Applying a periodic disturbance $E_\omega(t) = E_0\exp(-i\omega t)$, equation (2.69) becomes:

$$P_\omega(t) \;=\; \epsilon_0(\epsilon^*(\omega)-1)E_\omega(t) \tag{2.70}$$

with

$$\epsilon^*(\omega) \;=\; \epsilon^{'}(\omega) - i\epsilon^{''}(\omega) \tag{2.71}$$

where $\epsilon^*(\omega)$ is the complex dielectric function. The real part is proportional to the energy stored reversibly in the system while the imaginary part is proportional to the energy loss. The ratio between the energy loss and the energy stored is the loss tangent ($\tan(\delta) = \epsilon^{``}/\epsilon^{`}$). The complex dielectric function and the time dependent dielectric function $\epsilon(t)$ are connected by:

$$\epsilon^*(\omega) \;=\; \epsilon^{'}(\omega) - i\epsilon^{''}(\omega) = \epsilon_\infty - \int_0^\infty \frac{\mathrm{d}\epsilon(t)}{\mathrm{d}t}\exp(-i\omega t)\mathrm{d}t \tag{2.72}$$

The dependence on angular frequency of the complex dielectric function is due to the different processes: (i) microscopic fluctuations of molecular dipoles, (ii) the propagation of mobile charge carriers, (iii) the separations of charges at interfaces giving rise to an additional polarization.

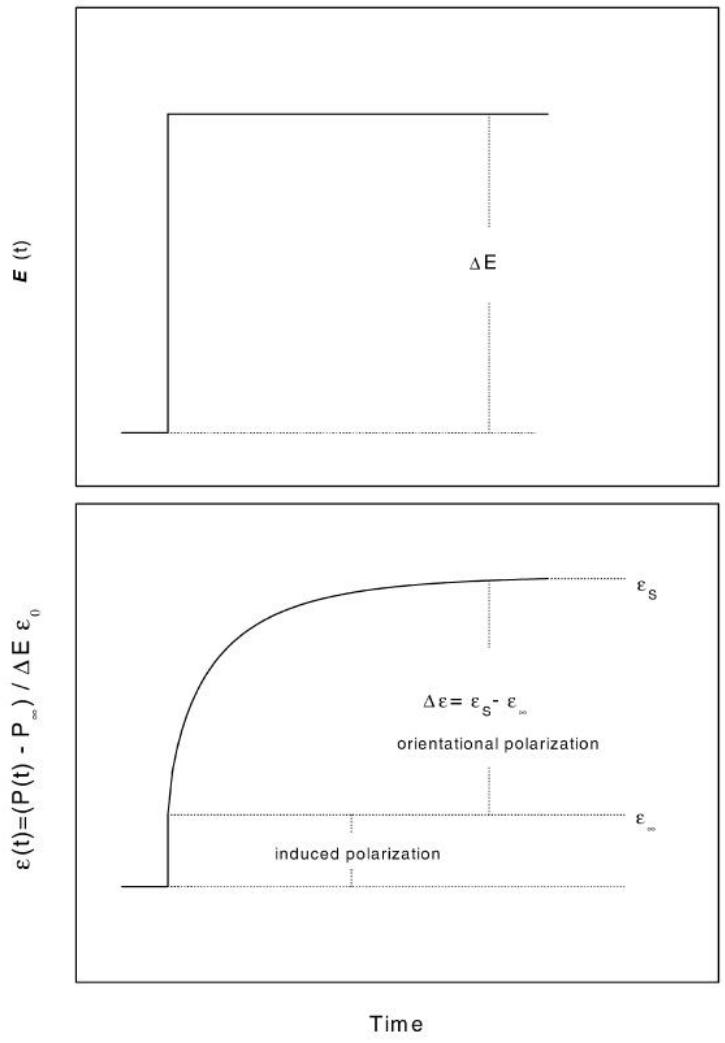

Figure 2.9: Schematic relationships between the time dependence of the electric field ΔE, the polarization P and the time dependent relaxation function $\epsilon(t)$ [80]

2.2.3 Dielectric spectroscopy instruments

The dielectric experiments were performed at the Materials Physics Center - Centro de Fsica de Materiales (CFM) in San Sebastián. The complex dielectric ϵ^* has been measured using the broadband dielectric spectrometers *Novocontrol Alpha* for the frequency range investigation between 10^{-2} to 10^6 Hz, while the high frequency measurements (10^6-10^9) have been performed using an Agilent rf impedance analyzer 4192B.

Fourier correlation analysis

The complex dielectric function, defined as Eq. 2.71, can be derived at low and intermediate frequencies (10^{-3}–10^7 Hz) by measuring the complex impedance $Z^*(\omega)$ of a parallel plate capacitor. In fact, for a capacitor C^* filled with a material under study the complex dielectric function is defined as:

$$\epsilon^*(\omega) \; = \; \epsilon^{'}(\omega) - i\epsilon^{''}(\omega) = \frac{C^*}{C_0} \tag{2.73}$$

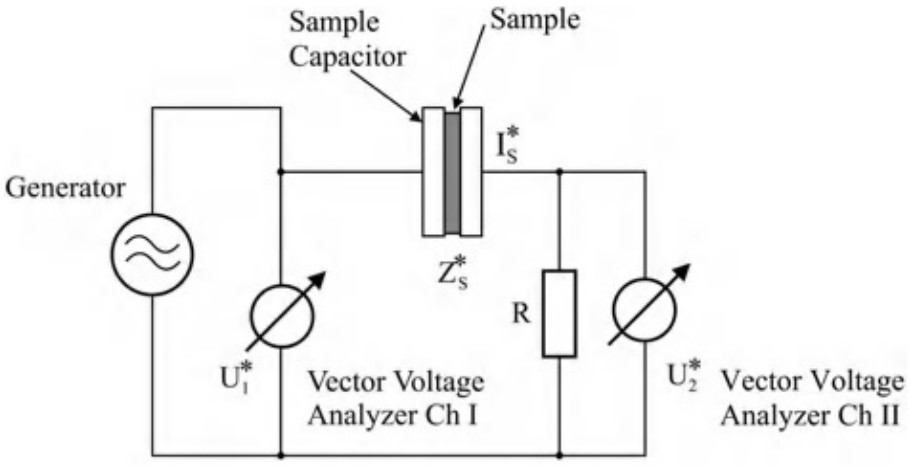

Figure 2.10: Scheme of a Fourier correlation analyser [80]

where C_0 is the vacuum capacitance of the arrangement. Considering that the complex capacitance is related to the complex impedance as:

$$C^*(\omega) = \frac{1}{i\omega Z^*(\omega)} \tag{2.74}$$

using Eq. 2.74 in Eq. 2.73 we obtain:

$$\epsilon^*(\omega) = \frac{1}{i\omega Z^*(\omega) C_0} \tag{2.75}$$

A convenient way to determine the complex impedance Z^* is using a circuit as that illustrated in Fig. 2.10 plus a correlation analysis of the measured voltages. A sine wave voltage $U_1^*(\omega)$ is applied to the sample capacitor and the sample current $I_s^*(\omega)$ is measured by convert it into a voltage with a resistor $U_2^*(\omega) = I_s^*(\omega)R$. The complex sample impedance $Z_s^*(\omega)$ is simply calculated from the measured data by:

$$Z_s^*(\omega) = \frac{U_s^*(\omega)}{I_s^*(\omega)} = R\left(\frac{U_1^*(\omega)}{U_2^*(\omega)} - 1\right) \tag{2.76}$$

where $U_s^*(\omega)$ is the sample voltage.

However, this set-up with the resistor R suffers from several limitations. At low frequencies the high impedance limits sensitivity because of the extremely low current to be detected. Furthermore, at high frequencies the measured current can be significantly influenced by small inductances (cables) and contact quality when the sample impedance is small. Therefore, a combination of the Fourier correlation analysis and dielectric converter is normally used to overcome these problems. The converter consists in an electrometer of variable gain to match the huge impedance range required for dielectric relaxation spectroscopy. In addition, in order to improve the measurement sensitivity, the combined measurement under the very same conditions for the sample of a reference capacitor $Z_R^*(\omega)$ can be performed. By doing so, the measured impedance for the sample results independent of the varying circuit elements. In summary, the combination of Fourier correlation analysis with dielectric converter and reference capacitor measurement allow performing dielectric experiments over a broad frequency range with a high accuracy.

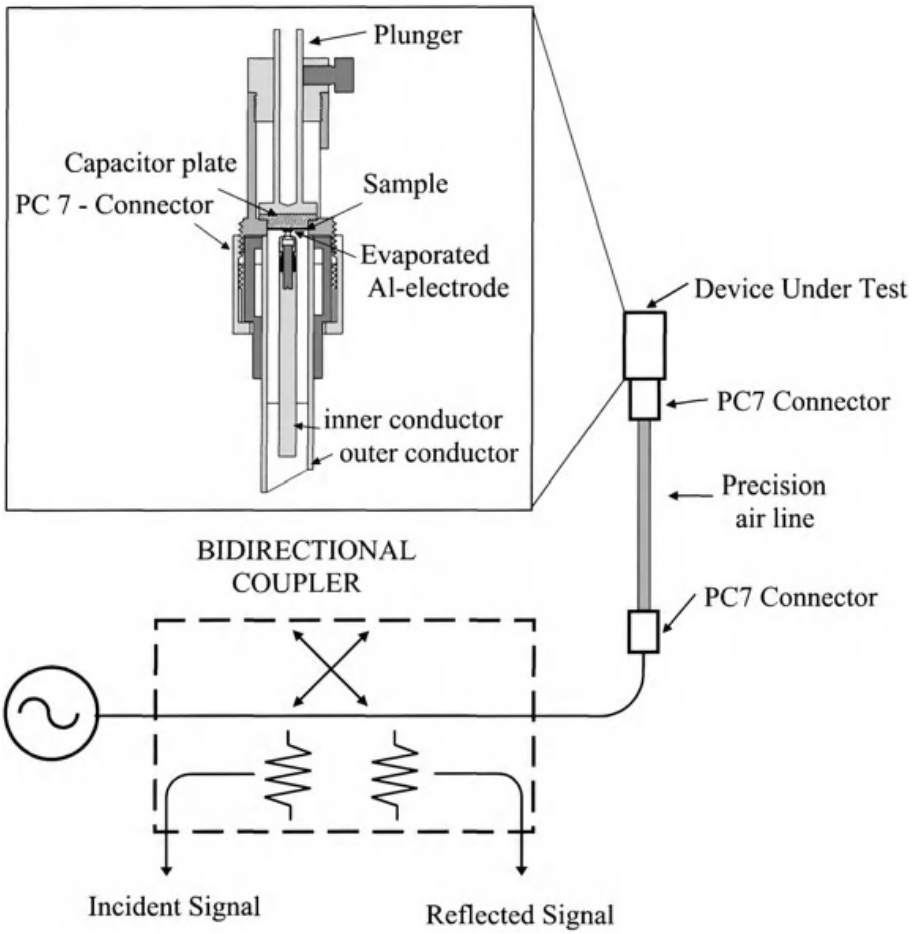

Figure 2.11: Scheme of the coaxial line reflectometer with sample head [80]

RF Reflectometry

In the frequency range 10^6-10^9 Hz the measurements of the sample impedance start to be significantly affected by the circuit elements. This results in the presence of standing waves which contribution cannot be neglected. This can be avoided by means of microwave techniques taking into account the measurement line as the main part of the measured impedance. In Fig. 2.11 the scheme the measurement technique used to investigate the sample at high frequencies is shown. The sample capacitor is used as the termination of a precision coaxial line. The complex reflection factor r^* of the line (length l) depending on the sample impedance is measured with a microwave reflectometer. The incoming and reflected waves are separated with two directional couplers and are measured in amplitude and phase. The complex reflection coefficient r^* is defined as the ratio of the complex amplitudes of these two waves at the point of reference.

$$r^*(x) = \frac{U^*_{refl}(x)}{U^*_{inc}(x)} \tag{2.77}$$

The resulting spatial dependency for the complex amplitude of the total voltage $U^*(x)$ and the total current $I^*(x)$ are respectively:

$$U^*(x) = U^*_{inc}(x)(e^{-i\beta x} + r^*(x)e^{i\beta x}) \tag{2.78}$$

$$I^*(x) = \frac{U^*_{inc}(x)}{Z_0} + \frac{U^*_{refl}(x)}{-Z_0} = \frac{U^*_{inc}(x)}{Z_0}(e^{-i\beta x} + r^*(x)e^{i\beta x}) \tag{2.79}$$

where Z_0 is the characteristic impedance of the transmission line. From Eq. 2.78–2.79 we obtain that at $x = 0$:

$$Z^*_s(\omega) = \frac{U^*(\omega)}{I^*(\omega)} = \frac{1 + r^*}{1 - r^*} Z_0 \tag{2.80}$$

This equation shows that this method is suitable as far as the sample impedance is of the same order than the line impedance Z_0, thus limiting the frequency range for a given set-up. Moreover, in order to perform experiments in this frequency range, the characteristic propagation of the system has to be carefully controlled. The actual experiment usually involves a calibration procedure, where well known impedances have to be used. The analysis of these signal measured over the complete frequency range allows modelling the characteristic line propagation.

2.3 Complementary experimental techniques

2.3.1 X-ray diffraction

Wide angle X-Ray scattering

Wide Angle X-Ray Scattering (WAXS) measurements to decipher the short-range order were performed on a Bruker D8 Advance diffractometer working in parallel beam geometry. By using a Gobel mirror, the originally divergent incident X-ray beam from a line focus X-ray tube (Cu, operating at 40 kV and 40 mA) is transformed into an intense and parallel beam that is free of Kβ radiation. The parallel beam optic required in the secondary beam path is achieved by an equatorial axial Soller slit of 0.2°. The linear detector LYNXEYE used presents an active area of 14.4 mm x 16 mm.

Small angle X-Ray scattering

Small Angle X-Ray Scattering (SAXS) was used to probe the large-scale structure. Experiments were conducted on a Rigaku 3-pinhole PSAXS-L equipment operating at 45 kV and 0.88 mA. The MicroMax-002+ XRay Generator System is composed by a microfocus sealed tube source module and an integrated X-Ray generator unit which produces CuK transition photons of wavelength =1.54 Å. The flight path and the sample chamber in this equipment are under vacuum. The scattered X-Rays are detected on a two-dimensional multiwire X-Ray Detector (Gabriel design, 2D-200X). This gas-filled proportional type detector offers a 200 mm diameter active area with c.a. 200 micron resolution. The azimuthally averaged scattered intensities were obtained as a function of wavevector q, $q = 4\pi\lambda^{-1}sin(\theta)$. Reciprocal space calibration was done using silver behenate as standard.

2.3.2 Differential scanning calorimetry

Differential scanning calorimetry (DSC) is a technique of thermal analysis widely used in the investigation of polymer materials. The heat flow rate difference into

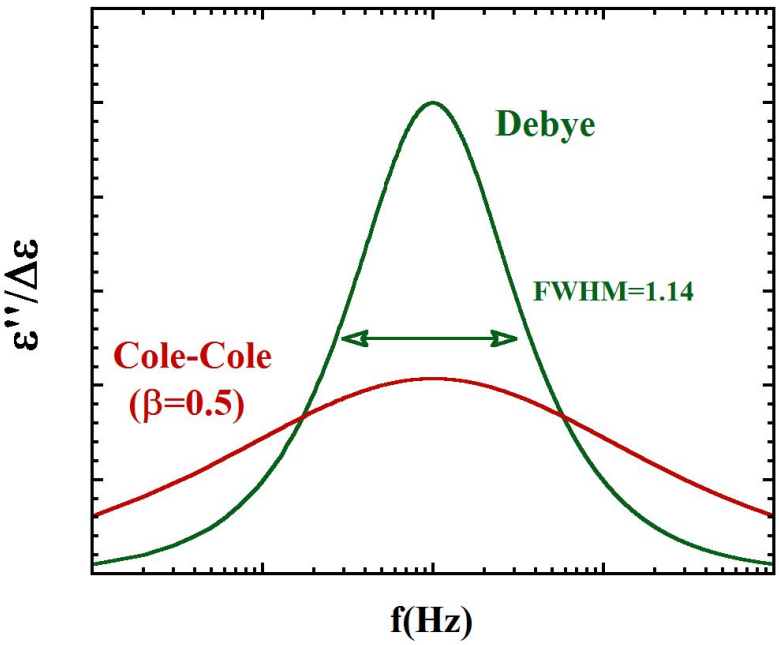

Figure 2.12: Comparison between Debye function (Eq 2.81) and Cole-Cole function (Eq 2.82) with $\beta = 0.5$.

a substance and a reference is measured as a function of temperature while the substance and reference are subjected to a controlled temperature program. Among the applications of DSC, the easy and fast determination of the glass transition temperature, the heat capacity jump at the glass transition and the melting and crystallization temperatures are the most relevant in this work. A special type of DSC is the *modulated differential scanning calorimetry* in which a temperature modulation is overlaid on a linear heating or cooling rate. This technique has a number of advantages, above all the simultaneous measurement of heat effects that are reversible and not reversible at the timescale of the oscillation.

2.4 Models and Interpretation

2.4.1 DS: relaxation processes data analysis

In dielectric spectroscopy, relaxation processes are characterized by a peak in the imaginary part $\epsilon^{''}$ and a step-like decrease of the real part $\epsilon^{'}(\omega)$ of the complex dielectric function $\epsilon^* = \epsilon^{'}(\omega) - i\epsilon^{''}(\omega)$ with increasing frequency. The frequency of maximal loss ν_p is related to a characteristic relaxation rate $\omega_p = 2\pi\nu_p$ or relaxation time $\tau_p = 1/\omega_p$ of the fluctuating dipoles. From the shape of the loss peak the distribution of relaxation times can be deduced by using model functions. The easiest model is the *Debye* function:

$$\epsilon^*(\omega) = \epsilon_\infty + \frac{\Delta\epsilon}{1 + i\omega\tau_D} \tag{2.81}$$

where $\Delta\epsilon = \epsilon_s - \epsilon_\infty$ is the dielectric relaxation strength with $\epsilon_s = \lim_{\omega\tau \ll 1} \epsilon^{'}(\omega)$ and $\epsilon_s = \lim_{\omega\tau \gg 1} \epsilon^{'}(\omega)$. The Debye relaxation time τ_D is related to the position of

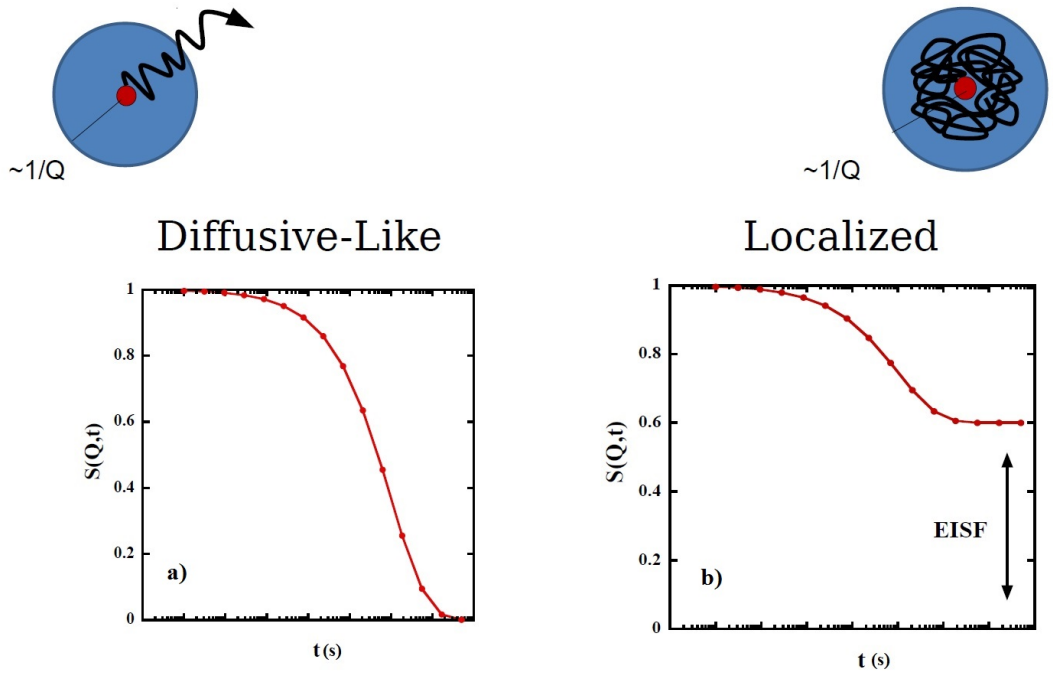

Figure 2.13: Representive intermediate scattering functions for a diffusive-like process (a) and for a localized process (b).

maximal loss by $\omega_p = 2\pi\nu_p = 1/\tau_D$. The loss peak is symmetric with a half width ω_D of 1.14 decades. Commonly the half width is much broader than the predicted by (2.81) and the shape can be also asymmetric. A symmetric broadening of the dielectric function can be described by the *Cole-Cole* function:

$$\epsilon^*_{CC}(\omega) = \epsilon_\infty + \frac{\Delta\epsilon}{(1+i\omega\tau_{CC})^\beta} \tag{2.82}$$

where $0 < \beta \leq 1$ characterizes the broadening. Notice that for $\beta = 1$ the Debye function is obtained. The Cole-Cole relaxation time τ_{CC} gives the position of maximal loss by $\omega_p = 2\pi\nu_p = 1/\tau_{CC}$. A comparison between the Debye function and the Col-Cole function is shown in Fig. 2.12.

An asymmetric broadening of the spectra can be described by means of the *Havriliak-Negami* function:

$$\epsilon^*_{HN}(\omega) = \epsilon_\infty + \frac{\Delta\epsilon}{(1+(i\omega\tau_{HN})^\beta)^\alpha} \tag{2.83}$$

where $0 < \alpha \leq 1$ and $0 < \beta \leq 1$ are the shape parameters that describe the symmetric and the asymmetric broadening of the complex dielectric function. The position of maximal loss depends on the parameters β and γ according to

$$\omega_p = \frac{1}{\tau_{HN}}\left[\sin\frac{\beta\pi}{2+2\alpha}\right]^{1/\beta}\left[\sin\frac{\beta\alpha\pi}{2+2\alpha}\right]^{1/\beta} \tag{2.84}$$

2.4.2 QENS: localized motions data analysis

In order to intuitively classify the motions involved in a glass-forming system, we can define a virtual sphere in the real space with radius $\sim 1/\mathbf{Q}$, being $\mathbf{Q}$ the wave-

vector explored in the experiment, containing the scattering center. If at a given time the scattering center escapes from the virtual sphere, the motion is diffusive-like, otherwise a localized process is occurring . First, we assume the simplest localized motion, that is the jump between two equivalent positions (1 and 2). In this scenario, at $t = 0$ the scattering center is in its initial position 1(2) and after a time t it can remain in the same position or jump to position 2(1). We define the probabilities of jump or not jump at time t respectively as

$$p_+(t) = \frac{1}{2}[1 + \mathrm{e}^{-\Gamma t}] \tag{2.85}$$

$$p_-(t) = \frac{1}{2}[1 - \mathrm{e}^{-\Gamma t}] \tag{2.86}$$

where Γ is the frequency with which the scattering center returns to its initial position. Reminding that the intermediate scattering function can be expressed by:

$$S(\mathbf{Q}, t) = \left\langle \mathrm{e}^{i\mathbf{Q}[\mathbf{r}(t)-\mathbf{r}(0)]} \right\rangle \tag{2.87}$$

and using eq.2.85 and 2.86, we obtain:

$$S(\mathbf{Q}, t) = 2p_+ + 2p_-\mathrm{e}^{i\mathbf{Qd}} = A(\mathbf{Q}) + [1 - A(\mathbf{Q})]\mathrm{e}^{-\Gamma t} \tag{2.88}$$

with $\mathbf{d}$ the distance between the jumps and $A(\mathbf{Q}) = 1/2[1 + \mathrm{e}^{i\mathbf{Qd}}]$. In Fig. 2.13(b), a qualitative example of the intermediate scattering function is shown. At $t = 0$, the intermediate scattering function $S(\mathbf{Q}, t) = 1$ that is the probability of finding the scattering center in its initial position is 1. For higher values of t, approaching the characteristic time of the jump $1/\Gamma$, $S(\mathbf{Q}, t)$ decays reaching the constant value $A(\mathbf{Q})$ at $t \gg 1/\Gamma$. In sec.2.1.5, it has been shown that for $t \to \infty$, the intermediate scattering function assumes a constant value $\neq 0$ when the motion is confined in a volume. Therefore, we can associate the value $A(\mathbf{Q})$ at which the $S(\mathbf{Q}, t)$ decays for a localized motions with the EISF defined in sec.2.1.5. It is possible to generalize the localized motions assuming different numbers of jump positions and different geometries. Independently from the definition of the EISF, the general intermediate scattering function for a localized motion is defined by:

$$S(\mathbf{Q}, t) = EISF(Q) + [1 - EISF(Q)]\phi(t) \tag{2.89}$$

where $\phi(t)$ contains the time-dependence of the process. We can note that the geometry of the local motions not only affects the elastic intensity by the EISF factor, but also the quasi-elastic intensity by the factor (1-EISF).

2.4.3 Inelastic neutron scattering: methyl group dynamics data analysis

The modelization of the methyl group dynamics is important in this thesis because the polymer investigated contains three meethyl groups in its monomer. In polymeric materials, at temperatures well below the glass transition region, we can well approximate that the main chain dynamics is completely frozen while small side units, as methyl groups, can still move. Under this condition, the interaction between the methyl group and its environment can be described by an effective

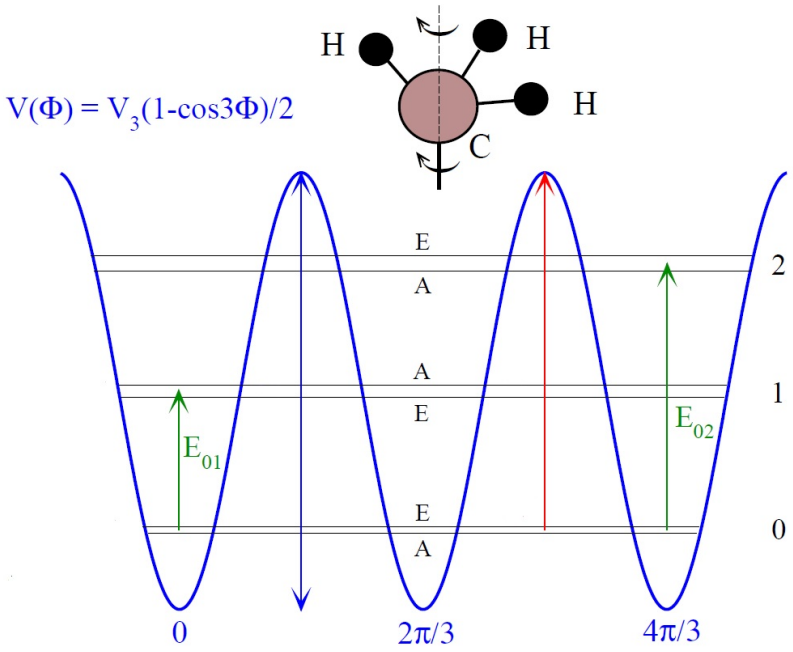

Figure 2.14: Picture of methyl group rotation about its C_3-axis, and level scheme for a purely threefold potential with barrier height V_3.

mean-field rotational potential [77, 81]. The strength of the C-H covalent bond allows to neglect the internal degrees of freedom in comparison with both translational and rotational motions of the group as whole. Therefore, the methyl group can be regarded as a rigid rotor. As a consequence, the mean-field potential only depends on the characteristic angular coordinate ϕ, which is measured in the plane perpendicular to the C_3-symmetry axis.

In order to explain the protocol used in this work, first I will focus the attention on the case of methyl group dynamics in molecular crystals. At very low temperature ($T \sim 1\ K$), methyl group motions can be described by threefold rotational potential:

$$V(\phi) = \frac{V_3}{2}(1 - \cos(3\phi)) \tag{2.90}$$

where V_3 correspond to the maximum and the amplitude of the potential $V(\phi)$. The corresponding Hamiltonian is given by:

$$H_R = -B\frac{\partial^2}{\partial\phi^2} + V(\phi) \tag{2.91}$$

where $B = \hbar^2/2I$ is the rotational constant of the rigid rotor, with I the moment of inertia of the methyl group around its threefold symmetry axis. $V(\phi)$ must be invariant under $2\pi n/3$ rotations, with $n = \pm 1, \pm 2$, ..., because of the threefold symmetry. Therefore, $V(\phi)$ can be expanded as a Fourier series:

$$V(\phi) = \sum_{n=1}^{\infty} \frac{V_{3n}}{2}[1 - \cos(3n\phi + \delta_{3n})] \tag{2.92}$$

In a first approximation only the threefold term is retained, while the higher-order terms contribute just as small corrections to the main term. Hence Eq.2.91 becomes:

$$H_R = -B\frac{\partial^2}{\partial\phi^2} + \frac{V_3}{2}(1-\cos(3\phi)) \tag{2.93}$$

The energy levels of the single well described by $V(\phi)$ are the so-called librational levels and the transitional energies from the librational ground state to its excited levels are the librational energies E_{0i}. The coupling of the wavefunctions of the individual wells splits the librational levels. The resulting sub-levels are denoted as A and E, the latter consisting of the degenerate doublet (E_a, E_b). At very low energy, $T \sim 1$ K, $k_BT \ll E_{0i}$ and the occupation probability of the excited librational states is negligible. Therefore, the rotor oscillates coherently between the three wells with an oscillation frequency equal to the tunnelling frequency ω_t [77]. As the temperature increases, the thermally activated hopping over the rotational barrier occurs and a classical picture of the methyl groups dynamics is commonly accepted. In Fig. 2.14 the quantized energy levels of a threefold potential are shown.

From a neutron scattering experimental point of view, the spectra for methyl groups dynamics at $T \sim 1$ K shows a central elastic peak and two inelastic peaks of resolutions width. The inelastic peaks are related to the transition $A \leftrightarrow E$ within the ground librational state, while the elastic peak includes the ground state transitions $E_a \leftrightarrow E_b$. Increasing the temperature, the inelastic peaks are shifted toward the elastic peaks and become broader. Simultaneously , a quasi-elastic component appears around the elastic peak. Finally, at around $\sim 50-70$ K, the quasi-elastic and inelastic components merge in a single quasi-elastic line well described by a Lorentzian function. The corresponding HWHM follows an Arrhenius-like dependence on temperature:

$$\Gamma = \Gamma_\infty \exp\left(\frac{-E_a}{k_BT}\right) \tag{2.94}$$

where E_a is the classical activation energy, defined as the difference between the top of the potential barrier and the ground state, and Γ_∞ is a temperature independent factor that typically takes values of $\sim 5-10\ meV$. The tunnelling frequency ω_t, first librational energy E_{01} and classical activation energy E_a are direct functions of the potential barrier V_3. The numerical relations [77] are given by:

$$E_a(K) = 0.598V_3^{1.05} \tag{2.95}$$

$$E_{01}(meV) = 0.470V_3^{0.548} \tag{2.96}$$

$$\hbar\omega_t(meV) = 0.655\left(1+\frac{V_3}{2.67}\right)^{1.06}\exp\left[-\left(\frac{V_3}{4}\right)^{0.5}\right] \tag{2.97}$$

Clearly, polymeric materials are disordered systems and, therefore, it is not possible to apply directly the equations describing methyl group dynamics in molecular crystals to methyl groups of glass-forming polymers. Hence, the neutron scattering data investigated in this work were interpreted in the framework of the *rotation rate distribution model* (RRDM) [82]. It is assumed that the only effect of the structural disorder on methyl group dynamics is to introduce a distribution of rotational barriers $g(V_3)$, originated from the different local environments felt by the individual methyl groups. In a first approximation, we can assume a Gaussian distribution of the purely threefold rotational barriers:

$$g(V_3) = \frac{1}{\sqrt{2\pi}\sigma_V}\exp\left[-\frac{(V_3-\langle V_3\rangle)^2}{2\sigma_V^2}\right] \tag{2.98}$$

where $\langle V_3 \rangle$ is the average barrier and σ_V the standard deviation of the distribution. The functional relations Eqs.2.95−2.97 allow for a straightforward transformation between $g(V_3)$ and the corresponding distributions of activation energies of classical hopping $f(E_a)$, rotational tunnelling frequency $h(\hbar\omega_t)$ and librational energies $F(E_{0i})$:

$$g(V_3)dV_3 = f(E_a)dE_a = F(E_{0i})dE_{0i} = -h(\hbar\omega_t)d\hbar\omega_t \tag{2.99}$$

CHAPTER

3

STRUCTURAL CHARACTERIZATION OF PDMAEMA, PDMAEMA/THF 30 WT% AND PDMAEMA/H_2O 30 WT%

In this chapter the structure of PDMAEMA in the dry state and in mixture (at 70% polymer concentration) with tetrahydrofuran (THF) and water will be discussed. Two different techniques were used to investigate the samples: X-ray and neutron scattering diffraction. Such a combination allow us to have a complementary information about the structural properties of the samples: while X-rays interact with the spatial distribution of the valence electrons, and therefore are sensitive to the heavy atoms, neutrons are scattered by atomic nuclei. As a consequence, by means of isotopic (H/D) substitution, neutron diffraction allows to carry out a selective study of the polymer in mixture. The chapter is organized as following: first, the structural characterization of the polymer in the dry state will be shown, then the structure of PDMAEMA/THF mixture and finally the results on PDMAEMA aqueous solution will be presented.

3.1 Experimental Details

3.1.1 Sample

Poly(dimethylaminoethyl methacrylate) in its protonated (hPDMAEMA) and deuterated (dPDMAEMA) forms was purchased from Polymer Source. The average molecular weight of hPDMAEMA was $M_w = 57000$ g/mol, with polydispersity M_w/M_n= 3.0, while for dPDMAEMA $M_w = 80000$ g/mol and M_w/M_n= 2.0. In order to

evaporate possible trapped solvent, PDMAEMA (Polymer Source) as received was annealed 7 h at T=373 K under vacuum. The mixtures containing 30 wt% of solvent were prepared by mixing the dry polymer with the appropirate amounts of THF, dTHF H_2O and D_2O (Sigma Aldrich) during a few days.

3.1.2 Calorimetry and Diffraction Conditions

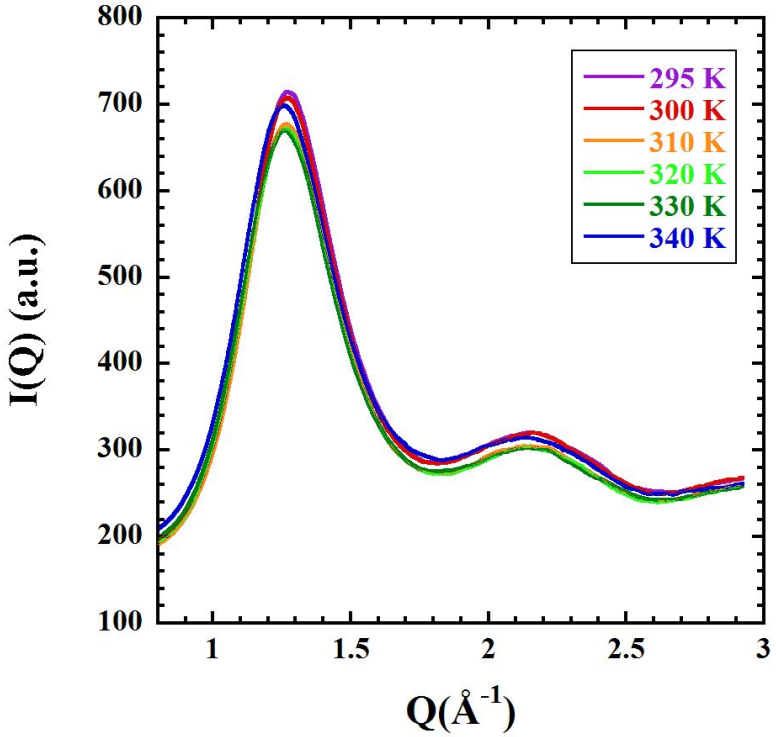

Figure 3.1: WAXS diffraction pattern of PDMAEMA measured at different temperatures.

Wide angle X-ray scattering (WAXS) measurements on PDMAEMA were performed, under vacuum, in reflection (θ-2θ configuration) varying the scattering angle 2θ from 4 to 30°with a step of 0.05°. The measuring time employed was 10 s/point. In small angle X-ray scattering (SAXS) experiments, samples in mixture (PDMAEMA/THF and PDMAEMA/H_2O) were sandwiched between mica windows and placed in hermetic cells, while dry PDMAEMA was placed without windows. All the measurements were performed under vacuum and in transmission geometry. Two sample-to-detector distances were used: 0.5 m ($0.1 < Q(\text{Å}^{-1}) < 1.6$) and 2 m ($0.008 < Q(\text{Å}^{-1}) < 0.15$). Measuring times of about 20 min were employed. Neutron diffraction with polarization analysis measurements were carried out by using the diffuse scattering spectrometer DNS (MLZ, Garching, Germany) on PDMAEMA, PDMAEMA/THF, PDMAEMA/dTHF, dPDMAEMA/THF, PDMAEMA/H_2O and PDMAEMA/D_2O. An incident neutron wavelength of $\lambda = 4.2$ Å was used covering a

range in momentum transfer Q from Q=0.2 Å^{-1} to Q=2.67 Å^{-1}. Background correction was done by subtracting the intensity scattered by an empty aluminum sample holder. Differential scanning calorimeter (DSC) TA Instrument Q2000 was used to determine the glass transition temperature T_g of the samples (sample weights about 10 mg). Hermetic aluminium pans were used for all the samples. Modulated DSC measurements were performed on PDMAEMA, PDMAEMA/THF and PDMAEMA/H_2O with average heating rate of 3 K/min and amplitude of modulation ±0.5 K with a period of t_p = 60 s.

3.2 Structure of PDMAEMA

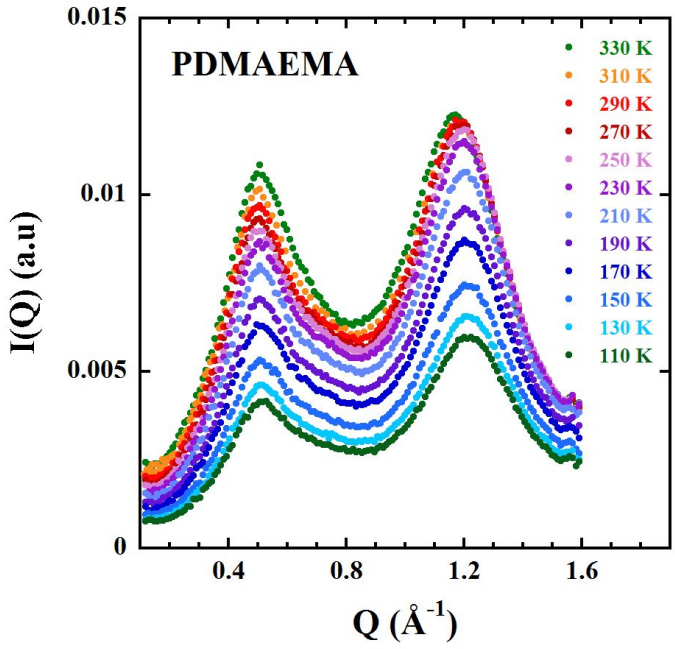

Figure 3.2: SAXS diffraction pattern of PDMAEMA measured at different temperatures.

Wide angle X-ray scattering (WAXS) results on PDMAEMA are shown in Fig. 3.1. The experiment was carried out at different temperatures above the glass transition, from 295 to 340 K. Two peaks are observed in the diffraction pattern of the dry polymer: one intense and relatively narrow at $Q \sim 1.2$ Å^{-1}, while the latter, broader and less intense, at $Q \sim 2.2$ Å^{-1}. In glass-forming polymers the peaks at around ~ 1.2 $\mathring{A}^{-1}$ are usually attributed to inter-chain structural correlations while peaks at higher Q correspond to intra-chain correlations, that are related to the atomic distances within the monomer. The position of the maximum of the high peak centered at higher Q-values does not change as temperature increases. On the contrary, the peak at low Q-values shows a temperature dependence of its position. Such a behaviour is in agreement with the interpretation of the origin of the underlying

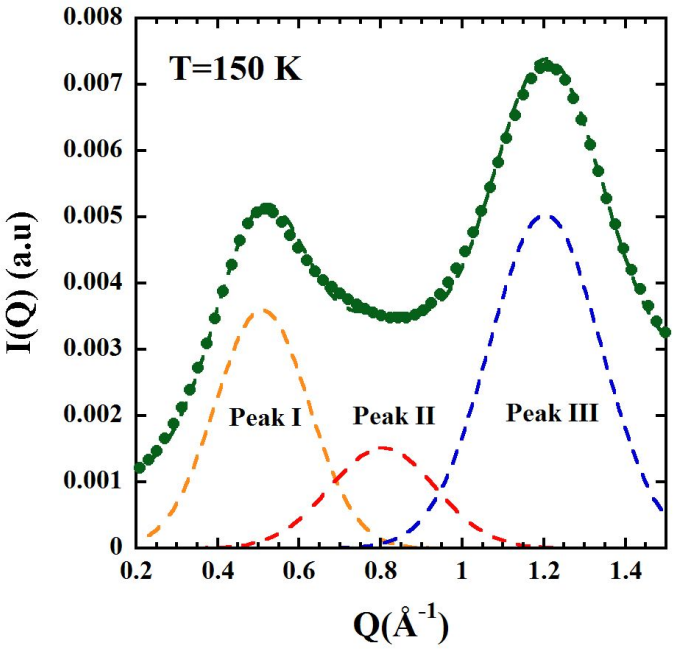

Figure 3.3: X-ray diffraction pattern of PDMAEMA at T=150 K. Dashed green line shows the fit with the model described in the text. Dotted lines refer to curves describing peak I (yellow), peak II (red) and peak III (blue).

correlations. In fact, it has been reported in literature [83, 84, 85, 86] that the position of the inter-chain maximum changes with temperature, especially above the temperature of glass transition. On the contrary, the intra-chain peak maximum does not appear affected by temperature changes. This was explained by the fact that the interactions between polymer chains are of the Van der Waals type, while the interactions within the chain are governed by covalent bonding. In Fig. 3.2 results obtained by small angle X-ray scattering are shown. They have been carried out in a temperature range from 110 to 330 K, that is including temperatures in the glassy state of the system and temperatures above the T_g. We notice two main peaks centred at about ~ 1.2 Å^{-1} (we will call it peak III), in agreement with WAXS measurements, and ~ 0.5 Å^{-1} (peak I). At low temperature, peak I appears quite asymmetric. This suggests the presence of an unresolved contribution centred at around ~ 0.8 Å^{-1} (peak II). In order to extract information on the temperature dependence of the maximum position and shape of the peaks, SAXS data were fitted by the sum of three Gaussian functions. The Gaussian functions are expressed by:

$$I(Q) = I_0 \exp\left[-\left(\frac{Q - Q_m}{\sigma} \right)^2 \right] \tag{3.1}$$

where I_0 is the intensity of the peak, Q_m the position of the maximum and σ is related to the width of the peak (full width half maximum FWHM $= 2\sqrt{2\ln(2)}\sigma$). As an example, the result of the fitting procedure at T=150 K is shown in Fig. 3.3. The temperature dependence of the parameters is shown in Fig. 3.4–3.6. Due to the complex molecular composition of PDMAEMA monomer, it is not trivial to

relate these contributions to specific correlations between molecular groups. However, comparing the results obtained with those on similar polymers investigated by diffraction and molecular dynamics (MD) simulation in previous works, it is possible to provide a picture for the main structural features of PDMAEMA.
Starting from high Q-values, the average position of the maximum of peak III (Fig. 3.4(b)) is centred at $Q_m^{III} \sim 1.19$ Å^{-1}. Using Bragg's approximation, we can estimate an average distance of about $d_{III} = 2\pi/Q_m^{III} = 5.3$ Å. This value is close to that found for polymers characterized by long and relatively bulky side-groups –i.e polymers of the family of poly(n-alkyl methacrylates) [87], poly(n-alkyl acrylates) [88], poly(itaconates) [89], poly(alkylene oxides) [90], polystyrene [91] and poly(vinyl pirrolidone) [92] –. In those works, such a distance was related to correlations between atoms located in side groups of different monomers. This kind of polymers shares with PDMAEMA another relevant property, that is the presence of a 'pre-peak' (peak I) at low Q. In the system under investigation, such a peak corresponds to a distance between molecular groups of about $d_I \sim 12.3$ Å. This peak can be related to inter-mainchain distances [87]. In addition, MD simulation studies revealed a strong anti-correlation between, above all, side-group (SG) and main-chain (MC) atoms in the same Q-range.

Therefore, the presence of such a pre-peak has been related to a kind of nano-phase segregation between side groups and backbones leading to the existence of nano-domains rich in each of the polymeric subspecies [88, 93, 94]. Regarding peak II, diffraction and MD simulation studies on poly(methyl methacrylate) (PMMA) [95], poly(ethyl methacrylate)(PEMA) and poly(vinyl acetate) (PVAc) [96] have found a similar contribution and related it to correlations involving the backbone atoms –i.e, carboxyl group (COO), α-methyl groups (αMG) and MC–. In Figs.3.4–3.6 the thermal behaviour of the parameters characterizing the peaks can be seen in comparison with DSC results displayed in the corresponding panel(a). These plots show the temperature derivative of the reversible part of the specific heat, which shows a maximum at the glass-transition temperature of the sample. Below the glass transition temperature, all the structural peaks show the same temperature dependence: the maximum position shifts toward lower Q values when heating the sample. This behaviour, commonly found in structure factor peaks reflecting intermolecular correlations, is attributed to thermal expansion leading to an increase of intermolecular distances. However, approaching T_g, some changes occur. In fact, in peak III, the T-dependence becomes stronger when the thermal expansion changes from that in the supercooled liquid state to that in the glassy state. On the contrary, peak I displays the opposite tendency in addition to an increase of σ parameter (Fig. 3.5). We can interpret this peculiar behaviour as a signature of the complexity of this peak where both MC-MC,MG-MG and cross-correlations MC-MG occur. Finally, peak II does not appear to be affected by the glass transition as can be shown in Fig. 3.6.

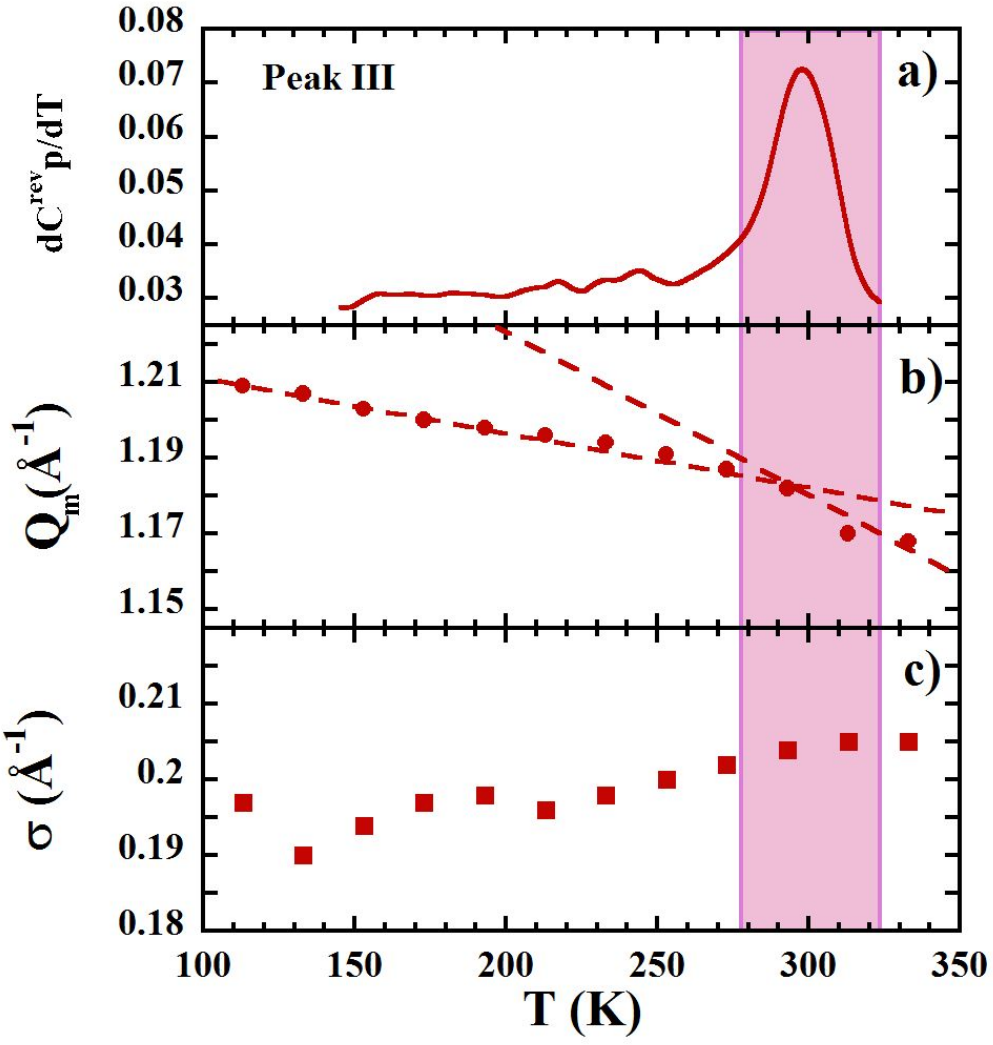

Figure 3.4: **a)** Temperature derivative of the reversible specific heat of dry PDMAEMA. **b)** Temperature dependence of the position of the maximum corresponding to peak III in Figure 3.3 in dry PDMAEMA. **c)** Temperature dependence of the width of peak III in dry PDMAEMA. The shadowed area indicates the region of the glass transition.

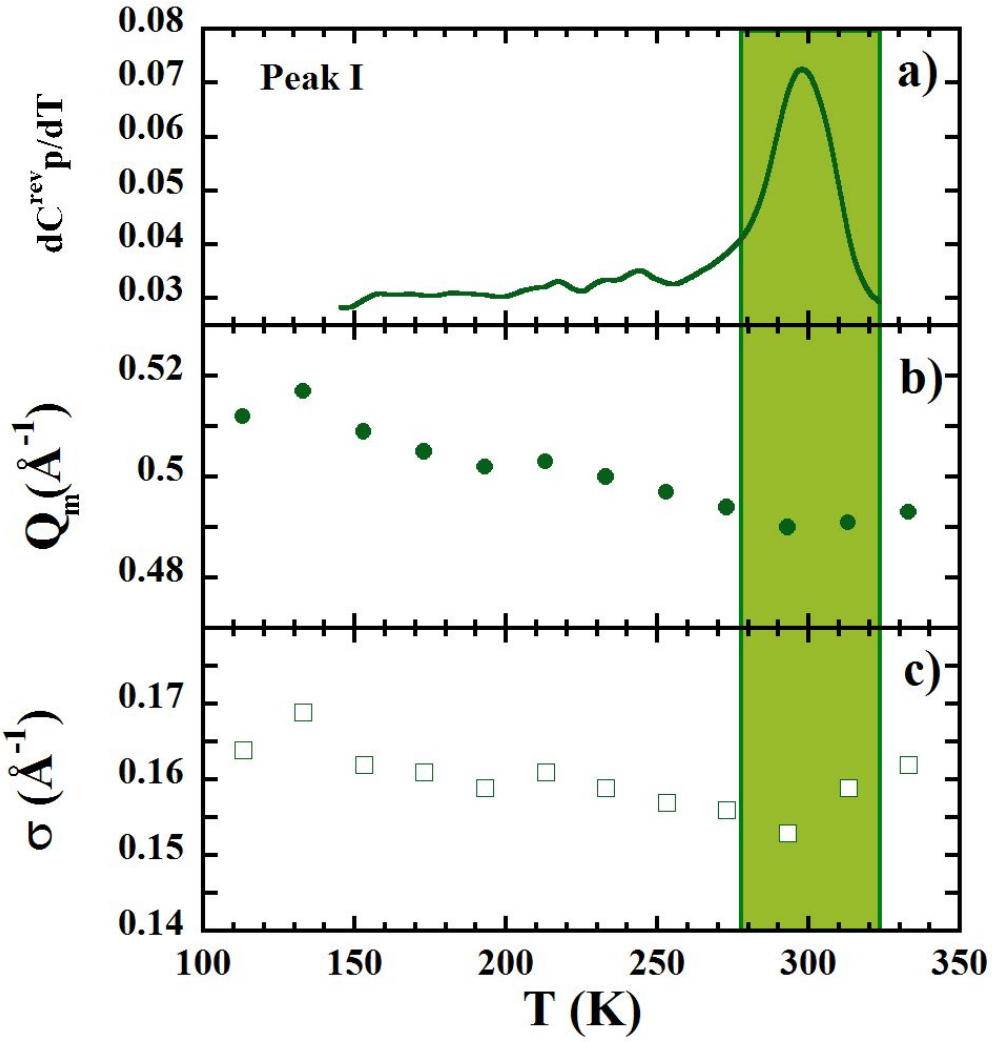

Figure 3.5: **a)** Temperature derivative of the reversible specific heat of dry PDMAEMA. **b)** Temperature dependence of the position of the maximum corresponding to peak I in Figure 3.3 in dry PDMAEMA. **c)** Temperature dependence of the width of peak I in dry PDMAEMA. The shadowed area indicates the region of the glass transition.

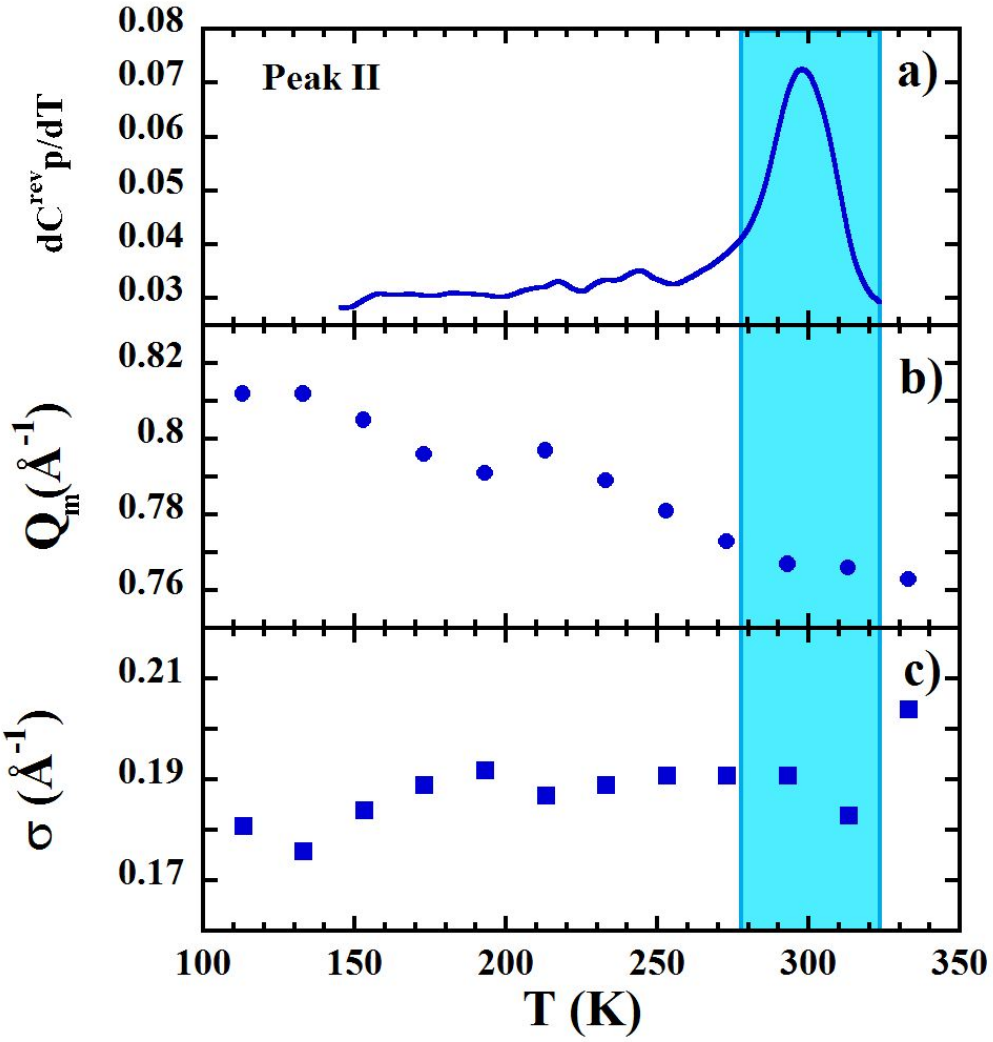

Figure 3.6: **a)** Temperature derivative of the reversible specific heat of dry PDMAEMA. **b)** Temperature dependence of the position of the maximum corresponding to peak II in Figure 3.3 in dry PDMAEMA. **c)** Temperature dependence of the width of peak II in dry PDMAEMA. The shadowed area indicates the region of the glass transition.

3.3 Structure of PDMAEMA/THF 30 wt %

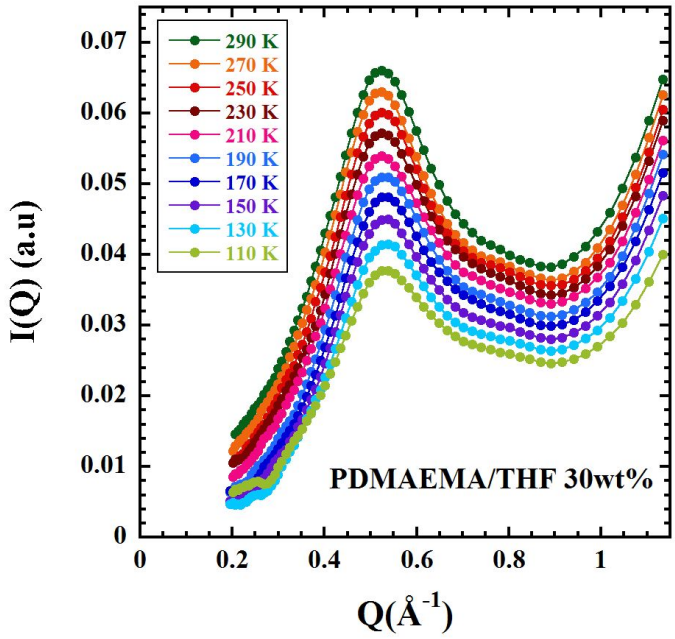

Figure 3.7: SAXS diffraction pattern of PDMAEMA/THF 30 wt % measured at different temperatures. Multiplicative factors have been applied to correct artefacts in the intensity due to mica expansion and show the curves with more clarity.

In the previous section the structural properties of PDMAEMA in the dry state have been characterized. Trying to reveal how the presence of solvent molecules affect the polymer structure, PDMAEMA/THF 30 wt % sample was investigated. It was not possible to perform WAXS measurements on this sample due to the lack of hermetic sample holder in reflection mode that could avoid THF evaporation. SAXS experiments were feasible (data shown in Fig. 3.7) by using a hermetic cell with parallel mica windows in the transmission geometry. Unfortunately, mica gives an intense Bragg peak that obligates us to limit the measurements in the Q range from 0.2 to 1.2 $Å^{-1}$. Therefore, additional information was sought in neutron diffraction experiments. In Fig. 3.8 DNS measurements on dry PDMAEMA and PDMAEMA/THF 30 wt % are shown. We can observe that peak III position is hardly affected by the presence of THF molecules ($\Delta d_{III} \approx 0.2$ Å). This peak appears somewhat narrower in THF mixture than in the dry state, as can also be observed comparing the SAXS diffraction patterns of both samples (see Q-range ~ 1 $Å^{-1}$ in Fig. 3.9 due to high-Q flank of peak III).

Next we tried to obtain a quantitative description of peaks I and II from the X-ray results. In Fig. 3.10 an example of the results of the application of the fitting procedure previously explained on small angle scattering data is shown. The peak III position was fixed from DNS measurements, while its width was allowed to change. The position of the maximum and the width of the pre-peak (peak I) assume values

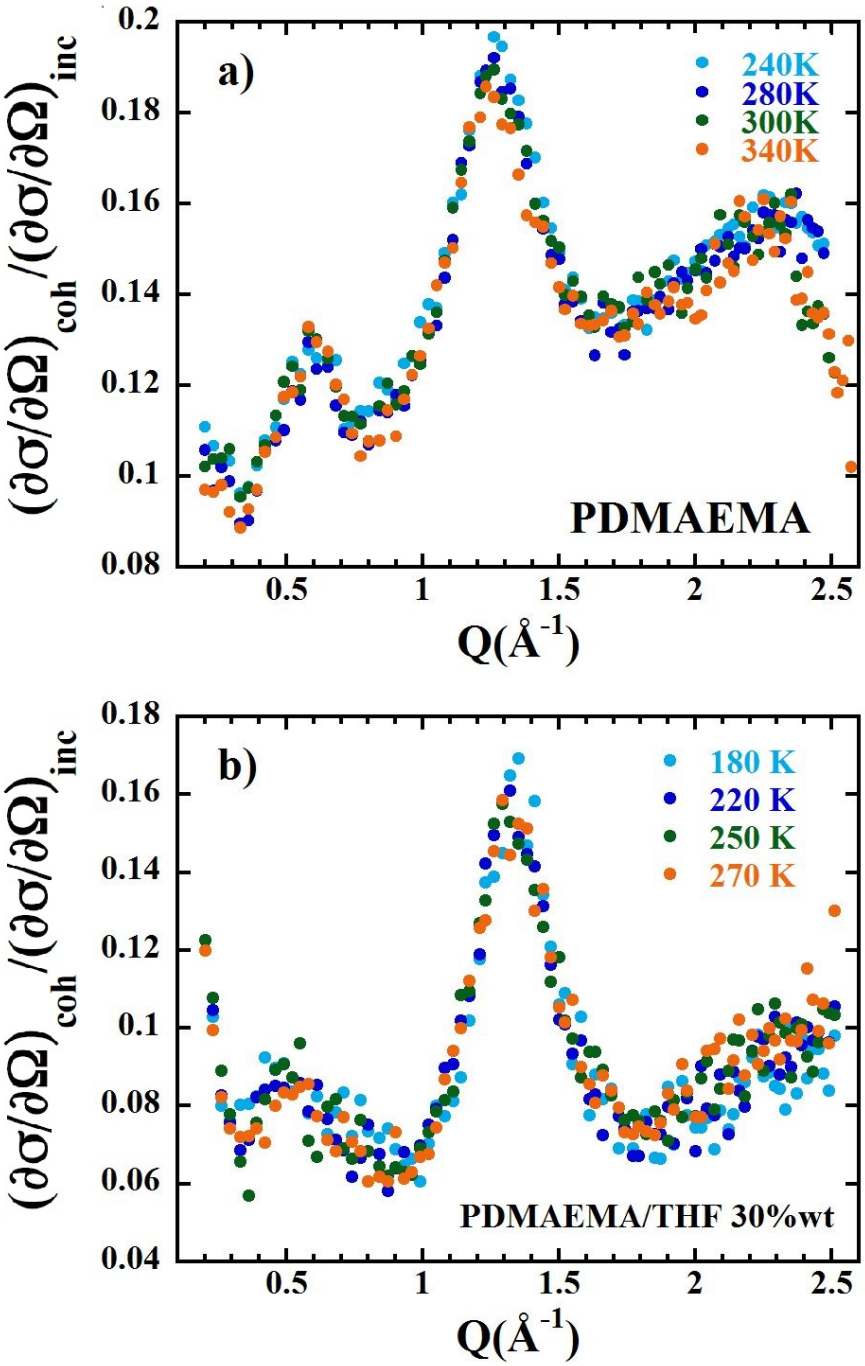

Figure 3.8: Ratio between the coherent and incoherent scattering cross sections measured at different temperatures on PDMAEMA (a) and on PDMAEMA/THF 30 wt %(b)

very close to those obtained for the dry polymer (see Fig. 3.11). Regarding peak II, we observe that the average position of the maximum is comparable to the one of PDMAEMA in the dry state (Fig. 3.12(b)). However, due to the insufficient information on the peak III shape and position, further discussion on the σ parameter

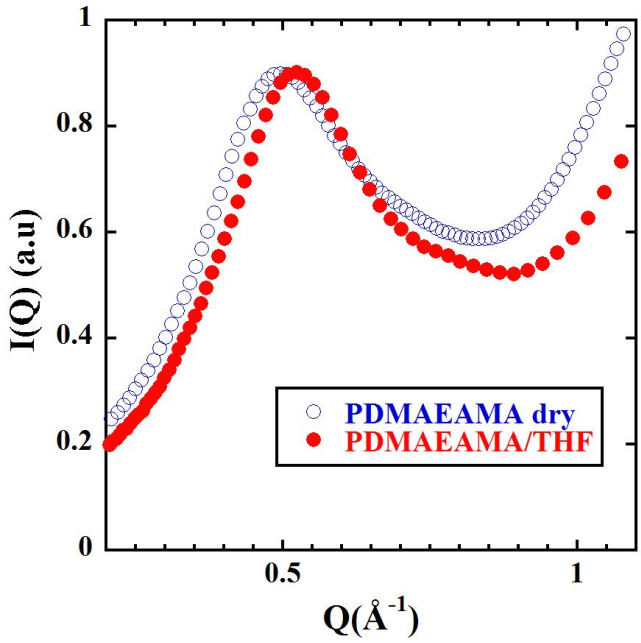

Figure 3.9: Comparison of X-Ray diffraction patterns obtained by SAXS on dry PDMAEMA (empty symbols) and on its mixture with THF (filled sumbols) at room temperature. The intensities have been scaled to coincide in the maximum of the peak.

value and temperature dependence is not possible. Regarding the T-dependence of the correlation distances, both peaks (peak I and II) show a shift toward lower Q values with increasing T as expected. Nevertheless, the temperature dependence of the position of peak I does not exhibit any crossover approaching the T_g in contrast with the corresponding contribution in dry PDMAEMA. Probably, this can be related to different cross-correlation contributions occurring in THF mixture.
Moreover, neutron diffraction measurements were performed on partial deuterated samples (dPDMAEMA/THF and PDMAEMA/dTHF) to provide the contrast between the components in the mixture (see Fig. 3.13). At low Q-values, the results on both samples show a strong increase of the coherent cross section. In the dPDMAEMA/THF sample, this contributions see to flatten around ~ 0.5 Å^{-1} . However, in PDMAEMA/dTHF (Fig. 3.13(b)), the coherent contribution continuously increases toward lower Q-values. This behaviour is supported by SAXS measurements on the mixture performed in the low Q-range at room temperature (Fig. 3.14). All these results lead to think that the low-Q scattering reflects the typical concentration fluctuations in a mixture without any clear signature of the presence of clusters with well-defined associated length scales.

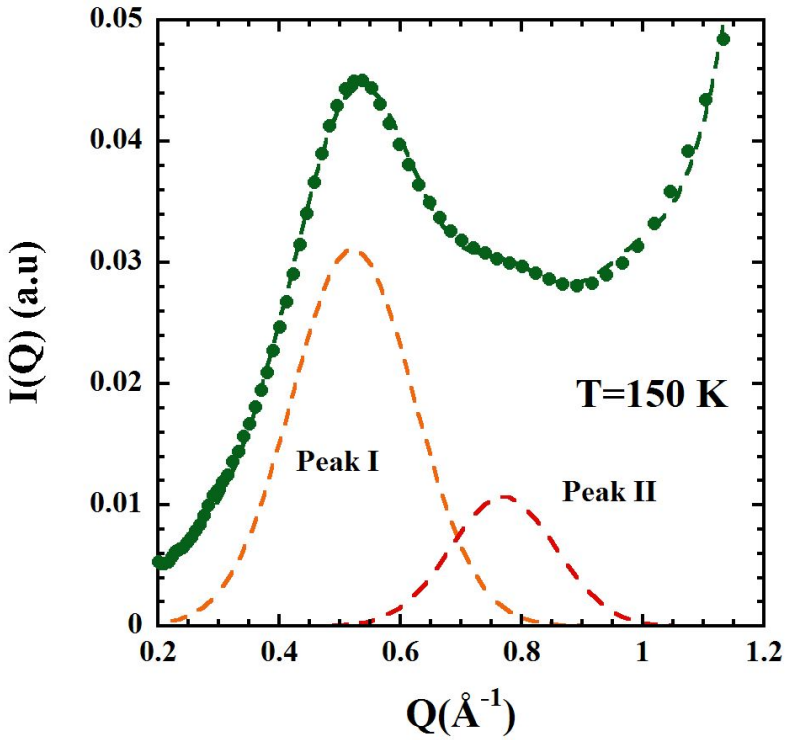

Figure 3.10: X-ray diffraction pattern of PDMAEMA/THF 30 wt % at T=150 K. Dashed green line shows the fit with the model described in the text. Dotted lines refer to curves describing peak I (yellow), peak II. The contribution of peak III (not shown) was built from the DNS information.

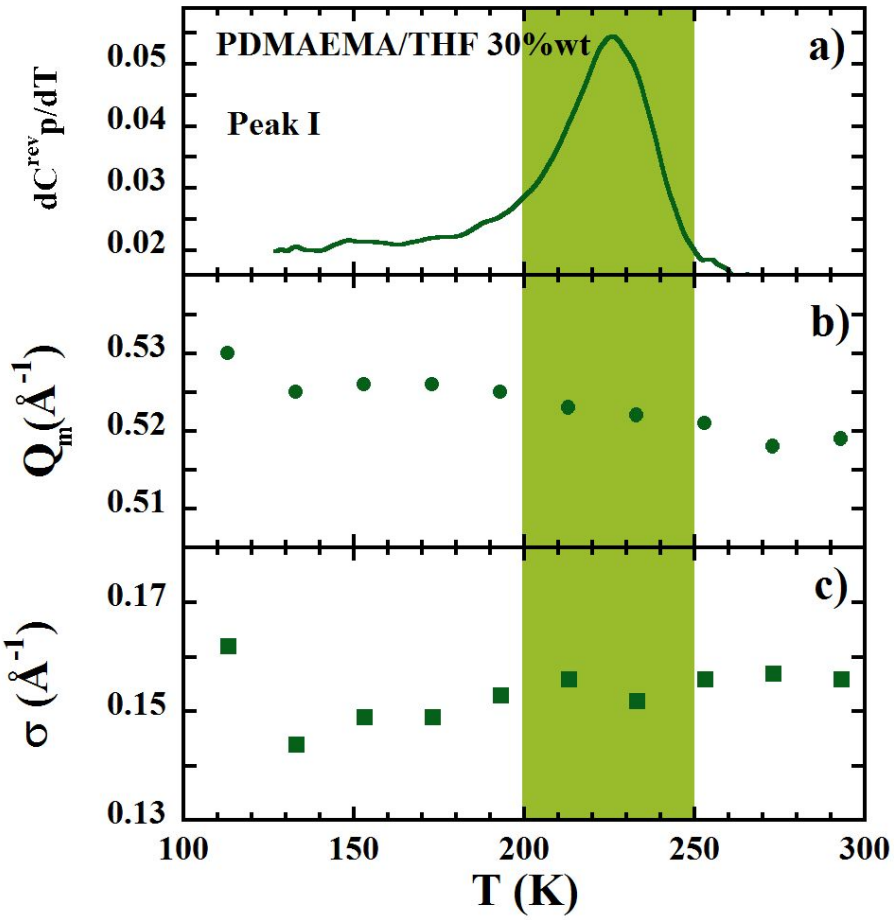

Figure 3.11: **a)** Temperature derivative of the reversible specific heat of PDMAEMA/THF 30 wt %. **b)** Temperature dependence of the position of the maximum corresponding to peak I in Figure 3.10 in PDMAEMA/THF 30 wt % sample. **c)** Temperature dependence of the width of peak I in PDMAEMA/THF 30 wt %. The shadowed area indicates the region of the glass transition.

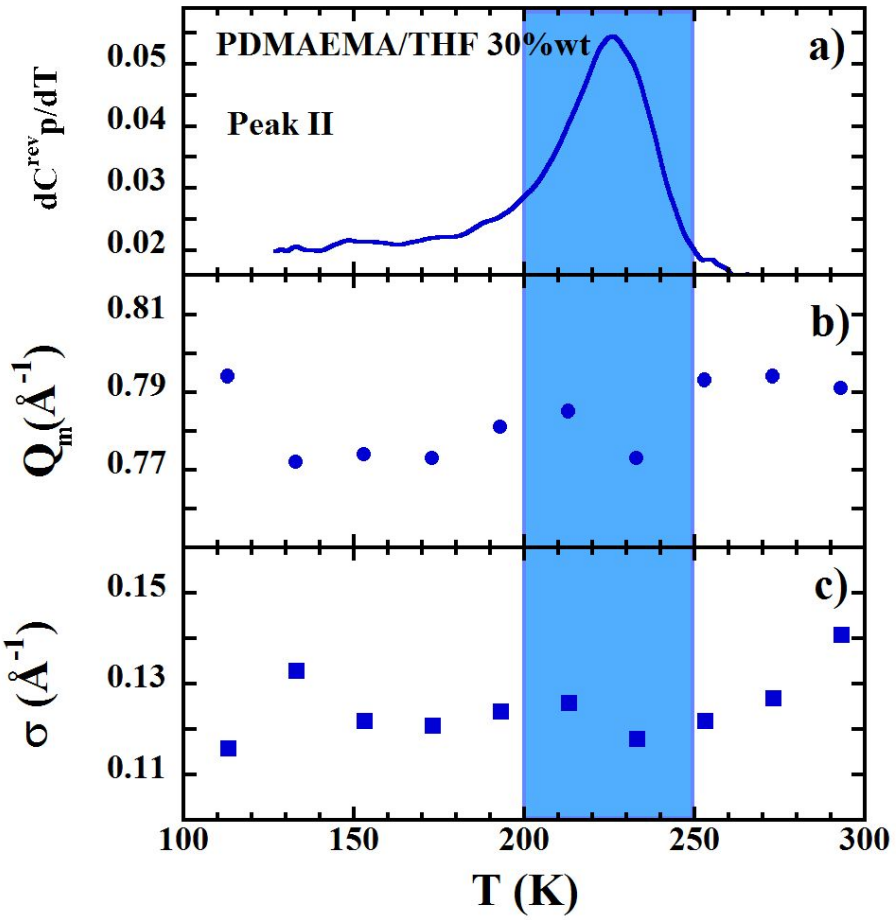

Figure 3.12: **a)** Temperature derivative of the reversible specific heat of PDMAEMA/THF 30 wt %. **b)** Temperature dependence of the position of the maximum corresponding to peak II in Figure 3.10 in PDMAEMA/THF 30 wt % sample. **c)** Temperature dependence of the width of peak II in PDMAEMA/THF 30 wt %. The shadowed area indicates the region of the glass transition.

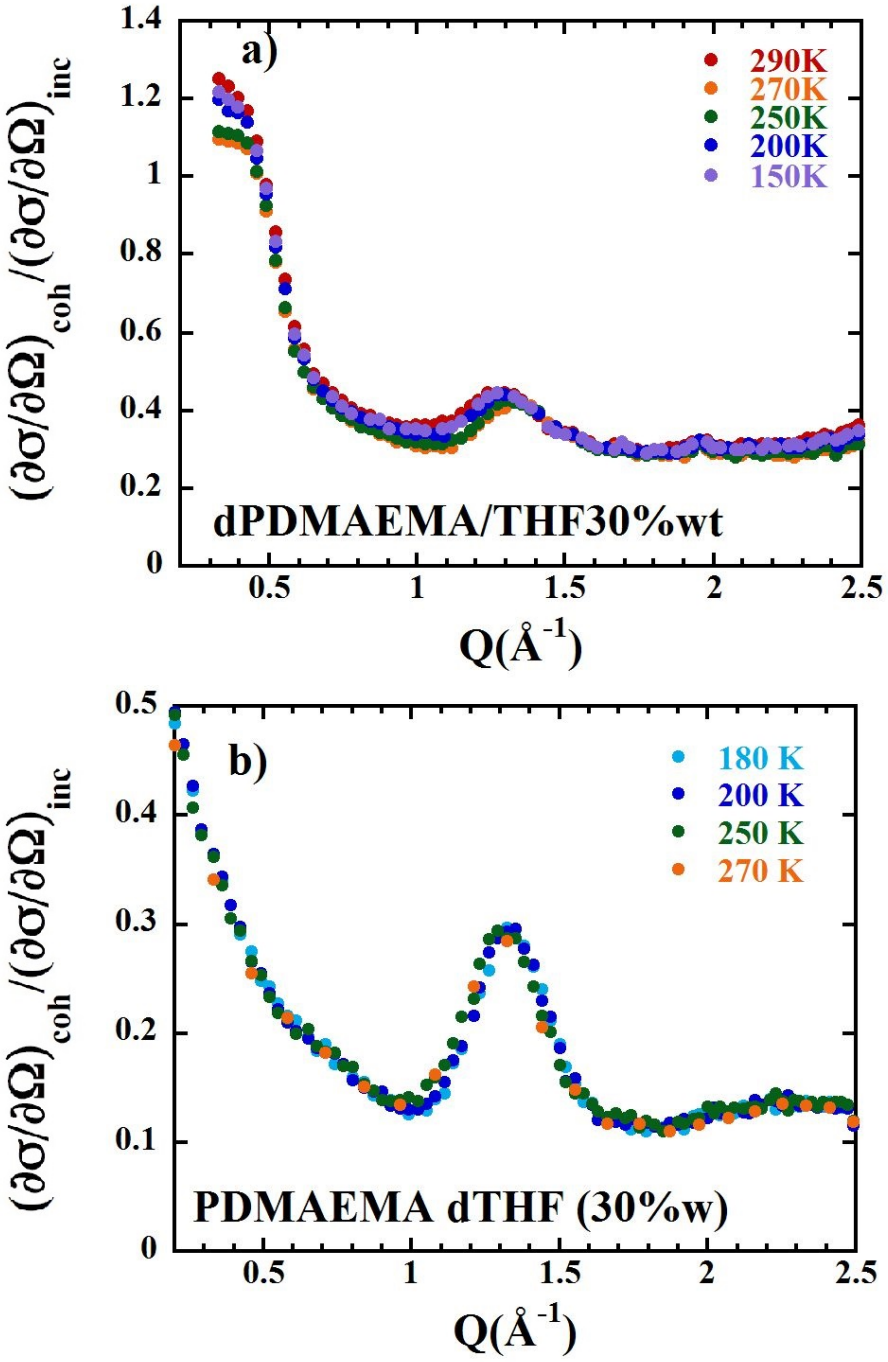

Figure 3.13: Ratio between the coherent and incoherent scattering cross sections measured at different temperatures on dPDMAEMA/THF 30 wt % (a) and on PDMAEMA/dTHF 30 wt %(b)

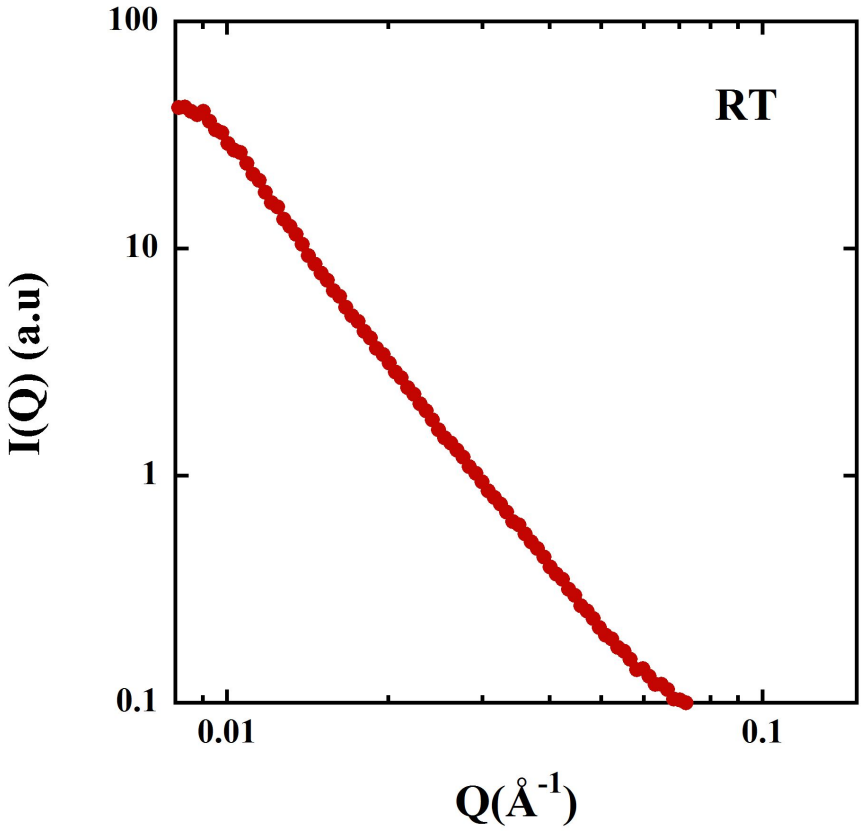

Figure 3.14: X-Ray diffraction pattern obtained by SAXS on PDMAEMA in mixture with THF at room temperature.

Summarizing, *i)* we have seen that the presence of THF molecules mainly affect the distribution of the SG/SG correlation distances even though its average distance $d_{III} = 2\pi/Q_m^{III}$ appears to be slightly shifted. *ii)* The overall nano-domain structure associated to the pre-peak is essentially the same in the dry polymer and in the mixture. *iii)* THF molecules appear to be homogeneously distributed within the sample since there is not sign of solvent clusters in the results obtained by both SAXS and DNS (where only density fluctuations are observed).

3.4 Structure of PDMAEMA/H_2O 30 wt %

Finally, the structure of PDMAEMA/H_2O 30 wt % (corresponding to $\sim$ 4 water molecules per monomer) was studied. As expected, some relevant changes were observed in this sample, due to the presence of hydrogen bonds. Starting from DNS measurements on polymer in mixture with deuterated water (Fig. 3.15(a)), we can observe a very intense peak at low Q values ($\sim$ 0.25 Å^{-1}). The large difference between b_D and b_H induces a large contrast between molecules containing deuterated and protonated nuclei. This peak can be attributed to the presence of regions rich in deuterated water dispersed all over the sample, giving rise to a well defined correlation distance. At the two lowest temperatures (180 and 220 K), the intensity and the position of the peak maximum are comparable. Increasing the temperature, we can observe a shift toward lower Q values of the maximum and, especially, an increase of the intensity up to almost double its value at 280 K. The presence of such a peak was confirmed by small angle neutron scattering (SANS) [97] measurements performed on PDMAEMA and PDMAEMA/D_2O 30 wt % samples at room temperature (Fig. 3.16), where a peak centred at around $\sim$ 0.2 Å^{-1} is found in the polymer in deuterated water mixture. The position of this contribution is in agreement with the shift toward lower Q values observed in the DNS data. These Q-values correspond to large average correlation distances in the range of $25 < d < 31$ Å. It is well known the tendency of water molecules of form clusters, that is to join together instead of being uniformly distributed in the sample. Therefore, it would be reasonable to relate this scattering contribution to the presence of water clusters, and thereby the deduced characteristic spatial length to the average distance between them.

Moving toward higher Q values (Fig. 3.15(b)), a broad peak is found in the range from 1 to 2 Å^{-1}. The shape of such a peak appears highly dependent on the temperature range. In fact, at high temperature it is centred at around 1.2 Å^{-1} and is characterized by a strong asymmetry, whereas at the two lowest temperatures investigated (180 and 220 K), the peak appears more symmetric and the maximum is shifted toward higher Q values. A very similar temperature dependence has been observed for water confined in mesoporous MCM-41 [98, 99]. For comparison, in Fig. 3.17 the neutron diffraction spectra of D_2O in MCM-41 measured by *Floquet at al.* are shown. At high temperature, the confined water neutron diffraction signal appears as a wide bump located at around Q_m = 1.85 Å^{-1}, whereas, at low temperature, T =173 K , the signal looks much more like a diffraction peak centred at smaller Q value (1.7 Å^{-1}).

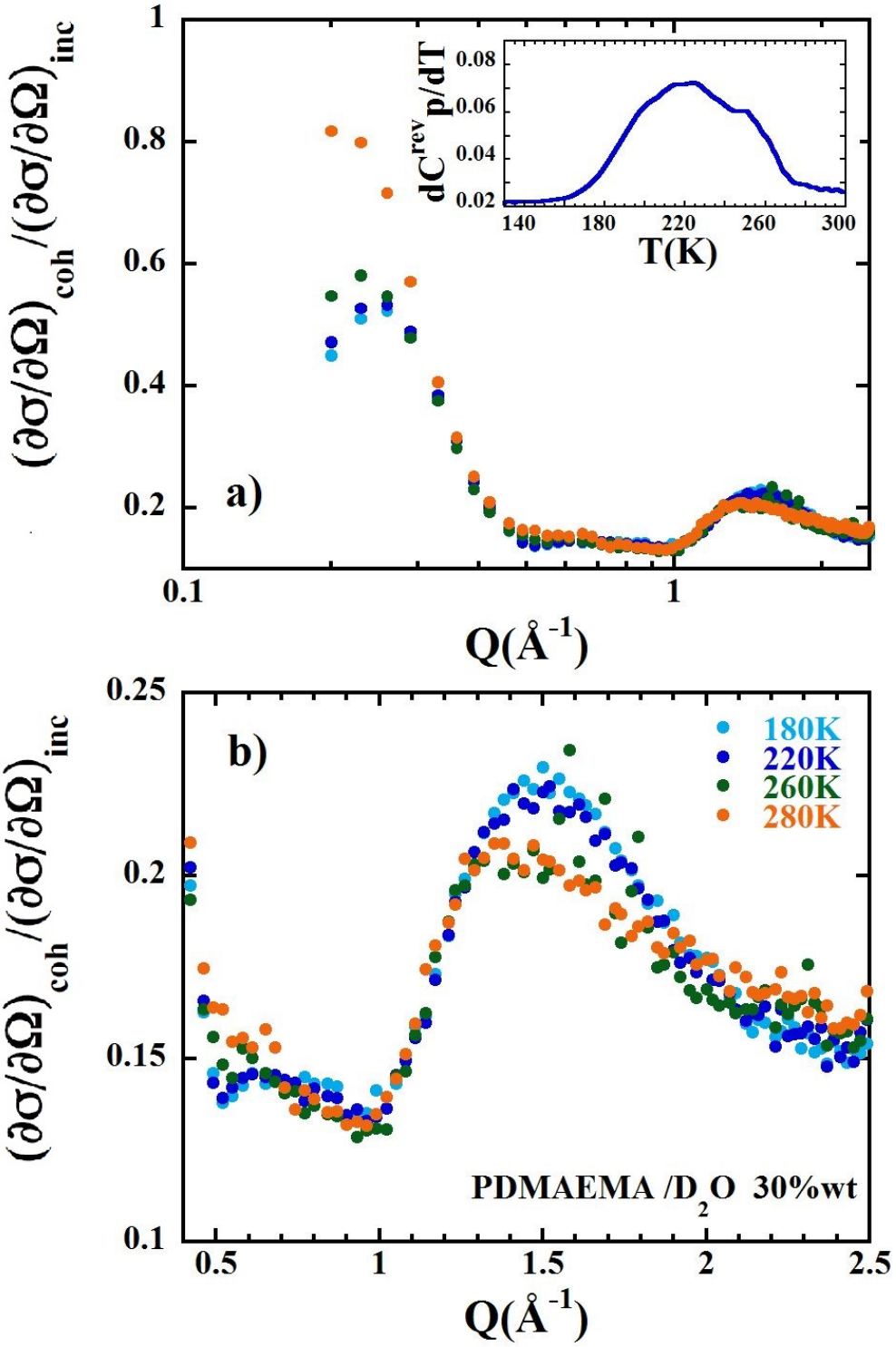

Figure 3.15: Ratio between the coherent and incoherent scattering cross sections measured by DNS at different temperatures on PDMAEMA/D_2O 30 wt %. *Inset*: Temperature derivative of the reversible specific heat of PDMAEMA/H_2O 30 wt %.

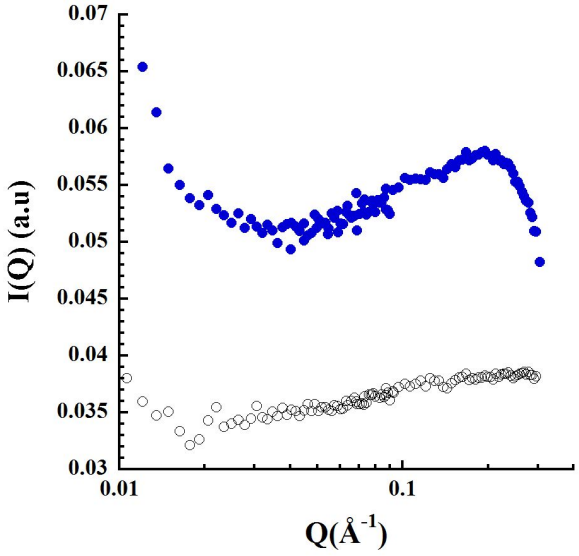

Figure 3.16: Diffraction patterns obtained by SANS on dry PDMAEMA (empty symbols) and on PDMAEMA/D_2O 30 wt % (filled sumbols) at room temperature.

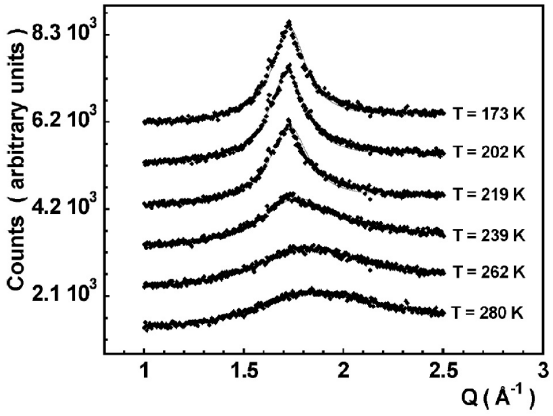

Figure 3.17: Measured neutron diffractograms of confined water D_2O sorbed in MCM-41 sample for different temperatures in the range 173280 K studied by *Floquet et al.*

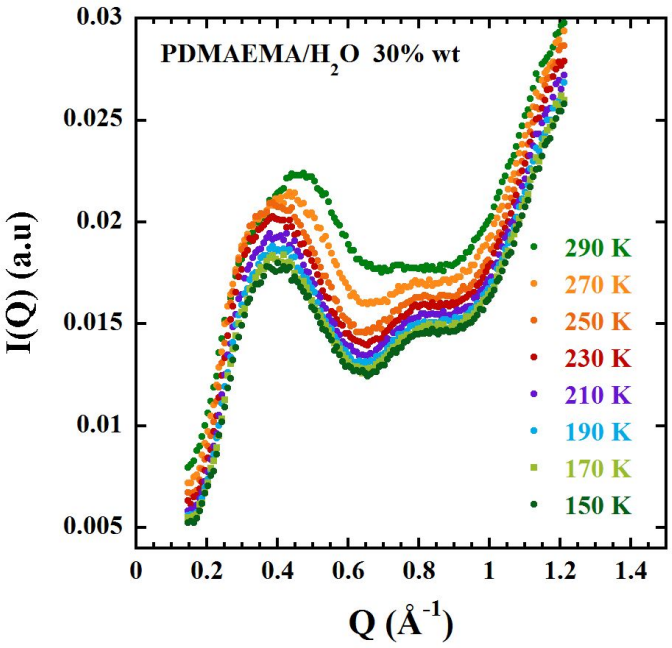

Figure 3.18: SAXS diffraction pattern of PDMAEMA/H_2O 30 wt % measured at different temperatures.

A combined study of neutron diffraction and empirical potential structure refinement (EPSR) simulations [99], suggested that the mesoscopic arrangement of water molecules in the pore could change as a result of the modified water-water and water-substrate interactions. Upon cooling, the H-bonds between water molecules are strengthened, while those between water and the wall atoms become weaker. Therefore, at low T the pore appears more uniformly filled while the walls are less wet and water molecules are arranged in a cubic-ice-like structure [98]. In Fig. 3.15(inset) we can see the temperature derivative of the specific heat of the sample measured by differential scanning calorimetry (DSC). It shows a very broad glass transition process that is complete at $\sim$ 220 K. Such a temperature coincides with the appearing of the well defined water peak in DNS spectra. We may suggest the emergence of an extra finite size effect produced by the 'frozen' main-chains of PDMAEMA that would restrict the water molecules mobility.

So far the DNS results on the cluster peak and peak III have been discussed. The characterization of peak I and peak II was performed on the SAXS results, where these peaks were better resolved (Fig. 3.18). To avoid water evaporation, the same experimental setup employed for the THF mixture was used. As a consequence, also in this case, it is not possible to resolve the peak related to the SG/SG correlation distances (peak III). Comparing the spectra of the water mixture with that of the polymer in the dry state and in THF mixture, it is clear that the peak I is strongly affected by the presence of water molecules. In the fitting procedure of SAXS results it was necessary to add a further Gaussian function to describe such a peak. Fig. 3.19 shows an example of the fitting results at room temperature. The temperature dependence of Q_m parameters of both curves describing peak I are shown in Fig. 3.20

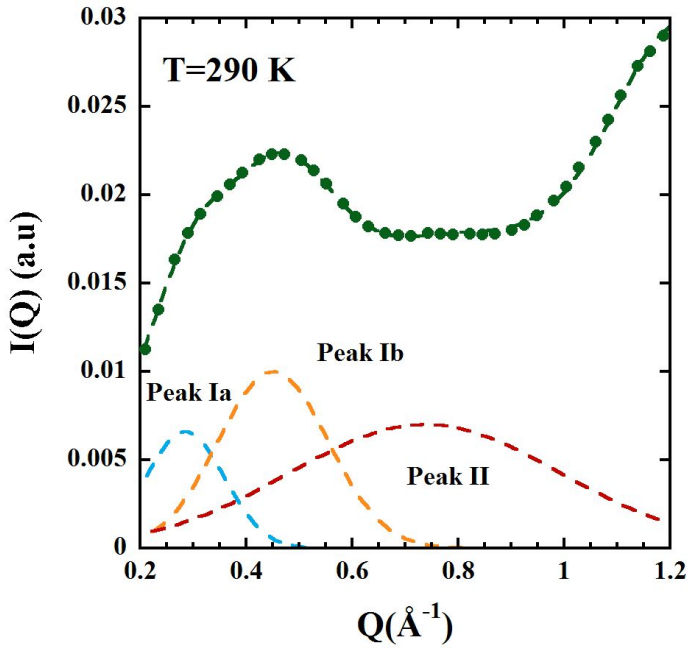

Figure 3.19: X-ray diffraction pattern of PDMAEMA/H_2O 30 wt % at room temperature. Dashed green line shows the fit with the model described in the text. Dotted lines refer to curves describing peak Ia (light blue), peak Ib (yellow) and peak II (red). The contribution of peak III (not shown) was built from the DNS information.

in comparison to that of the dry polymer. The peak at lower Q (peak Ia) is centred at values close to those characterizing the peak observed by DNS and SANS, suggesting a relation with water cluster distances, while the other curve (peak Ib) is located at Q_m values smaller than that of the pre-peak (peak I) of the dry polymer. Assuming this peak Ib in the mixture to be related to the nano-domains in the polymer, the difference between the average distances between nano-domain in dry PDMAEMA and in PDMAEMA/H_2O is $\Delta d_{Ib} \approx 2$ Å.

Regarding the peak at around 0.8 Å^{-1} (peak II, as previously named), the position of its maximum is close to that of PDMAEMA. However, as in the case of the THF mixture, it is not possible to extract information on its width, even though it must be mentioned that the fitting procedure seems to demand a much broader peak as shown in Figs. 3.19-3.21. This suggests either a wider distribution of the correlation distances associated to this peak or the presence of a further peak that cannot be resolved by SAXS measurements. The splitting of peak II into two peaks could be attributed to the presence of regions where the polymer would be hydrated coexisting with other regions without presence of water. This picture would be suggested by the finding of water clusters mentioned above. In any case, the observed effect could be related to a stronger heterogeneity within the sample.

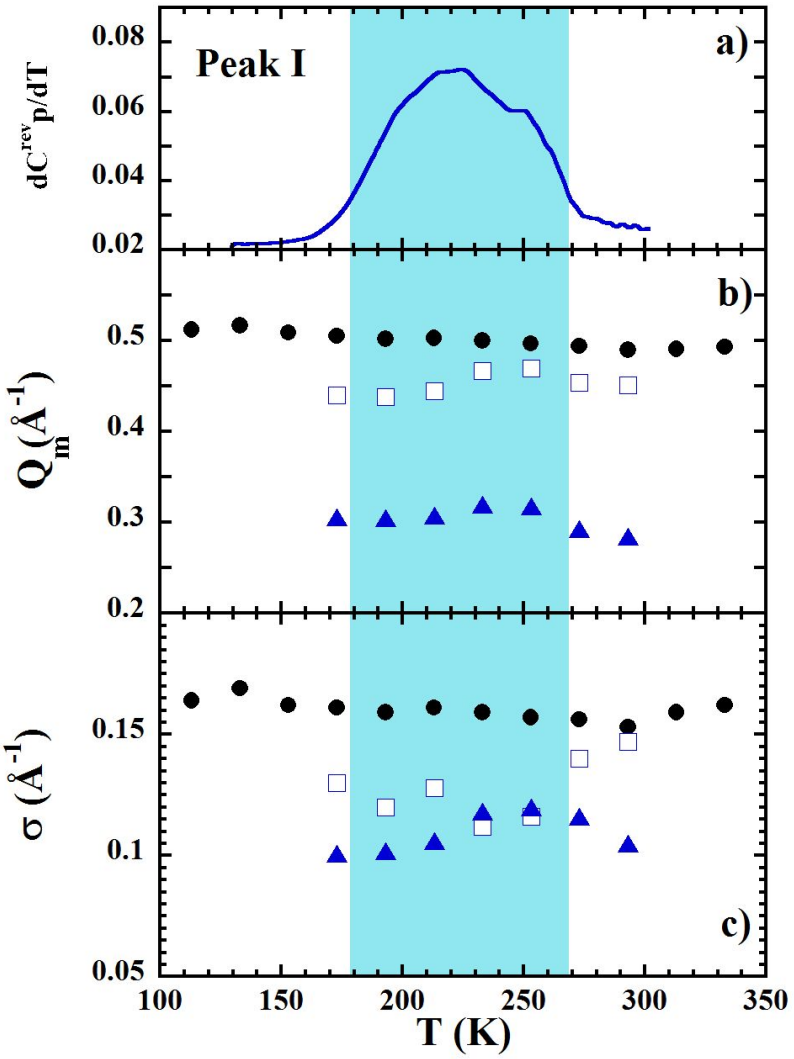

Figure 3.20: **a)** Temperature derivative of the reversible specific heat of PDMAEMA/H_2O 30 wt %. **b)** Temperature dependence of the position of the maximum corresponding to peak Ia (blue triangles) and peak Ib (empty squares) in Figure 3.19. As a comparison, black circles refer to the positions of peak I of dry PDMAEMA. **c)** Temperature dependence of the width peak Ia (blue triangles) and peak Ib (empty squares) of PDMAEMA in water mixture and peak I of dry PDMAEMA (black circles). The shadowed area indicates the region of the glass transition.

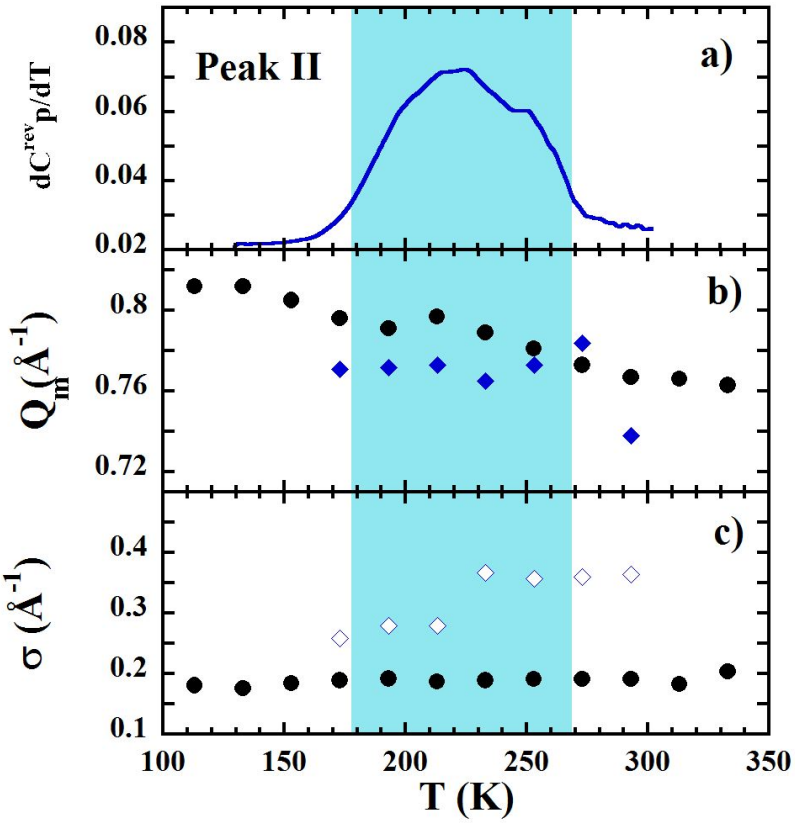

Figure 3.21: **a)** Temperature derivative of the reversible specific heat of PDMAEMA/H_2O 30 wt %. **b)** Temperature dependence of the position of the maximum corresponding to peak II (blue diamonds) in PDMAEMA water mixture (see Fig. 3.19) and peak II (black circles) in dry PDMAEMA. As a comparison, black circles refer to the positions of peak I of dry PDMAEMA. **c)** Temperature dependence of the width peak II (empty diamomds). As a comparison, black circles refer to the width of peak I of dry PDMAEMA. The shadowed area indicates the region of the glass transition.

Concluding, the presence of water molecules induces several differences in the structural properties of the sample compared with those of PDMAEMA in the dry state and in THF mixture. *i)* First, water molecules tend to join together giving rise to clusters, as evidenced by neutron diffraction and confirmed by X-ray diffraction. *ii)* As a consequence, the distances between nano-domains become larger than in PDMAEMA and PDMAEMA/THF samples. *iii)* The presence of water clusters leads to a non-uniform hydration of the polymer. This would explain the stronger heterogeneity suggested by the fitting curve in the Q range from 0.6 to 1.0 Å^{-1}. *iv)* The diffraction pattern in the Q-range $\sim$ 1–2 Å^{-1} shows the temperature dependence reported for water confined in other systems in the literature, suggesting a change in the water-water interactions and an extra finite size effect upon the vitrification of the polymer matrix.

CHAPTER

4

INFLUENCE OF PLASTICIZERS IN THE DYNAMICS OF THE POLYMER COMPONENT (30 WT%-SOLVENT CONCENTRATION)

In this chapter, the influence of plasticizers on the dynamical processes of PDMAEMA –α-relaxation, local motions of the side group and methyl group rotation– will be discussed. Dielectric spectroscopy and neutron scattering techniques were used to investigate the polymer dynamics. This combination consented to explore the samples over a wide range in frequency (DS) and, by using deuterated solvents (NS), to 'isolate' the polymer dynamics in the mixtures. As commented in the Introduction, THF and water were chosen with the purpose of elucidate the role of the H-bonds on the dynamical changes (due to their different interactions with the polymer).

4.1 Experimental Details

Sample

Polymer as received was annealed for 7 h at T = 373 K under vacuum to evaporate possible trapped solvent, while the mixtures containing 30 wt% of solvent were prepared by mixing the dry polymer with the appropriate amounts of THF, dTHF, H_2O or D_2O (Sigma Aldrich) during a few days. Dielectric spectroscopy and differential scanning calorimetry (DSC) experiments were performed on samples with protonated solvents, while those with deuterated solvents were used to isolate the polymer component in the neutron scattering experiments.

Sample	Instrument	incident wavelength (λ) (Å)(* analysing energy)	energy resolution (FWHM) (μeV)
PDMAEMA/*THF*	FOCUS	6.0	~ 45
	IRIS	6.65 *	17.5
	SPHERES	6.27 *	0.62
PDMAEMA/D_2O	TOFTOF	6.0	~ 48
	TOFTOF	7.0	~ 25
	SPHERES	6.27 *	0.62
PDMAEMA	TOFTOF	6.0	~ 55
	TOFTOF	8.0	~ 25

Table 4.1: Experimental configurations used for QENS measurements

Calorimetry and Dielectric Spectroscopy conditions

Broadband dielectric spectrometer Novocontrol Alpha-S and high frequency dielectric spectrometer Agilent E4991A RF-Impedance Analyzer were used to measure the complex dielectric function $\epsilon^*(\omega) = \epsilon^{'}(\omega) - i\epsilon^{''}(\omega)$, covering a frequency range of 10^{-2}-10^9 Hz. The samples were prepared forming a parallel-plate capacitor between parallel gold-plated electrodes with a diameter of 20 and 10 mm for low and high frequency measurements respectively. Measurements were carried out under isothermal conditions every 5 K with a temperature stability better than 0.1 K. The maximum temperature for the dry polymer (370 K) was chosen to avoid degradation, while for the plasticized samples we performed measurements up to 300 K to avoid a significant solvent evaporation. Differential scanning calorimeter was used to determine the glass transition temperature T_g of the samples (sample weights about 10 mg). Hermetic aluminium pans were used for all the samples. Modulated DSC measurements were performed on PDMAEMA, PDMAEMA/THF and PDMAEMA/H_2O with average heating rate of 3 K/min and amplitude of modulation $\pm$0.5 K with a period of $t_p = 60$ s.

Inelastic neutron scattering conditions

Complementary information on methyl-group dynamics is provided by the inelastic librational peaks contained in the vibrational density of states (VDOS). The VDOS of the hydrogens of the dry polymer and the plasticized polymer with dTHF and deuterated water were obtained from the inelastic neutron scattering (INS) data collected by using TOSCA. The dry sample was loaded in an aluminium foil sachet closed in a flat aluminium sample holder sealed by indium wire, while for the mixtures indium wire-sealed liquid cells were used. All samples were investigated at T = 10 K.

Quasielastic neutron scattering conditions

Four different spectrometers were used to carry out the QENS measurements: the direct-geometry time-of-flight instruments FOCUS and TOFTOF, the inverted-geometry time-of-flight spectrometer IRIS and the backscattering spectrometer SPHERES.

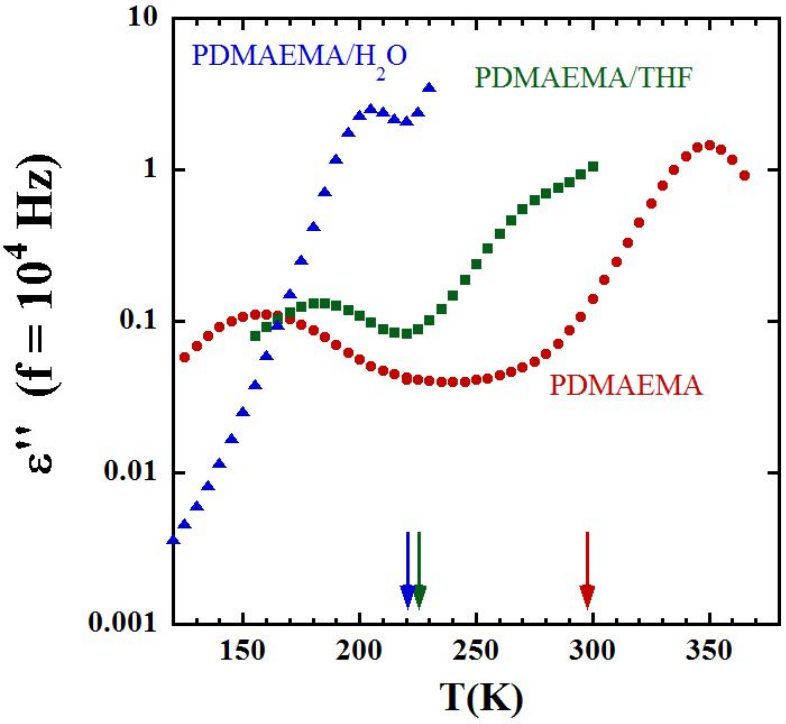

Figure 4.1: Isochronal curves of dielectric loss obtained for $f = 10^4\ Hz$. Blue triangles: PDMAEMA/H_2O; green squares: PDMAEMA/THF; red circles: PDMAEMA. Arrows show the locations of T_g determined from DSC (inflection point), T_g^{DSC}

.

Each sample was investigated using a combination of spectrometers and/or incident wavelengths (see Table 4.1), in order to cover a wide dynamic window. The time windows accessed were approximately from 10^{-13} to 10^{-9} s for the polymer in dTHF and deuterated water solutions and from 10^{-12} to 10^{-10} s for the dry sample. For all experiments, flat aluminium sample holders were used. For the samples in solution, the cells were sealed using indium wire to avoid solvent loss. The thicknesses of the sample holders were chosen in order to obtain a transmission close to 90% to neglect possible multiple scattering contributions. Vanadium in flat aluminum cell was measured at room temperature to correct the detector efficiency. All data were corrected for the sample holder contribution by subtracting the intensity scattered by an empty cell. The resolution function was determined measuring the samples at 10 K. Dry PDMAEMA and PDMAEMA/dTHF samples were investigated at T = 250 K, 270 K, 290 K, while the PDMAEMA/D_2O system was studied at T= 250 K.

4.2 Experimental Results

4.2.1 Calorimetry and Dielectric Spectroscopy

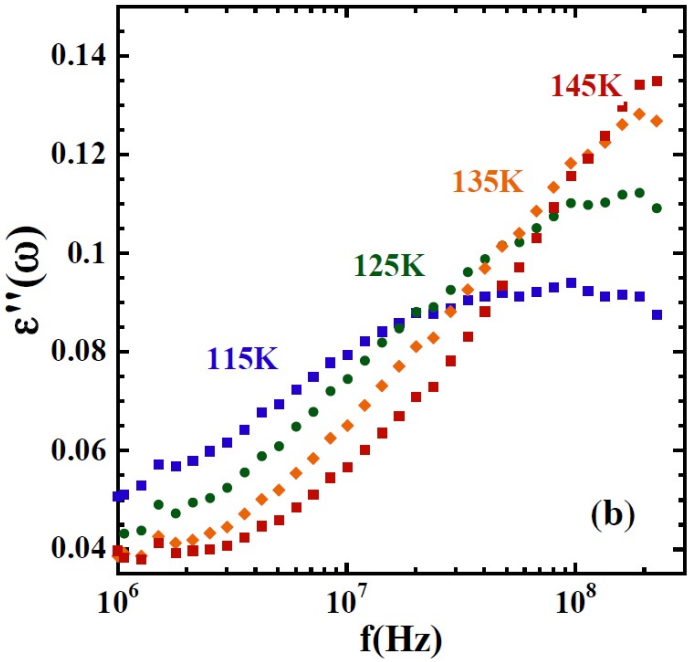

Figure 4.2: Dielectric loss measured on PDMAEMA/THF with Agilent E4991A RF-Impedance Analyzer at the different temperatures indicated

.

Dielectric spectroscopy measurements on dry PDMAEMA reveal two broad temperature-dependent processes (Fig. 4.1). The main peak, relevant at higher temperatures, is related to the segmental (α) relaxation while that at low temperature can be attributed to a secondary relaxation. Adding THF we observe a strong shift toward lower temperature of the main peak associated to the shift of T_g, as confirmed by DSC experiments (inflection point at T_g^{DSC}(PDMAEMA) = 299 K, $T_g^{DSC}(PDMAEMA/THF)$ = 227 K). The secondary relaxation peak in PDMAEMA/THF appears slightly shifted ($\sim$ 20 K) toward higher temperature with respect to that in bulk. We note that these data result from the combined contributions of the two components in the system (polymer/THF). In PDMAEMA/H_2O only an intense peak in the low temperature region is present. This peak is related to the dynamics of water molecules and seemingly covers the polymer secondary relaxation due to the high signal given by the strong water dipole moment. At high temperature it is not possible to distinguish the segmental relaxation in this sample due to the huge conductivity contribution. Finally, high-frequency measurements on THF mixture reveal a further process (Fig. 4.2).

4.2.2 Inelastic Neutron Scattering

Due to the high value of the hydrogen incoherent cross section, the neutron intensity scattered by all the samples is basically due to the incoherent scattering contribution

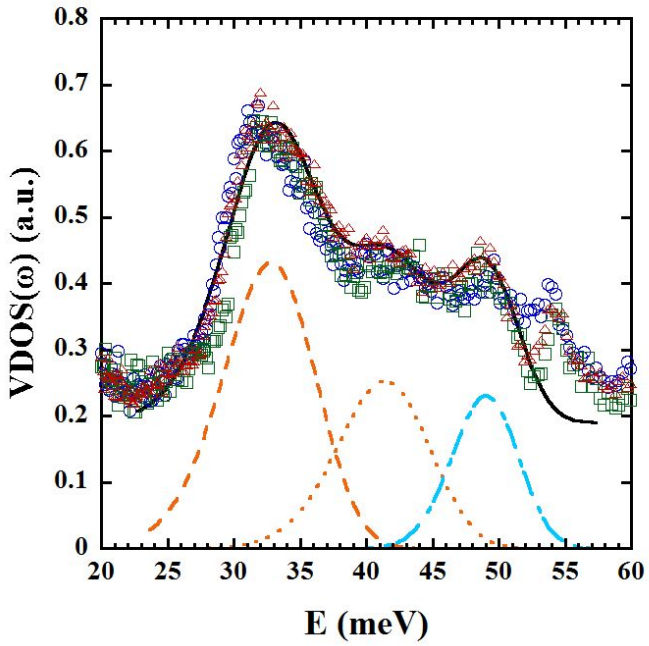

Figure 4.3: H-weighted vibrational density of states of PDMAEMA in the dry state (red triangles), and in the mixtures with *d*THF (green circles) and with D_2O (blue squares) at T = 10 K. The intensities of the mixtures have been scaled to match that of dry PDMAEMA. Solid line is a fit with the different contributions indicated by the dotted, dashed and dashed-dotted lines (see the text).

from PDMAEMA hydrogen atoms. TOSCA results on the three samples are shown in Fig. 4.3. In the energy range from 20 to 53 meV, we observe three peaks. The strongest peak is found at lower energy. Comparing the data of the three samples, we do not find any significant difference, e. g. an energy shift or an extra broadening.

4.2.3 Quasielastic Neutron Scattering

For the ulterior analysis of the QENS results, data were transformed into time domain, following a procedure which allows deconvolution of data from the instrumental resolution, thereby facilitating the combination of results from different spectrometers. Experimental intermediate scattering functions $S^{exp}(Q,t)$ were obtained by Fourier transforming to time domain the QENS data obtained at a given temperature and Q-value on each spectrometer. These functions were deconvoluted from the resolution function dividing them by the corresponding $S^{exp}(Q,t)$ obtained from the spectrum measured at 10 K. Figure 4.4 shows as an example the such obtained final intermediate scattering functions of PDMAEMA hydrogens in the PDMAEMA/dTHF sample for some representative Q-values and two different temperatures. As can be seen, by applying this procedure to data measured on three spectrometers (FOCUS, IRIS and SPHERES in this case), almost three decades in time are covered.

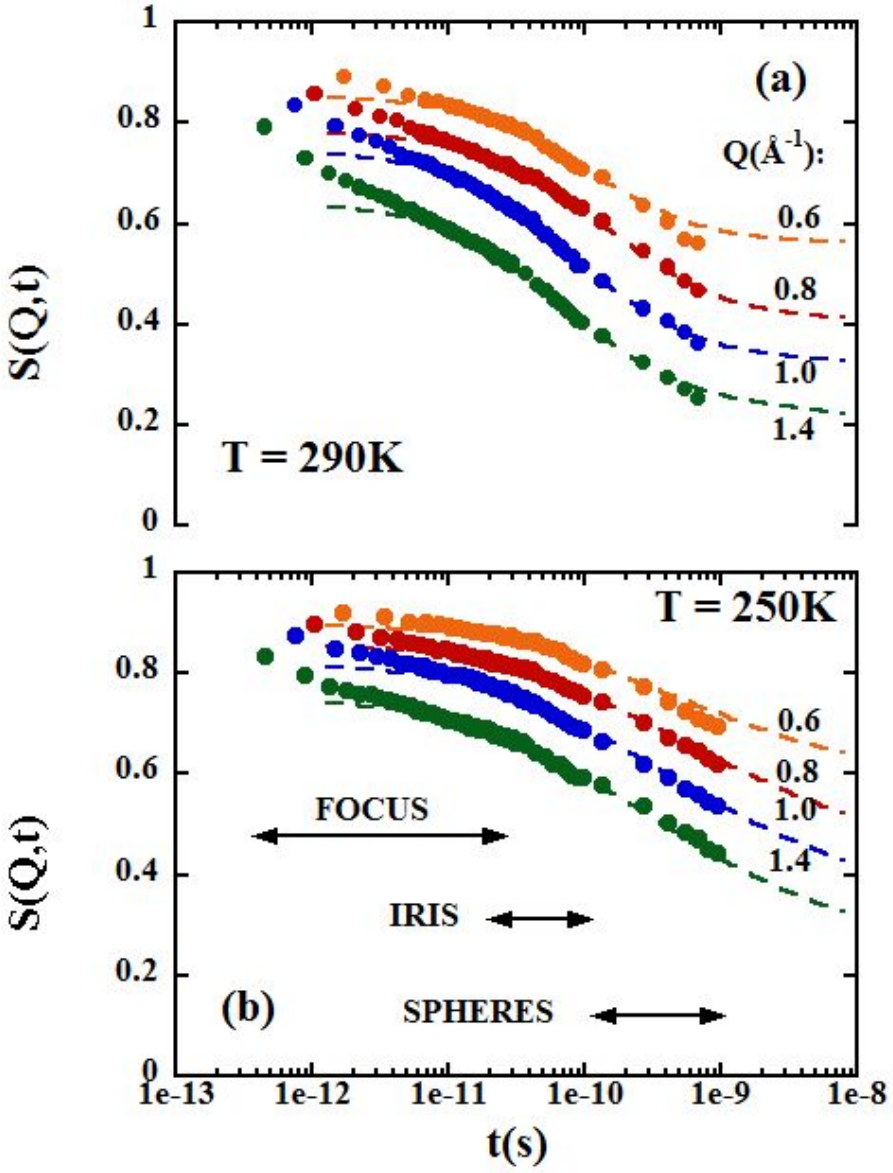

Figure 4.4: Intermediate scattering function of H-atoms of the polymer component in the PDMAEMA/dTHF sample at T = 290 K (top) and T = 250 K (bottom) and the different Q-values indicated. The dashed lines show the fits with the model described in the text.

The intermediate scattering functions show more pronounced decays at higher temperatures, with a tendency to reach a plateau in the long-time regime. For a given temperature, the characteristic time for the decay does not show a clear Q-dependence. These features suggest the occurrence of spatially localized motions in the window investigated.

4.3 Modellization and Data Analysis

4.3.1 Dielectric Spectroscopy

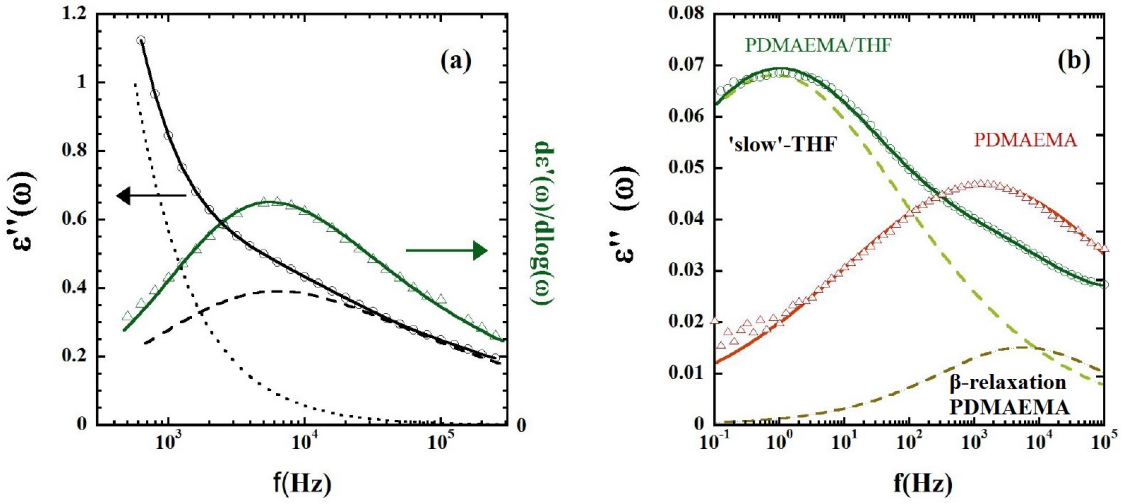

Figure 4.5: **a**)DS results at high temperature (T=270 K) showing the α-relaxation contribution of PDMAEMA/THF mixture. Circles show the experimental $\epsilon''(\omega)$ described by the imaginary part of Eq. 4.1 (continuous line). Dashed line represents HN function and dotted line the conductivity contribution. Triangles show the derivative $\partial\epsilon'(\omega)/\partial log(\omega)$ fitted by Eq. 4.2 (continuous line). **b**) Results on PDMAEMA/THF (circles) and the dry polymer (triangles) at 130 K, in the glassy state. For comparative purposes, bulk polymer data have been multiplied by 0.7 in order to take into account the amount of polymer in the mixture. The dashed lines show the two Cole-Cole components used to describe PDMAEMA/THF data.

In the high temperature region above the glass-transition temperature, polymer motions are dominated by the α-relaxation. In such regime, the dielectric permittivity of polymers can usually be fitted with the sum of the contributions from the α-relaxation (described by a Havriliak-Negami function) and the conductivity:

$$\epsilon^*(\omega) = \epsilon^{'}(\omega) - i\epsilon^{''}(\omega) \; = \; \epsilon_\infty + \frac{\Delta\epsilon}{[1+(i\omega\tau_{HN})^\alpha]^\beta} - i\frac{\sigma_0}{\epsilon_0\omega} \tag{4.1}$$

Here, ϵ_∞ is the high-frequency limit permittivity, $\Delta\epsilon$ is the dielectric strength, τ_{HN} is the characteristic relaxation time, α and β are the shape parameters of the α-process, σ_0 is the DC conductivity and ϵ_0 is the vacuum permittivity. Usually the data analysis is performed on the imaginary part of the permittivity $\epsilon^{''}(\omega)$, where the relaxation process leads to a peak. However, adding THF, it is not possible to

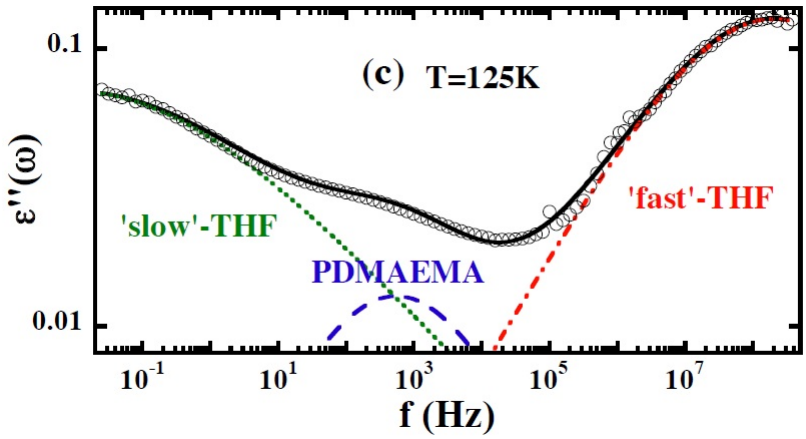

Figure 4.6: Dielectric loss measured on PDMAEMA/THF at T=125 K. Solid line is the description in terms of the three Cole-Cole contributions represented by the dashed ('slow' THF-process), dotted (PDMAEMA β-relaxation) and dashed-dotted ('fast' THF-process) curves.

clearly resolve the high temperature process (α-relaxation of the polymer) from the large conductivity contributions to $\epsilon^{''}(\omega)$ (see, e.g, Fig. 4.5(a)). Therefore, the data analysis was carried out on the real part of $\epsilon^{*}(\omega)$, $\epsilon^{'}(\omega)$, where conductivity does not contribute. In particular, we considered the derivative of $\epsilon^{'}(\omega)$ with respect to $\log(\omega)$, since this function displays a maximum at similar frequency as the $\epsilon^{''}(\omega)$ relaxational counterpart. Thus, the characteristic time τ_{max}, defined as the inverse of the frequency ω_{max} at the $\epsilon^{''}(\omega)$-peak, $\tau_{max} = 1/\omega_{max}$, was calculated for both PDMAEMA and PDMAEMA/THF samples by fitting:

$$\frac{\partial\epsilon'(\omega)}{\partial\log\omega} \propto \Re\left[\frac{(i\omega\tau_{HN})^{\alpha}}{[1+(i\omega\tau_{HN})^{\alpha}]^{\beta+1}}\right] \tag{4.2}$$

and using the relationship:

$$\tau_{max} = \tau_{HN}\left[\frac{\sin(\frac{\alpha\beta\pi}{2+2\beta})}{\sin(\frac{\alpha\pi}{2+2\beta})}\right]^{1/\alpha} \tag{4.3}$$

An example of the quality of the fit is shown in the left panel of Fig. 4.5 for PDMAEMA/THF results. Due to the high conductivity produced by water molecules, it is not possible to observe the structural relaxation of PDMAEMA in aqueous solution even using the representation $\partial\epsilon'(\omega)/\partial\log(\omega)$. Figure 4.7(a) shows the inverse-temperature dependence of the relaxation times obtained for the α-process of dry PDMAEMA and PDMAEMA/THF samples. The curvature clearly shows the non-Arrhenius character expected for the dynamics in the supercooled liquid state. The curves were fitted with the usually invoked Vogel-Fulcher-Tammann (VFT) equation:

$$\tau = \tau_0 \exp\left(\frac{B}{T-T_0}\right) \tag{4.4}$$

VFT parameters are shown in Table 4.2. As we have already mentioned in the Introduction, the fragility index m, describing how fast dynamics change approaching

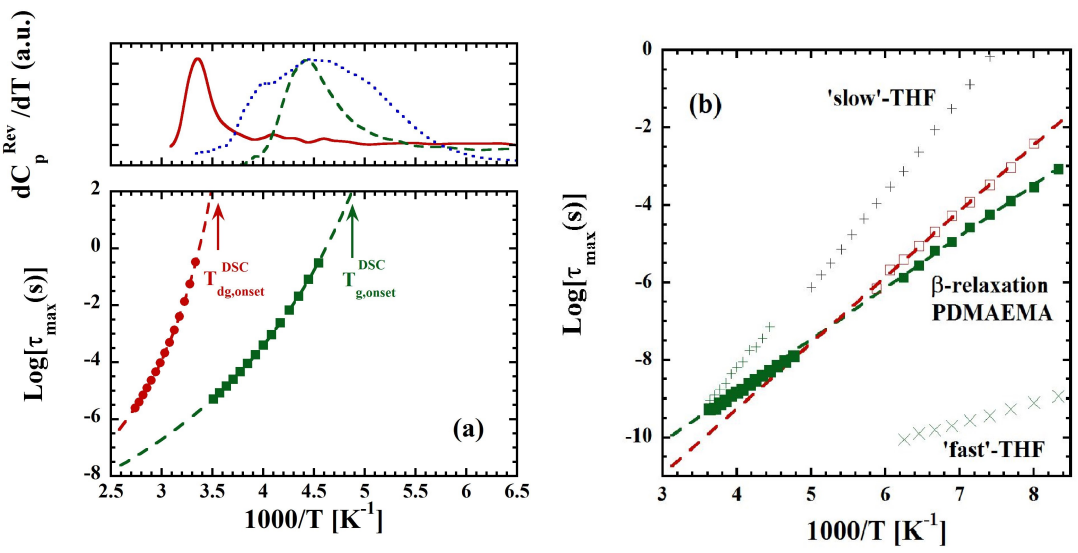

Figure 4.7: **a**) Top: Temperature derivative of the reversible specific heat of PDMAEMA (red solid line), PDMAEMA/THF (green dashed line) and PDMAEMA/H_2O (blue dotted line). Arrows mark the position of the onset temperature for the DSC glass transition. Bottom: Inverse temperature dependence of the characteristic times of the α-relaxation obtained from DS. Red circles represent data from PDMAEMA in the dry state, while green squares in the mixture with THF. Dashed lines are fits with the VFT expression (Eq. (4.4)). **b**) Relaxations attributable to the polymer component in the dry state (empty red squares) and in PDMAEMA/dTHF (filled green square). Crosses correspond to 'slow' and 'fast' THF components.

the glass transition temperature, is mathematically defined as:

$$m = \left.\frac{\partial \log\tau}{\partial(T_g/T)}\right|_{T=T_g} \tag{4.5}$$

We calculated this index starting from VFT results and defining $T_g = T_g^{DS}$ as the temperature at which the relaxation time reaches a value of $\tau = 100\ s$. The T_g^{DS} values of PDMAEMA in the dry state and in the mixture with THF are shown in Table 4.2, in comparison with the values deduced from DSC measurements. This table also includes the such obtained values of the fragility index.

The spectral shape of the α-process differs, as usually found, from that of a single Debye process. The width of this relaxation is represented as function of the characteristic time in Fig. 4.8(a) for both systems.

At lower temperatures –below T_g– only local motions leading to secondary relaxations are expected to take place. In Fig. 4.5(b) spectra of dry PDMAEMA and PDMAEMA/THF are shown at $T = 130$ K. The dry sample shows a broad and nearly symmetric peak –the polymer β-relaxation– suggesting a distribution of mobilities. In order to describe this contribution, a Cole-Cole function was used:

$$\epsilon^*_{CC}(\omega) = \epsilon_\infty + \frac{\Delta\epsilon}{[1 + (i\omega\tau_{CC})^{\alpha_{cc}}]} \tag{4.6}$$

	PDMAEMA	PDMAEMA/THF	PDMAEMA/H_2O
$\log(\tau_0(s))$	-11.7 ± 0.1	-11.4 ± 0.1	-
B(K)	1666 ± 6	1881 ± 6	-
T_o(K)	231.1 ± 0.3	142.0 ± 0.3	-
T_g^{DS}(K)	287 ± 1	204 ± 1	-
T_g^{DSC}(K)	299 ± 1	227 ± 1	220 ± 3
m	148	95	-
$T_{g,onset}^{DSC}$(K)	285 ± 1	205 ± 1	176 ± 1

Table 4.2: Vogel-Fulcher-Tammann parameters of the characteristic time of the α-relaxation and fragility index of PDMAEMA in the dry state and with THF. T_g values determined from DS and DSC are also given for the three systems. For DSC, values correspond to the inflection point of the $C_p(T)$ (T_g^{DSC}) and to its onset ($T_{g,onset}^{DSC}$)in the heating ramp.

with τ_{CC} ($\equiv \tau_{max}$) the Cole-Cole characteristic relaxation time and α_{CC} the shape parameter. In PDMAEMA/THF three dynamic processes can be distinguished in this temperature range; therefore, a combination of three Cole-Cole functions was used in the fitting procedure (see the contributions as dashed lines in Fig. 4.5(b) and as dashed-dotted and dotted lines in Fig. 4.6). The characteristic times obtained from such description of the dielectric results of PDMAEMA in the dry state and in the mixture are shown in Fig. 4.7(b).

At this point, we discuss on the origin of the different secondary relaxations observed in PDMAEMA/THF mixture (see Fig. 4.5(b)–4.7(b)). Based on the strong intensity of the process at lower frequency, it has to be attributed to a relaxation involving THF molecules. A similar process has been reported for mixtures of THF with tristyrene [58]. In the other extreme, the process occurring at highest frequencies is absent in the dry polymer and in the aqueous mixture. Therefore, we can relate this dynamics to THF molecules. Thus, we will refer to these processes as 'slow'-THF and 'fast'-THF processes respectively. They will be analysed in detail in the next chapter. To interpret the origin of process at intermediate frequencies, in Fig. 4.5(b) we have included the β-relaxation results obtained for the dry polymer at the same temperature, properly weighted in order to represent the expectation for the β-contribution of the polymer –if it were unaffected by the presence of the solvent– in the permittivity loss measured on the mixture with THF. The characteristic time of this contribution is rather close to that corresponding to the high-frequency process in THF mixture. We thus may identify such a process in PDMAEMA/THF as the β-relaxation of the polymer component. We note, however, that this relaxation is affected by the presence of THF molecules.

As expected for thermally activated processes, the relaxation times characteristic for the sub-T_g relaxations follow an Arrhenius temperature dependence:

$$\tau = \tau_o \exp\left(\frac{E_a}{k_B T}\right) \tag{4.7}$$

with the parameters shown in Table 5.1.

Symmetric broadening of spectra can be attributed to the presence of distributions of relaxation times in the glassy state due to the disorder. We may consider

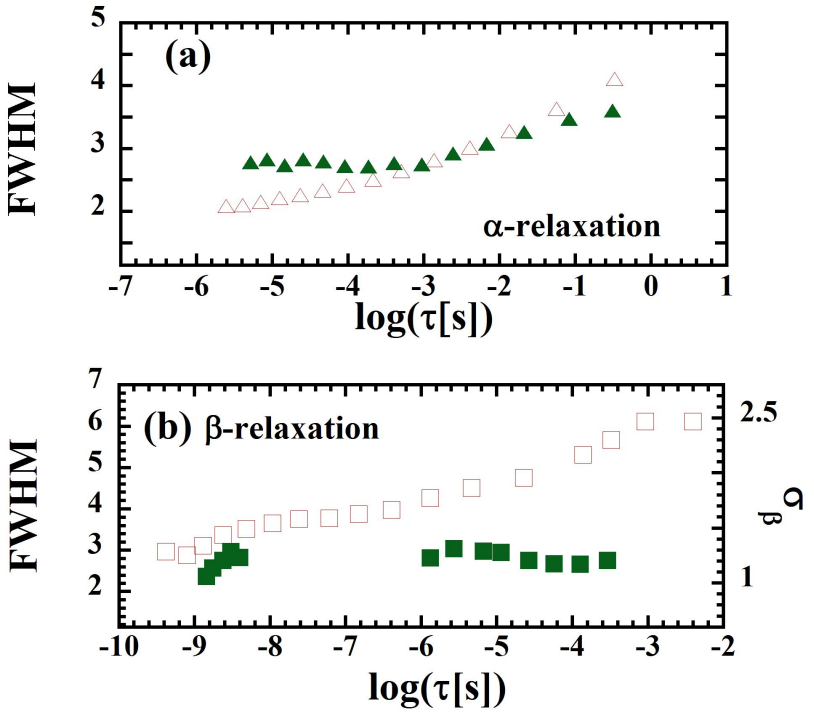

Figure 4.8: Full width at half maximum of loss peak corresponding to the α-relaxation (a) and β-relaxation (b) of the polymer as function of the characteristic time. Empty symbols refer to dry PDMAEMA, while filled symbols to PDMAEMA/THF. In (b), the scale on the right shows the equivalent width of the corresponding Gaussian distribution of relaxation times σ_β.

the logarithmic relaxation times distributed according to a Gaussian function:

$$h[log(\tau)] = \frac{1}{\sqrt{2\pi\sigma^2}} \exp\left(-\frac{\left[\log(\tau) - \overline{\log(\tau)}\right]^2}{2\sigma^2}\right) \tag{4.8}$$

Here, $\overline{log(\tau)}$ is the average logarithm of the characteristic time (position of the maximum of the distribution function), $\overline{log(\tau)} \equiv log(\tau_{CC})$. For the β-process, the width of such distribution (we shall call it σ_β) has been calculated starting from the shape parameter α_{CC} of the Cole-Cole function by the empirical equation:

$$\sigma_\beta = \frac{6.9 \times 10^{-4}}{\alpha_{CC}^4} - 3.8163 \log(\alpha_{CC}) \tag{4.9}$$

This equation resulted from the CC fit of the loss-curves generated with a superposition of Debye relaxations according to Eq. 4.8 for various σ-values in the range from 0.1 to 0.5. The so-obtained results are represented in Fig. 4.8(b) as function of the characteristic time.

	dry PDMAEMA	PDMAEMA/THF
$\log[\tau_o(s)]$	-16.1 ± 0.1	-14.1 ± 0.2
E_a(meV)	337 ± 5	262 ± 5

Table 4.3: Arrhenius parameters of the characteristic time of the β-relaxation of PDMAEMA in dry state and in THF mixture

4.3.2 Methyl Groups Dynamics

In its monomer PDMAEMA contains three methyl groups of two different kinds –two located at the end of the side group (SG-MG) and one directly linked to the main chain (MC-MG)–. In Chapter 3, it has been illustrated that in the glassy state of polymeric materials the interaction between the methyl group and its environment is often well approximated by an effective threefold rotational potential[77] . The associated lowest librational transitions E_{01}, E_{02} assume values typically in the range 10-60 meV and can be directly detected by INS. Thus, investigating the librational energies of the polymer methyl groups provides a straightforward mean –usually easier than studying the classical rotational hopping times at higher temperatures– to extract information about the potential barrier V_3. We recall the relationship between E_{01} and V_3 (Eq. 2.96). The polymer methyl groups dynamics were thus investigated identifying and characterizing the librational peaks in the VDOS revealed by TOSCA (see Fig. 4.3). In all cases, the VDOS presents a pronounced and relatively broad peak centred at about 33 meV followed by other less intense peaks. The first two peaks are in the energy range where the first librational transition usually manifest [77]. We may assume that they correspond to the two kinds of methyl group in PDMAEMA. At first sight, one can realize that the effect of plasticizers on these peaks, if any, is negligible. To describe the data we invoked the rotational rate distribution model [82, 100, 77] that assumes a Gaussian distribution of potential barriers:

$$g(V_3) \;=\; \frac{1}{\sqrt{2\pi}\sigma_{V_3}}\exp\left[-\frac{(V_3-\overline{V_3})^2}{2\sigma_{V_3}^2}\right] \tag{4.10}$$

Here, $\overline{V_3}$ is the average value of the potential barrier and σ_{V_3} the standard deviation of the distribution. Via Eq. 2.96, the distribution of barriers translates in the following distribution of librational energies:

$$F(E_{01}) \;=\; \frac{1.82}{0.47}E_{01}^{0.8}\frac{1}{\sqrt{2\pi}\sigma_{V_3}}\exp\left(\frac{-\left((\frac{E_{01}}{0.47})^{1.82}-(\frac{\overline{E_{01}}}{0.47})^{1.82}\right)^2}{2\sigma_{V_3}^2}\right) \tag{4.11}$$

The parameters characterizing the underlying distributions of potential barriers were obtained from the two first peaks in the VDOS, which were attributable to the first librational energies of the two kinds of methyl groups. We described this range of the VDOS with the superposition of two functions expressed by Eq. 4.11 and weighted by pre-factors, plus a flat background; we also included in the fitting function an additional broadened peak to account for the third maximum, in order to take into account possible contributions of this peak in the high-energy flank of the second one. The result of such fitting procedure for the data on the dry sample is the solid line in Fig. 4.3. The parameters deduced for the two first peaks on all samples are

shown in Table 4.4. The area of the first peak was about two times the area of the second one. Considering the two kinds of methyl groups in PDMAEMA, we can relate the former to the librations of the methyl groups of the side chain (SG-MG), and the latter to the libration of the methyl group of the main chain (MC-MG). We note that the outcome of these TOSCA results is crucial for the analysis of QENS data, since it provides valuable information about the dynamics of the methyl-group rotations contributing to the quasielastic signal in the temperature range investigated, allowing thereby fixing quite a number of parameters in the model function used in the QENS analysis.

Table 4.4: Parameters characterizing the methyl-group dynamics of dry PDMAEMA and PDMAEMA in mixtures with $dTHF$ and with D_2O obtained from TOSCA experiments.

Parameters	First Peak			Second Peak		
	Dry	THF	D_2O	Dry	THF	D_2O
$\overline{E_{01}}$(meV)	33.03	33.4	32.2	41.3	41.9	40.08
σ_{V_3}(K)	410	390	435	455	435	505
$\overline{V_3}$(K)	2293	2344	2193	3449	3541	3374

4.3.3 Intermediate Scattering Functions

The function accessed by QENS is mainly dominated by the incoherent scattering function from all the hydrogens in the sample. This is obtained from the superposition of the individual hydrogens as: $S(Q,t) = N^{-1}\sum_{\alpha=1}^{N} S_\alpha(Q,t)$ (in the following, we will skip the label 'inc'), where the index α refers to the kind of hydrogen in the PDMAEMA component. So, α can be: main-chain methylene hydrogen (MC-ME) (2 hydrogens out of 15 per monomer unit); main-chain methyl-group hydrogen (MC-MG) (3 out of 15); side-group methylene hydrogen (SG-ME) (4 out of 15) or side-group methyl-group hydrogen (SG-MG) (6 out of 15). At the temperatures where QENS experiments were performed, molecular motions are expected to be spatially localized. As shown in Chapter 2, the intermediate scattering function describing a localized motion is given by:

$$S(Q,t) \;=\; A\,[EISF + (1 - EISF)\phi(t)] \tag{4.12}$$

The pre-factor A parametrizes the fast contributions (fast motions like vibrations leading to the decay of correlations at times shorter than those accessible by the instruments). For sake of simplicity, we assumed this vibrational parameter to be the same for all hydrogen atoms in PDMAEMA. The information about the geometry of the local motion is given by the elastic incoherent structure factor (EISF), while the dynamic information (time dependence) is contained in the function $\phi(t)$ (further information can be found in Chapter 2). Due to the heterogeneities of the amorphous systems investigated, in the general case we expect $\phi(t)$ to result from a distribution of single exponential functions:

$$\phi(t) \;=\; \int h[log(\tau)]\exp(-t/\tau)\mathrm{d}log(\tau) \tag{4.13}$$

Now we define the model functions for each kind of hydrogen in our polymer.

(i) *Main-chain hydrogens*:

(i.a) *Main-chain methylene hydrogens.* Given the temperature range investigated, we assumed that segmental motions are completely frozen. This implies that main-chain methylene hydrogens only vibrate around their equilibrium positions leading to an elastic contribution, i. e., $S_{MC-ME}(Q,t) = A$.

(i.b) *Main-chain methyl-group hydrogens.* As for the MC-ME hydrogens, we assume that motions related to segmental relaxation are frozen. However, MC-MG hydrogens may display an additional mobility, namely rotations. From the analysis of TOSCA results (second peak of the VDOS) we have deduced a value of the average potential barrier for main-chain methyl group rotations $\overline{V_3}$ of about 3500 K (see Table 4.4). This implies that in the temperature range here considered, these hydrogens undergo stochastic jumps (rotations) among the three equivalent positions in the 3-fold potential. The scattering function for such motion is given by Eq. 4.12 with

$$EISF_{MG} = \frac{1}{3}\left(1 + 2\frac{\sin(Qr_{HH})}{Qr_{HH}}\right) \tag{4.14}$$

being $r_{HH} = 1.78$ Å the distance between hydrogens in a MG. The time dependence $\phi(t)$ in Eq. 4.12 was fixed from TOSCA results, since they provide full information about the distribution of potential barriers $g(V_3)$ which finally translate in a distribution of rotational rates. The activation energy of stochastic jumps is related with the barrier via Eq. 2.96. Using this relationship, the distribution function of activation energies $H(E_a)$ was calculated from the $g(V_3)$ deduced by the TOSCA analysis [Eq. 4.10]. The obtained curve $H(E_a^{MG})$ was then fitted by a Gaussian distribution in order to calculate its width and average value ($\sigma_{E_a^{MG}}$ and $\overline{E_a^{MG}}$). The characteristic time corresponding to a given activation energy is expressed as:

$$\tau_{MG} = \Gamma_\infty^{-1}\exp\left(\frac{E_a^{MG}}{k_B T}\right) \tag{4.15}$$

Thus, a Gaussian $H(E_a^{MG})$ translates into a log-normal distribution of characteristic times $h[\log(\tau_{MG})]$ [Eq. 4.8] with a width $\sigma_{MG} = (\sigma_{E_a^{MG}} log(e))/(k_B T)$ and $\overline{\log(\tau_{MG})}$ defined from Eq. 4.15 with $E_a^{MG} = \overline{E_a^{MG}}$. For the Γ_∞ parameter the value $\Gamma_\infty =$ 5 meV, typically found in polymers [77], was chosen. We note that by fixing this value of Γ_∞, all parameters involved in the scattering function of MC-MG hydrogens were fixed (except the common pre-factor A).

(ii) *Side-group hydrogens.* By dielectric spectroscopy we have detected and characterized a secondary (β) relaxation related to the polymeric component. The reorientational motions of the dipole moment –located in the side-group– giving rise to this relaxation, could then be attributed to dynamical processes involving the side-group atoms in PDMAEMA. We would then expect that the dynamic function describing the time evolution of the localized atomic motions underlying the β-process –we shall call it $\phi_{SG}(t)$– could reflect the distribution of mobilities observed by dielectric spectroscopy (i. e., Eq. 4.13 with Eq. 4.8 and Eq. 4.9). We thus have assumed for this function $\phi_{SG}(t)$ a distribution of exponentials corresponding to a Gaussian distribution of $\log(\tau_{SG})$. Regarding the EISF characterizing these localized processes, a plausible geometry would be that of a confined motion on a

disc of radius R:

$$EISF_{SG} = \frac{1}{6}\Big(1 + 2j_0(QR) + 2j_0(QR\sqrt{3}) + j_0(2QR)\Big) \tag{4.16}$$

This kind of geometry was found to work describing the incoherent scattering function of hydrogens in polyethylene [101] (PE). The spatial extent of the motion – parametrized by the radius R– would depend on the particular kind of hydrogens within the side-group (note that all hydrogens in the side-group shall participate in this process).

(ii.a) *Side-group methylene hydrogens.* These atoms are assumed to undergo vibrations and the above-described side-group motions within a disc. We found that a suitable value for R was 3 Å, which is rather close to that reported for hydrogen motions in semicrystalline PE [101] .

(ii.b) *Side-group methyl-group hydrogens.* In this case, we estimated that the radius of the disc is determined by the distance between the centers of mass of the methyl groups (this distance is 3.3$\mathring{A}$). That is, $R = r_{SG-MG} = 1.65$ Å. Moreover, we considered the contribution of the methyl group rotations. The scattering function corresponding to this motion was constructed in an analogous way as above described for the MC-MG hydrogens, based on the TOSCA results of the first librational peak. Assuming simultaneous occurrence of both localized motions (side-group localized motions on a disc and rotations around the corresponding methyl carbon), the total intermediate scattering function for SG-MG hydrogens was built as the product of the two functions corresponding to these individual processes. Summarizing, the model intermediate scattering function used to describe the QENS results was:

$$\begin{aligned} S(Q,t) = A\{ & \frac{2}{15} + \frac{3}{15}\left[EISF_{MG} + (1 - EISF_{MG})\phi_{MG}^{MC-MG}(t))\right] + \\ & + \frac{4}{15}\left[EISF_{SG}^{SG-ME} + (1 - EISF_{SG}^{SG-ME})\phi_{SG}(t))\right] + \\ & + \frac{6}{15}\left[\left(EISF_{SG}^{SG-MG} + (1 - EISF_{SG}^{SG-MG})\phi_{SG}(t))\right) * \right. \\ & \left. * \left(EISF_{MG} + (1 - EISF_{MG})\phi_{MG}^{SG-MG}(t))\right)\right] \} \end{aligned} \tag{4.17}$$

In the fitting procedure with Eq. 4.17 we fixed all the parameters characterizing the geometry of the motions of the hydrogens of PDMAEMA, as well as the time dependence of the methyl group rotations from the TOSCA data analysis. Thus, the only free parameters left were A, and σ and $\overline{\log(\tau)}$ in $\phi_{SG}(t)$. We started with the case of the PDMAEMA/dTHF mixture where QENS data are of the best quality (wider dynamic window and T-range and time-scale of localized SG-motions better centred in the QENS window).

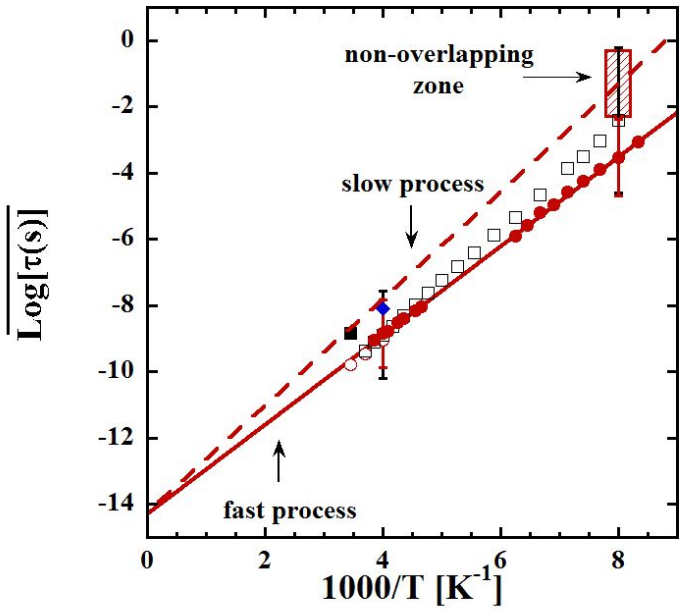

Figure 4.9: Arrhenius plot of the relaxation times of the polymer component revealed by DS in THF mixture (red filled circles) and dry PDMAEMA (empty squares). The Q-averaged QENS results are represented as empty circles for PDMAEMA/dTHF, blue diamond for PDMAEMA/D_2O and filled square for dry PDMAEMA. In these fits, Eq. 4.17 was used (f=1 in Eq. 4.19 has been assumed (see the text)). Solid line is an Arrhenius fit of the DS data of PDMAEMA in the mixture with THF, which is assumed to represent the fast component of the β-relaxation in the dry system. Dashed line is the deduced slow component of this process (see the text). Bars represent the width of the distribution function deduced from the values of the FWHM shown in Fig. 4.8(b).

At 250 K, the width of the distribution of the relaxation times of side-group motions was fixed imposing the σ_β obtained from dielectric spectroscopy results on the β-process (see Fig. 7(b)). The only free parameters were then the pre-factor A and the average characteristic time for the localized motion of hydrogens underlying the β-relaxation. The curves obtained by this fitting protocol match very well the data at times longer than approximately $\sim$ 10 ps, as shown in Fig. 4.4(b). Obviously, the fast contributions cannot be well parametrized by a simple pre-factor for times shorter than this value. The values obtained for the average logarithm of the characteristic time for the side-group motion [$\overline{\log(\tau)}$ in Eq. 4.8] are displayed in Fig. 4.10 as function of Q. They are practically Q-independent, as it would be expected for a localized motion. The resulting Q-averaged value $< \overline{\log(\tau)} >_Q$ agrees very well with the DS time $\overline{\log(\tau_{DS})}$ (see Fig. 6(b)). Such a nice agreement fails at higher temperatures. At the highest T investigated (290 K), the data are not compatible with the broad distribution of characteristic times extrapolated from the lower-T DS data. Leaving also σ_β as free parameter in the fitting procedure (see fitting curves in Fig. 4.4(a)), we obtained a markedly lower σ_β value ($\sim$0.48 vs 1.03). Regarding the characteristic time, we also found a nearly Q-independent behaviour. The resulting value $< \overline{\log(\tau)} >_Q$ (shown in Fig. 4.9 as empty circles) is nearly indistinguishable from that extrapolated from DS study. At 270 K, taking into account this result, we fixed the value of σ_β to that interpolated between those used at 250 K and 290 K ($\sigma_\beta = 0.75$, $T = 270K$). The resulting $< \overline{\log(\tau)} >_Q$ is included also in Fig. 4.9 showing a good agreement with DS results as well. For the dry polymer, we fixed the value of σ_β to that extrapolated from DS results. The obtained fitting curves describe reasonably well the data and are displayed in Fig. 4.11 for T=290 K. The value of $< \overline{\log(\tau)} >_Q$ for this temperature is included in Fig. 4.9 and is about a factor of 8 larger than that deduced from DS. In the case of the hydrated polymer, since no information about the dielectric β-relaxation is accessible due to the large water contribution, we fixed the σ_β value to that obtained by DS in the PDMAEMA/THF mixture. Figure 4.12 shows the good description of the incoherent scattering function achieved for the average value of the characteristic time displayed in Fig. 4.9. This characteristic time is significantly larger than that obtained for the mixture with THF.

4.4 Discussion

4.4.1 PDMAEMA α-Relaxation

We found, as usually reported [42, 44], a decrease of the glass transition temperature T_g of the polymer upon addition of solvents. This can be directly observed from the DSC investigation for the two mixtures (arrows in Fig. 4.1 and Fig. 4.7(a), top). The shift induced by both solvents is nearly the same, but the presence of water leads to a much broader signature of the glass transition (Fig. 4.7(a), top). This effect might be a consequence of the hydrogen bonds formed in the aqueous mixture. From the FWHM of the loss peak (Fig. 4.8(a)), we can see that the dielectric characterization of the PDMAEMA α-relaxation in the dry state reveals a strong dynamic heterogeneity at low temperatures, approaching T_g, that becomes less relevant as the temperature increases. In polymer mixture with THF, we observe an extra broadening at high temperature that could be associated to concentration fluctuations.

Regarding the T-dependence of the relaxation time, the polymer in the mixture with THF appears less 'fragile' in the Angell clasification [7] than in the dry system. As can be seen in Table.4.2, the parameter m drastically changes with THF addition, leading to a much less fragile behaviour. This observation is in agreement with typical plasticizing effects reported in literature (e.g. polyvinyl chloride (PVC) and PVC with dioctyl phthalate (DOP) [44], poly(vinyl methyl ether) PVME/H_2O [42]).

Now we focus on the changes induced in the glass-transition temperature of the polymer observed by DS and DSC. The shift deduced from DS analysis is 83 K, rather stronger than that obtained from DSC from the inflection point (i.e., from the maximum of the C_p^{Rev} derivative (see Fig. 4.7(a)). However, this apparent discrepancy between the observation by the two techniques disappears if we consider the onset temperature $T_{g,onset}^{DSC}$ (see Table 4.2 and Fig. 4.7(a) top). Noteworthy, the values of the glass-transition temperatures T_g^{DS} and $T_{g,onset}^{DSC}$ nearly coincide for both systems. This indicates that dielectric relaxation is very sensitive to the onset of the molecular motions involved in the glass-transition. In the particular case of PDMAEMA, this could be related with the fact that the dipole moment is mainly associated to the side-group. Such feature would also explain the above observed large broadening of the dielectric relaxation close to the glass-transition (~ 4 decades in both dry and mixture). Similar behaviour has been observed in other systems with bulky side groups like poly(n-alkyl methacrylates) (PnMAs) [102].

4.4.2 Methyl-Groups Dynamics

TOSCA experiments have allowed a detailed characterization of PDMAEMA methyl-group dynamics. The values of the average potential barrier and the widths of the distribution functions of the main-chain methyl-group are in the range of MC-MG in vinylic polymers as polyisobutylene (PIB) [103, 104, 105] , poly(α-methylstyrene) (PαMS) [106], and poly(methyl methacrylate) (PMMA) [106] . On the other hand, the values $\overline{E_a}$ for the side-group methyl group (SG-MG) rotations are lower than those of the MC-MG. This was also the case in PMMA (ester-methyl) [107, 108] and poly(ethyl methacrylate) (PEMA) [109] . The obtained results in the mixture quantitatively confirm that plasticization does not significantly produce either a shift of

the average value or an extra broadening of the distribution function of potential barriers.

4.4.3 Localized Side-Group Motions of PDMAEMA in the Glassy State

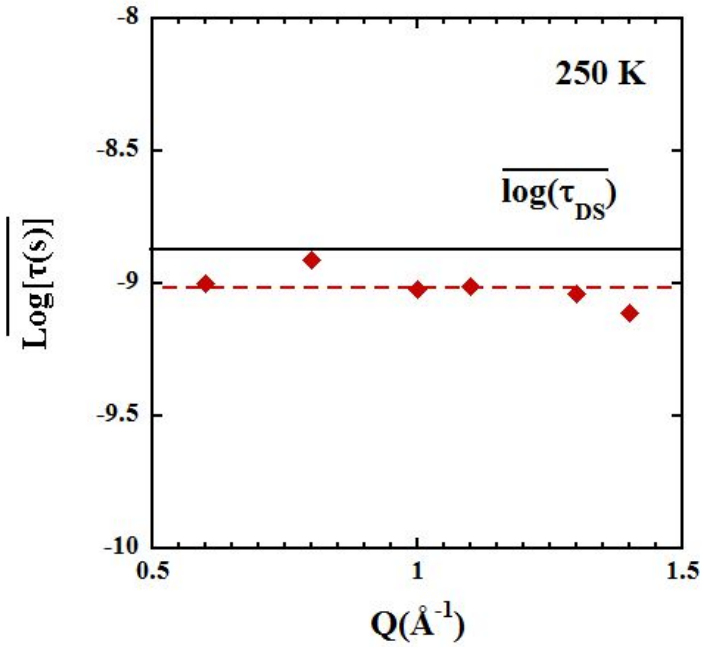

Figure 4.10: Momentum-transfer dependence of the average characteristic time associated to the local dynamics of side-group hydrogens in PDMAEMA in mixture with THF obtained from QENS at 250 K. Solid line indicates the result from the dielectric study on the β-relaxation at the same temperature. Dotted line shows the Q-averaged value of the QENS result $< \overline{\log(\tau)} >_Q$.

Dielectric spectroscopy reveals local motions under the so-called β-relaxation. A significant change of this process occurs in the presence of THF molecules. Polymer dynamics appear faster in THF solution and the apparent activation energy is affected by the presence of THF molecules (Table 5.1). Moreover, a strong reduction of the dielectric strength (Fig. 4.5(b)) and a narrowing of the characteristic relaxation times distribution (Fig. 4.8(b)) are found. These observations resemble the situation reported for PVC upon addition of DOP [44]. In that case, this was attributed, as in the case of Bisphenol-A Polycarbonate [48], to the presence of two distinct contributions (a fast and a slow component) to the dielectric β-relaxation of the neat polymer. At high temperature, the fast component would dominate the dipole reorientation, while, as the temperature decreases, the slow component would get more relevance. When comparing the results obtained for the dry polymer and in the mixture, we observe a rather good agreement at high temperature regarding both the characteristic time (points in Fig. 4.9) and the width of the distribution

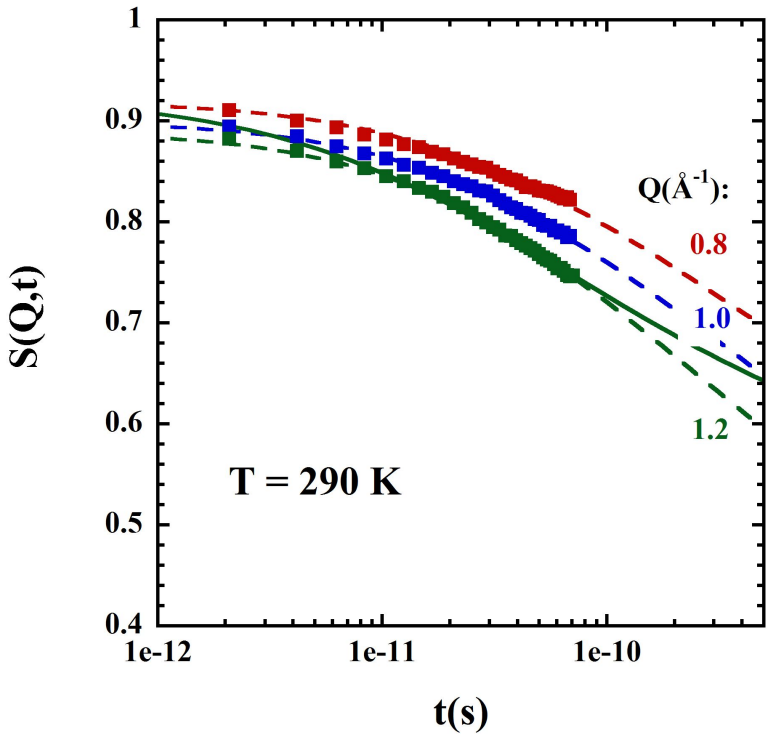

Figure 4.11: Intermediate scattering function of PDMAEMA hydrogens in the dry sample at T=290K and the different Q-values indicated described by Eq. 4.17 (dashed line). Solid line is the description of the highest-Q results by assuming a fraction of slow atoms (see the text).

(bars in Fig. 4.9). On the contrary, at low T the distribution in the mixture remains about the same as at high T, while in the dry polymer a much broader distribution is found. In addition, the average time of such distribution is larger in the dry polymer than in the mixture. These results could be rationalized on the basis of the existence of two components in the dry system. At high T the fast component would dominate in both samples. At low T, the β-process in the mixture would reflect only the fast component (with similar distribution width as at high T). This suggests to identify the fast component of the β-relaxation in the dry polymer with the single process detected in the mixture. Therefore, it would be characterized by the parameters shown in Table 5.1 corresponding to PDMAEMA in the mixture with THF. In the dry state, the presence of a slower component would be evidenced by the broader distribution and the larger average time at low T. We may estimate the relaxation time characteristic for the slow component τ^{slow} in the following way. First, a value can be estimated from the lowest temperature results (T=140 K). Assuming that the distribution width of the fast relaxation time of the dry polymer is similar to the one of the polymer in the mixture (as at high T), the non-overlapping zone of the bars at such low T (see Fig. 4.9) could be attributed to the distribution of the characteristic time of the slow component. Thus, such distribution spans over the range $-0.2 < \log(\tau(s)) < -2.4$. The characteristic time τ^{slow} could be determined

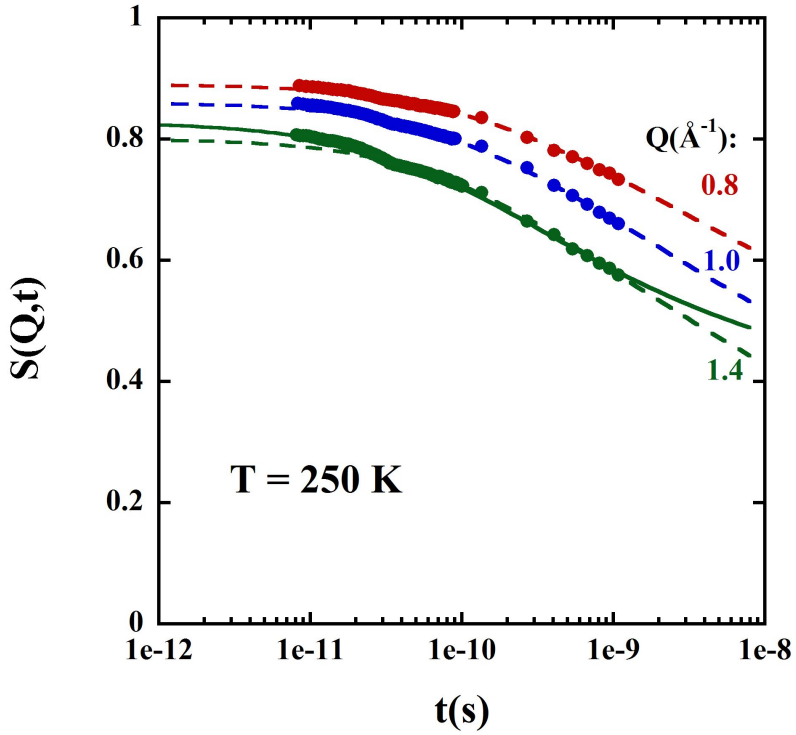

Figure 4.12: Intermediate scattering function of PDMAEMA hydrogens in PDMAEMA/D_2O at T=250K and the different Q-values indicated described by Eq. 4.17 (dashed line). Solid line is the description of the highest-Q results by assuming a fraction of slow atoms (see the text).

from the center of this interval, namely $\log[\tau^{slow}(s)](T = 140\ K) = -1.3$. Now, assuming an Arrhenius law with the same pre-factor as that for the fast component, the dotted line in Fig. 4.9 has been obtained for τ^{slow}. The corresponding activation energy would be ∼0.32 meV.

Dielectric spectroscopy provides an insight into the molecular motions through the dipole-dipole correlation function; direct information at atomic scale is revealed by QENS. The QENS results have allowed selectively following the hydrogen dynamics of the polymer component in the systems. For PDMAEMA in the mixture with THF at 250 K, they have revealed side-group localized motions with similar characteristics of the dielectric β-process. This agreement allows to assume that in this case QENS is sensitive to the microscopic motions responsible for the β-relaxation detected by DS. These data can be well described by assuming for the localized motions of side groups confined rotations on discs of 3 Å radius for methylene hydrogens and 1.65 Å radius for methyl-group hydrogens. Thus, we have been able to estimate the spatial extent of the localized motions involved in the β-relaxation of the polymer in the mixture with THF.

At higher temperatures –270 and 290 K– a narrowing of the distribution function of characteristic times has been observed with respect to that expected from DS results. We note that these temperatures are already relatively well above the glass

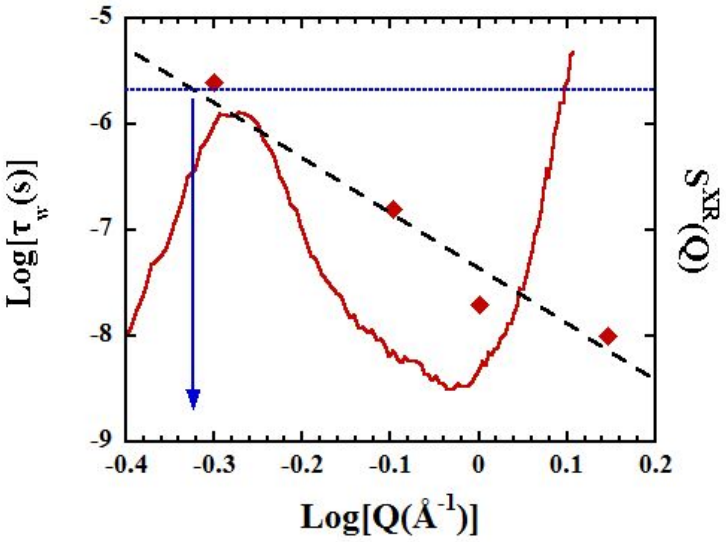

Figure 4.13: Wavevector dependence of the characteristic times of the stretched exponential function characterizing the intermediate scattering function of the α-relaxation in the mixture with THF at 290K. Dashed line is a power law $\tau_w \propto Q^{-2/\beta}$ corresponding to Gaussian behaviour. The horizontal dotted line indicates the value of the corresponding characteristic time τ_w deduced from the dielectric spectroscopy study and the vertical arrow marks the location of the Q-value at which this time matches the NS results. For comparison, the static structure factor measured by X-ray diffraction on this system has also been included (continuous line).

transition in the mixture. Therefore, this narrowing could be an apparent effect due to the additional dynamics –α-relaxation– superimposed to the localized motions at such high temperatures. We have thus fitted the QENS data at 290 K by assuming simultaneous occurrence of the α-process and β-process. The α-process would be characterized by a stretched exponential intermediate scattering function:

$$S_\alpha(Q,t) \;=\; \exp[-(t/\tau_w)^\beta] \tag{4.18}$$

with the β-parameter determined from the DS analysis ($\beta = 0.38$ for T=290 K). The model scattering function was thus built by multiplying Eq. 4.17 – with *all* parameters fixed as from DS and TOSCA experiments– with Eq. 4.18. Thereby, only two parameters were allowed to float: the pre-factor A and the Q-dependent characteristic time $\tau_w(Q)$. The resulting descriptions were very satisfactory, with the characteristic times displayed in Fig. 4.13. As expected, these times show a strong dispersion with Q, which can be rather well described by the power law $\tau_w \propto Q^{-2/\beta}$ corresponding to the Gaussian approximation [110, 111, 112, 113]. In this figure we have also included the value of the characteristic time obtained from DS for the α-relaxation. This value agrees with the value expected for $\tau_w(Q)$ at $Q \sim 0.4$ Å^{-1}.

It has usually been reported that such a coincidence occurs for $Q \sim 1\text{Å}^{-1}$ in glass-forming polymers [114]. However, for polymers like poly(vinyl acetate) (PVAc) and poly(alkylene oxide)s (PAOs) –also with relatively bulky side groups– it has been found that the matching takes place at lower Q-values, which have been identified –within the experimental uncertainties– with the Q-value Q_{max} corresponding to the inter-chain correlations of the static structure factor S(Q) [115, 116]. In Fig. 4.13 we have also represented the results for S(Q) as measured by X-ray diffraction on the PDMAEMA/THF sample. As can be seen in this figure, the coincidence of DS and QENS characteristic times for the α-relaxation of PDMAEMA in the mixture with THF also takes place around Q_{max}.

We now move to discuss the QENS results on the dry sample. From the previous analysis we have deduced a characteristic time scale for H-motions about 8-fold longer than that observed in the mixture with THF (see Fig. 4.9). Interestingly, the QENS time found for dry PDMAEMA is close to that estimated from DS for the slow component of the β-relaxation. This observation suggests the presence of a slow proton population in the dry polymer. Such a fraction of slowly moving atoms was not considered in the previous analysis. Therefore, we have reconsidered the model used to describe the QENS data on the dry polymer. In this high temperature range, DS results show coincident time scales for both, dry polymer and in the mixture. This is indicative of the existence of a common molecular motion, that can be identified as that detected and characterized by QENS in the mixture. Thus, for describing the intermediate scattering function of hydrogens in the dry sample, we assume a combination of a fraction f of protons undergoing the molecular motion in common and the rest *(1-f)* being much slower and giving an effectively elastic signal in the accessible dynamic window:

$$S^{dry}(Q,t) = fS^{mixture}(Q,t) + (1-f)A \tag{4.19}$$

Here $S^{mixture}(Q,t)$ is given by Eq. 4.17 and A is the common pre-factor accounting for faster processes. This model describes well the data of the dry polymer for all Q-values and temperatures investigated (250, 270 and 290 K) with a value of $f = 0.65$ (see as an example the solid line in Fig. 4.11).

When considering the outcome of the analysis of the QENS data on the aqueous mixture, we find a similar situation: the characteristic time found is again larger than that obtained for the THF mixture. Also in this case we may assume a slower component in the intermediate scattering function. Reanalyzing the data with Eq. 4.19 we also obtain a nice description of the experimental QENS data (see Fig. 4.12) with a value of $f = 0.75$.

After this synergetic approach combining the results from both DS and QENS techniques we can propose the following scenario: in the dry polymer, two (fast and slow) local molecular motions coexist, both controlling the dielectric relaxation –dipole reorientations– at low temperature. Addition of solvent molecules seems not to affect significantly the fast motion, but reduces the population involved in the slow process. This reduction is nearly complete in the THF mixture. However, water molecules produce only a partial reduction. The observed reduction of the slow motions in the mixtures could be attributed to the release of the steric hindrance and/or to a weakening of some interactions between side-groups. In the case of the THF mixture, there is a one-to-one ratio between solvent molecules and monomeric units, which would be sufficient for a nearly complete effect. In the water mixture,

there is a 4:1 ratio between water molecules and monomers. However, in Chapter 2 the structural properties of PDMAEMA/THF 30 wt% and PDMAEMA/H_2O 30 wt% have been discussed revealing that, while THF molecules appear to be homogeneously distributed within the sample, in the aqueous mixture the presence of water clusters have been observed. As a consequence, the coexistence of regions where the polymer would be hydrated and regions without presence of water has been invoked to explain the strong heterogeneity observed in the structure factor in Q range between 0.6 and 1 $Å^{-1}$. In this framework, the remaining slow fraction of side-groups hydrogens in the aqueous mixture would be due to the presence of those regions with a low hydration level.

CHAPTER

5

DYNAMICS OF TETRAHYDROFURAN AS A MINORITY COMPONENT IN A MIXTURE WITH PDMAEMA (30 WT%-SOLVENT CONCENTRATION)

This chapter deals with the characterization of the dynamics of the THF component in the 30 wt% THF mixture. With the purpose of assisting the reader, it might be useful to recall some relevant results shown in the previous chapters. Regarding the structural properties of PDMAEMA in the dry state and in PDMAEMA/THF, X-rays and neutron diffraction show a common peak at ~ 0.5 Å^{-1}. It has been related to the presence of a kind of nano-phase segregation between side-groups and main-chains leading to the existence of nano-domains rich in each of the polymeric subspecies. The size of such a domain is not affected by the presence of THF molecules. In addition, the presence of THF clusters has not been observed. We would thus expect that the THF molecules would be homogeneously distributed within the sample. Moving to the dielectric spectroscopy measurement reported in Chapter 4, at low temperature three processes in PDMAEMA/THF 30 wt% are identified (Fig. 1.6). The two main processes have been assigned to dynamics involving THF molecules –i.e. in the text we refer to them as 'slow' and 'fast' THF process– , while the weak relaxation, at intermediate frequencies, has been attributed to the β-relaxation of PDMAEMA. This process has been characterized in the previous chapter combining DS and QENS techniques. In the present chapter,

we employ the same combination to focus on the dynamics of the solvent molecules in PDMAEMA/THF 30 wt%.

5.1 Experimental Details

Sample

To exclude the presence of water molecules in pure polymer dPDMAEMA was annealed for 7 h at 370 K under vacuum. Concentrated mixture with THF 30%wt (1 molecule of THF/ polymer monomer) was prepared by mixing the dry polymer with the appropriate amounts of THF.

QENS Experimental Measurements

The cold neutron time-of-flight spectrometer TOFTOF was used to carry out QENS measurements providing information about the dynamics through the energy transfer analysis of the scattered neutrons. Using $\lambda = 7$Å, an energy resolution of 25 μeV was achieved. In the experiment, a flat aluminum sample holder sealed by indium wire was used in order to prevent solvent loss. The thickness of the sample holder was chosen in order to obtain a transmission close to 90%, to neglect possible multiple scattering contributions. Vanadium in a flat aluminum cell was measured at room temperature to correct the detector efficiency after the subtraction of the empty cell signal. The resolution function was determined measuring the sample at 10 K. *d*PDMAEMA/THF was investigated at 180, 200, 250 and 270 K.

5.2 Quasi-Elastic Neutron Scattering Results

QENS data acquired as function of momentum and energy transfer –i. e., of Q and $\hbar\omega$– were transformed into time domain and deconvoluted from the instrumental resolution following the procedure previously explained in Chapter 4. Figure 5.1 shows, as an example, the such obtained final intermediate scattering functions for some representative Q-values and two different temperatures. In the relevant Q-range for the QENS measurements, the incoherent fraction of the total (coherent plus incoherent) differential cross section of this sample amounts to about 0.75 in average, as can be deduced from the DNS data shown in Fig. 1.9(a) in chapter 3. These DNS data thus confirm that the incoherent contribution largely dominates the signal for this sample. We also emphasize that this incoherent contribution is basically due to the hydrogens in the THF component: the ratio between the incoherent cross section from these nuclei and the total incoherent cross section is 0.9. The intermediate scattering functions show more pronounced decays at the higher temperature, with a tendency to reach a plateau in the long-time regime. For a given temperature, the characteristic time for the decay does not show a clear Q-dependence suggesting the occurrence of spatially localized motions in the window investigated.

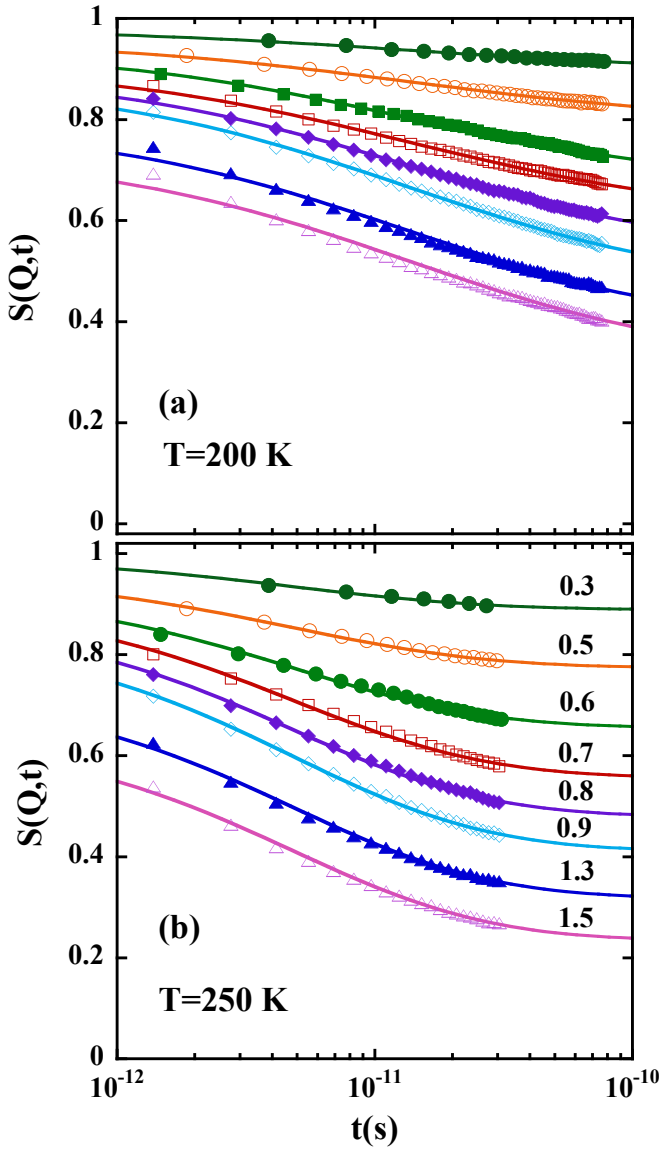

Figure 5.1: Intermediate scattering function of THF hydrogens in the mixture at different Q-values and $T = 200$ K (a) and $T = 250$ K (b). The Q-values are given in (b) in Å^{-1}. Data in (b) have been restricted to times shorter than 30 ps. Continues lines show the fits considering only the 'fast'-THF process with the model described in the text.

5.3 Data Analysis and Modelling

5.3.1 Dielectric Spectroscopy

In the previous chapter, the dielectric contribution related the polymer β-relaxation in THF mixture has been analysed. Now, we focus on the processes due to the THF molecules: the 'slow' and 'fast' ones. The characteristic times (obtained by using the fitting procedure described in chapter 4) and the width of the distributions (calculated via Eq. 4.9) are represented in Fig. 5.2 as functions of the inverse temperature. The relaxation times of both the 'slow' and the 'fast' processes of THF follow an Arrhenius temperature dependence. As a comparison, the Arrhenius parameters of the three processes in the mixture are shown in Table 5.1. Regarding the widths of the distributions, that corresponding to the PDMAEMA process shows a rather weak temperature dependence, in contrast to those related to the THF dynamics. In all cases, this parameter could be characterized, within the experimental uncertainties, by laws given by

$$\sigma = \frac{A_\sigma}{T} + \sigma_\infty \tag{5.1}$$

The parameters obtained are also compiled in Table 5.1.

	'fast'-THF	β-PDMAEMA	'slow'-THF
$\log[\tau_\infty(s)]$	-13.3 ± 0.5	-14.1 ± 0.2	-17.5 ± 0.2
E_a(meV)	104 ± 5	262 ± 5	459 ± 9
A(K)	185 ± 10	40 ± 8	280 ± 10
σ_∞	-0.01 ± 0.08	0.9 ± 0.1	0.12 ± 0.09

Table 5.1: Parameters characterizing the temperature dependence of the distributions of characteristic times (position of the maximum following the Arrhenius law and width obeying Eq. 5.1) of the sub-T_g processes identified in the PDMAEMA/THF mixture

5.3.2 Quasielastic Neutron Scattering

QENS experiments were performed at temperatures below or slightly above the glass transition of the sample, where THF molecular motions are expected to be spatially localized. Hence, the incoherent intermediate scattering function describing a localized motion was taken into account:

$$S(Q,t) = [EISF + (1 - EISF)\phi(t)] \tag{5.2}$$

Due to the heterogeneities of the amorphous systems investigated, a distribution of single exponential functions was assumed:

$$\phi(t) = \int h[\log(\tau)]\exp(-t/\tau)\mathrm{d}log(\tau) \tag{5.3}$$

From the DS investigation, we know that THF molecules are involved in two dynamical processes –the 'slow' and the 'fast' one–. Moreover, the DS study provided

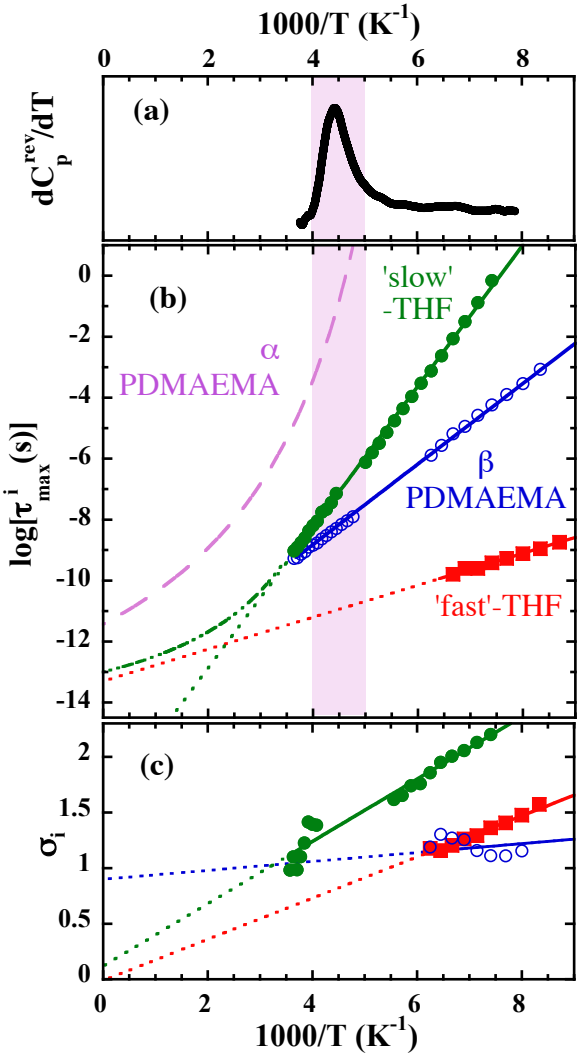

Figure 5.2: (a) DSC results (temperature derivative of the reversible part of the heat capacity in arbitrary units) on the hPDMAEMA/THF mixture. Inverse temperature dependence of the parameters characterizing the processes monitored by dielectric relaxation: (b) position of the maximum and (c) width of the distribution function of relaxation times. Filled circles correspond to the 'slow' THF-process, filled squares to the 'fast' THF-process and empty circles to PDMAEMA β-relaxation in the mixture. Lines in (b) are Arrhenius fits and in (b) correspond to the law (Eq. 5.1) with the parameters given in Table 5.1. Dotted lines are extrapolations. In (b) the Vogel-Fulcher law describing the behavior of the α-relaxation –attributable to the polymer component– is included (dashed curve), and the dashed-dotted line depicts a suggested Vogel-Fulcher extrapolation of the 'slow' THF-process toward high temperatures. The shadowed area indicates the width of the calorimetric glass-transition.

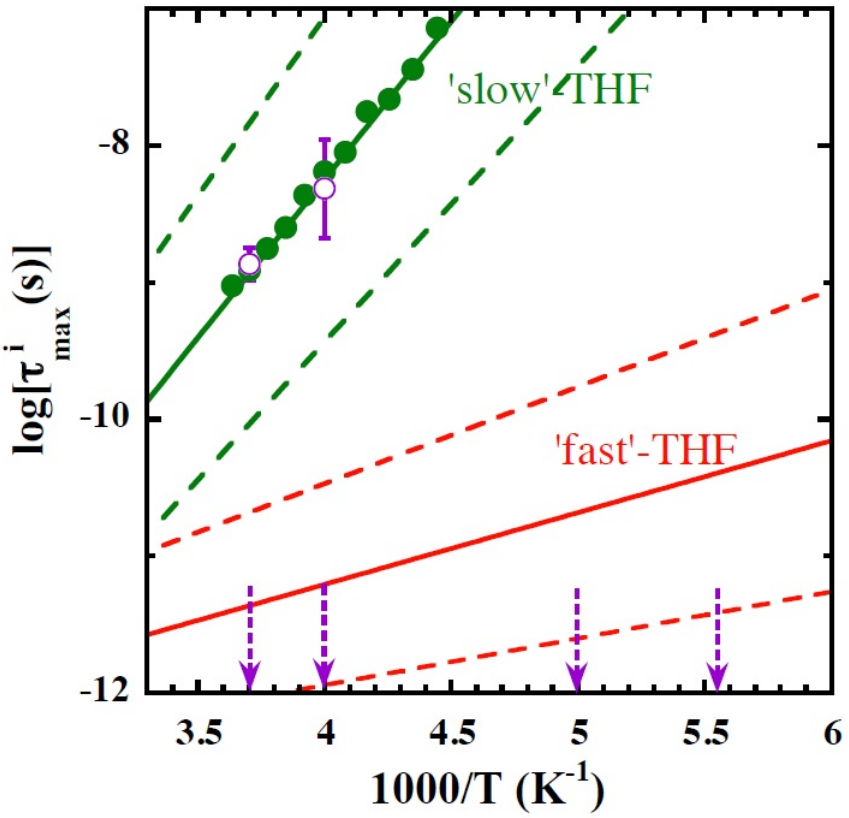

Figure 5.3: Magnification of the Arrhenius plot [Fig. 5.2(a)] in the region of interest for the QENS investigation (the location of the temperatures studied by QENS are indicated by the dotted vertical arrows). Only results referring to the THF component are represented. Solid lines are the Arrhenius fits shown in Fig. 5.2(a). Dashed lines represent the curves $\log\tau \pm \sigma$ of the THF contributions delimiting the region where the distribution function of characteristic times presents the most relevant contribution. The Q-averaged results obtained for the 'slow'-THF process from the QENS investigation are included as empty circles. The error bars show their variance (see Fig. 5.6).

valuable and accurate information about the distributions of relaxation times underlying both relaxational processes ($h_i^{DS}(\log\tau)$, with $\log(\tau_{CC})$ and σ following the Arrhenius equation and 5.1 with the parameters given in Table 5.1). These processes take place with rather different characteristic times (see Figs. 5.2 and 5.3). Taking into account the dynamic range covered by the QENS experiments ($\approx$ 1 to 100 ps), we would expect that the 'fast'-THF process dominates the decay of the intermediate scattering function at all the temperatures investigated. However, a contribution of the 'slow'-THF process could also be expected to be appreciable at long times in the high temperature range explored (see Fig. 5.3). With this information at hand, we applied the following strategy to analyze the QENS results:

Characterization of the 'Fast'-THF Process

As argued above, the main dynamic contribution to the QENS spectra is expected to be that of the 'fast'-THF process. The corresponding intermediate scattering function $S_f(Q,t)$ can be built invoking that of a localized motion (Eq. 5.2) with an a priori unknown $EISF = EISF_f$ and $\phi(t) = \phi_f(t)$ given by Eq. 5.3 with the distribution function of relaxation times fixed to that determined by DS for the 'fast'-THF process $h(\log\tau) \equiv h_f^{DS}(\log\tau)$. A global pre-factor A was also included in the fitting procedure, which parametrizes the even faster contributions (motions like vibrations leading to the decay of correlations at times shorter than those accessible by the instrument). With this model, very good fits were obtained at the two lowest temperatures investigated (see representative examples for 200 K in Fig. 5.1(a)). At higher temperatures, this description was acceptable if the time window considered was restricted to approx. $t \leq 30$ ps (see Fig. 5.1(b)). The so obtained values of the $EISF_f$ parameter are depicted in Fig. 5.4. They decrease with increasing Q and seem to reach a saturation value of about 0.5, at least at the lowest temperatures considered. This behavior can be well described by the $EISF$ corresponding to a jump between two equivalent positions,

$$EISF_{jump} = \frac{1}{2}\left(1 + \frac{\sin(Qd)}{Qd}\right) \tag{5.4}$$

were d is the jump distance. The fit of Eq. 5.4 to the obtained $EISF_f$ data delivers the characteristic jump lengths for the 'fast'-THF process d_f represented in the inset of Fig. 5.4. For the two lowest temperatures investigated, they are close to 3 Å, while there is a tendency of this parameter to increase at higher temperatures. We remind though that, in such a temperature range, QENS results could be significantly influenced by the 'slow'-THF process characterized by DS (see Fig. 5.3).

Characterization of the 'Slow'-THF Process

At 250 and 270 K the 'slow'-THF process indeed contributes to the long-time decay of the intermediate scattering function. This is illustrated in Fig. 5.5 for the case of 250 K and $Q = 0.8$ Å^{-1}. For these conditions, the dotted line shows the intermediate scattering function corresponding only to the 'fast'-THF process (and fast vibrational contributions) obtained as described in the previous analysis step. Obviously, this curve does not describe the tendency at long times ($t \geq 30$ ps approx.) of the experimental data. We thus analyzed the high-temperature QENS results considering the occurrence of both kinds of motions, aiming to obtain additional information on the 'slow'-THF process, in particular regarding its geometry. We assumed the a priori simplest scenario: simultaneous (independent) occurrence of the localized 'fast' and 'slow' processes in THF. This translates into the following intermediate scattering function:

$$S(Q,t) = A\{[EISF_f + (1 - EISF_f)\phi_f(t)][EISF_s + (1 - EISF_s)\phi_s(t)]\} \tag{5.5}$$

where the two intermediate scattering functions corresponding to each process are multiplied.

We tried to fix the maximum number of parameters in the fitting procedure. Therefore, we considered $EISF_f$ to be given by Eq. 5.4 with a temperature independent value of $d_f = 3$ Å (that deduced in the previous step for 180 and 200 K,

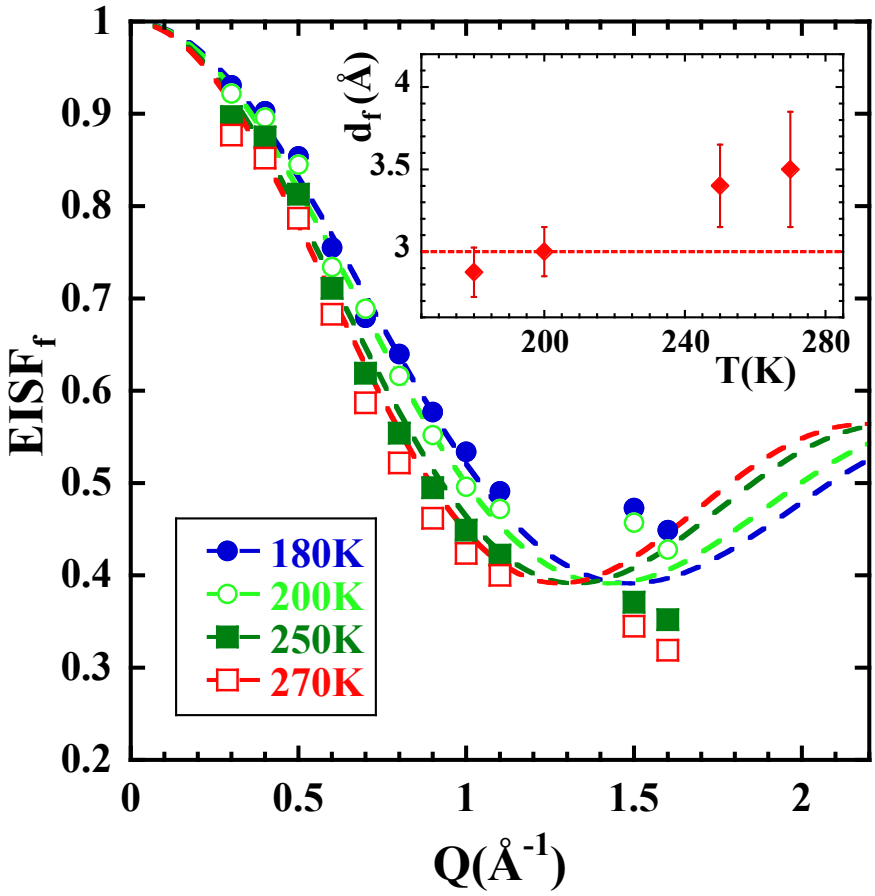

Figure 5.4: Wavevector dependence of the elastic incoherent structure factor corresponding to the 'fast' THF-process obtained from the analysis of the QENS results in terms of a unique contribution (and vibrations, see the text). Dashed lines are fits to the EISF corresponding to 2-sites jump. The resulting values of the jump distance d_f are represented as function of temperature in the inset.

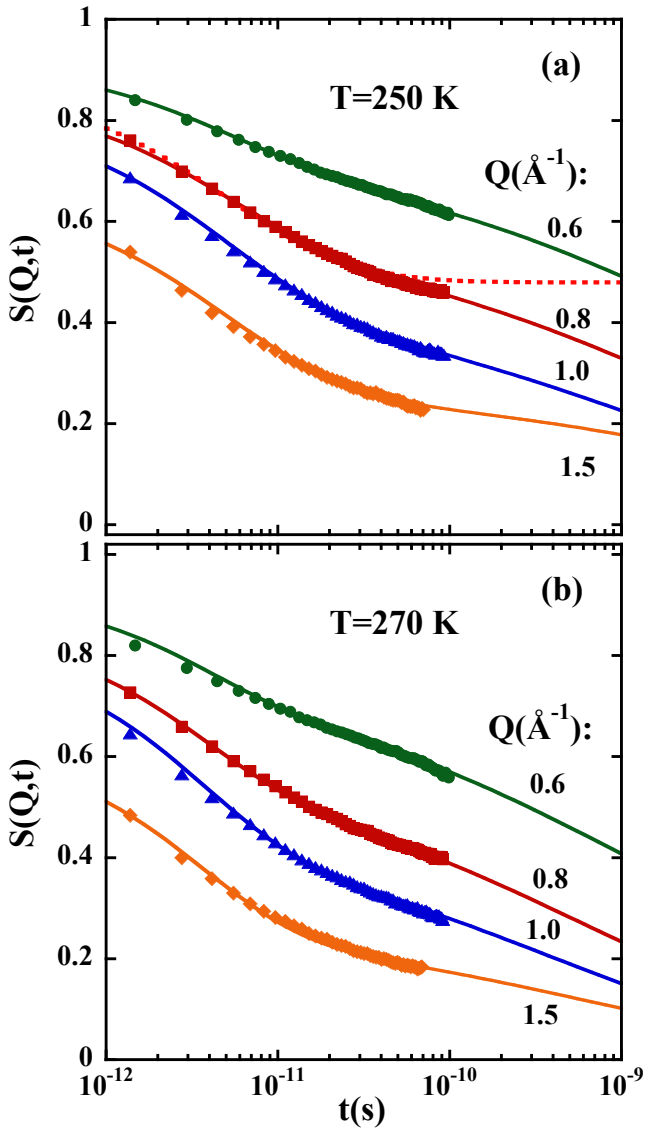

Figure 5.5: Intermediate scattering function of THF hydrogens in the mixture at $T = 250$ K (a) and $T = 270$ K (b) and the different Q-values indicated. Continues lines show the fits considering both, the 'fast' and the 'slow' THF process with the model described in the text (Eq. 5.5). For $Q = 0.8$ Å^{-1}, the description obtained assuming only the 'fast' contribution is shown for comparison as a dotted line.

where QENS data are free from slower contributions), and $\phi_f(t)$ to be completely fixed to that determined from DS. For the 'slow'-THF process, we assumed for $\phi_s(t)$ a Gaussian distribution of characteristic times with the width σ_s as determined from the DS study. Thus, only three parameters were allowed to float: the overall amplitude A, the average characteristic time $\overline{\log \tau_s}$ and $EISF_s$ of the 'slow'-process. From the Q-dependence of the QENS results, the most suitable functional form for the $EISF_s$ parameter was found to be that corresponding to motions lying within a sphere of radius r_s:

$$EISF_s \;=\; \frac{9}{(Qr_s)^6}\Big(\sin(Qr_s) - Qr_s\cos(Qr_s)\Big)^2 \tag{5.6}$$

with a value of $r_s \;\approx\; 4.3$ Å. The fitting curves obtained describe very accurately the experimental intermediate scattering functions, as can be seen in Fig. 5.5. The values of $\overline{\log \tau_s}$ used for these descriptions are represented in Fig. 5.6 as function of the scattering vector and compared with the dielectric counterparts at the same temperatures. The QENS results oscillate around the values determined from DS. This behavior could be due to the presence of coherent contributions in the intermediate scattering function (note the kind of modulation with the coherent component of the scattered intensity, see Fig. 1.9(a) in chapter 3), which are very difficult to take into account in the model function. We have calculated the Q-averaged value of this parameter as obtained from QENS, $\langle\overline{\log \tau_s}\rangle_Q$, as well as its variance. The results are displayed in Fig. 5.3 (empty circles and error bars) in comparison with the dielectric results. As can be seen in this context, the effect from coherent contributions is not so important, mainly at the highest temperature investigated. We can thus state that, within the uncertainties, the same relaxation times distribution is found from both, the dielectric and the QENS studies, also for this 'slow'-THF process.

5.4 Discussion

QENS qualifies both processes as localized motions taking place in a simultaneous way –i. e., as statistically independent events. Thanks to the combination of dielectric spectroscopy and QENS techniques, we have been able to characterize their associated distributions of characteristic times as well as their geometrical features. It is worth emphasizing that, within the uncertainties, for both processes we have been able to describe the QENS data with the relaxation times distribution determined from the dielectric spectroscopy investigation. In the following we discuss on the nature of the two THF-processes, in view of the obtained results and in the light of other works in the literature.

Let us assume that the elementary event underlying a given observed process is a simple activated jump over a barrier E_a. Then, its jump rate $1/\tau$ obeys an Arrhenius law $1/\tau = \nu_{vib}\exp[-E_a/(k_BT)]$, with ν_{vib} the attempt frequency –which should be typically of the order of the phonon frequencies in the system, i. e., $\nu_{vib} \;\approx\; 10^{13}s^{-1}$. Let us now assume that structural disorder induces different environments leading to a distribution of barriers $g(E_a)$. In the simplest case, $g(E_a)$ is a Gaussian function

$$g(E_a) \;=\; \frac{1}{\sqrt{2\pi}\sigma_{E_a}}\exp\left(-\frac{[E_a - \langle E_a\rangle]^2}{2\sigma_{E_a}^2}\right). \tag{5.7}$$

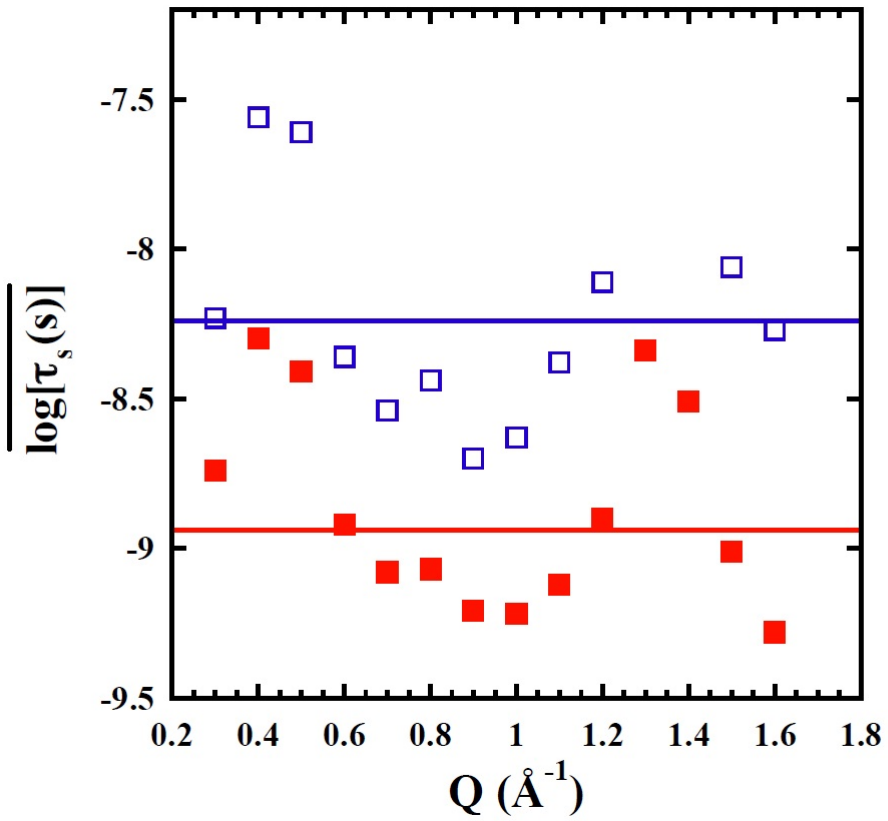

Figure 5.6: Wavevector dependence of the characteristic time deduced for the 'slow' THF process from the QENS investigation at 250 K (empty symbols) and 270 K (filled symbols). For 250 K, the slow contribution cannot be really resolved at 1.3 and 1.4 $Å^{-1}$. Horizontal lines indicate the corresponding values obtained from the dielectric study.

The existence of this distribution is accompanied by a Gaussian distribution of the logarithm of characteristic times τ where: (i) the average characteristic time displays the prefactor of the elementary process $1/\nu_{vib}$ and the average activation energy $\langle E_a \rangle$ and (ii) the width is simply given by $\sigma_{E_a} \log(e)/k_B T$. This means, if E_a is the only distributed magnitude for an ensemble of simply thermally activated processes leading to a given relaxation, then: (i) τ_∞ of the Arrhenius equation should have a meaningful value attributable to a real attempt frequency and (ii) σ_∞ in Eq. 5.1 should be zero.

These two conditions are fulfilled for the 'fast'-THF process. We can thus describe this relaxation as due to activated motions with activation energies distributed according a Gaussian function centered around an average value of $\langle E_a^f \rangle = 104$ meV with a width of $\sigma_{E_a}^f = 36.5$ meV. The value of $\langle E_a^f \rangle$ is in the range of typical energy barriers corresponding to simple molecular motions like e. g. methyl-group rotations, but the width is about twice as large as that usually found for such motions in glassy polymers [77] . A possible reason could be that the environments in the mixture are more heterogeneous than in bulk polymers. It is also worth commenting that the 'fast'-THF process here reported displays the same activation energy as the so-called δ-process observed by dielectric spectroscopy by Blochowicz et al. [58] on THF as minority component in mixtures with tristyrene (THF concentrations ϕ_{THF}=10, 20 and 33%). The characteristic times of such δ-process displayed a ϕ_{THF}-independent activation energy but decreasing average values with decreasing ϕ_{THF}. The 'fast'-THF process in PDMAEMA would roughly coincide with the infinite dilution limit of the δ-process observed in the mixtures with tristyrene. In that work, applying ^{2}H NMR spectroscopy they found that the motions involved in the δ-process could not be directly identified with conformational transitions between two different possible configurations reported from ab initio calculations reported by Rayon and Sordo [117]. An essential ingredient to be considered in order to describe the experimental ^{2}H NMR spectra was the geometrical distortion induced by the environment in the mixtures. In this way, Blochowicz et al. identified the occurrence of large angle jumps in THF and concluded that the origin of the δ-process should be due to an internal motion of the THF ring. From the QENS study we have deduced that the motions involved in this 'fast'-process lead to apparent hydrogen jumps between two positions separated by approx. 3 Å, in agreement with large angle jumps of the THF-ring as proposed from the ^{2}H NMR study. We also note that the scenario of very well dispersed THF molecules in the polymeric matrix would explain the coincidence of the 'fast'-THF process with the $\phi_{THF} \rightarrow 0$ limit of the δ-process reported in the mixtures with tristyrene.

Now we consider the 'slow'-THF process. It does not show any hint of Vogel-Fulcher like temperature dependence of the characteristic time in the whole temperature range investigated. In addition, DSC measurements do not reveal an additional glass-transition in the covered range (see Fig. 5.2(a)). Both observations obviously contradict that the 'slow'-THF process is a 'conventional' α-relaxation. Furthermore, the crossover from Vogel-Fulcher to Arrhenius temperature dependence in the vicinity of the glass-transition of the slower component reported for other binary mixtures cannot be resolved from our experimental results. The Arrhenius behavior of the 'slow'-THF process is found up to temperatures well above the glass-transition of the PDMAEMA component, where the 'slow'-THF process displays characteristic times as short at some nanoseconds. The crossover, if present in our system, would

have to be seek at even higher temperatures than those investigated in this work. The dashed-dotted line in Fig. 5.2(b) represents a speculative extrapolation of the average characteristic time of the 'slow'-THF process toward high temperatures following a Vogel-Fulcher dependence with a sensible prefactor of 10^{-13} s. To provide an experimental univocal proof such a behavior is unfortunately extremely difficult, given the high frequency/temperature region to be explored, implying probable solvent losses and merging of the process with the 'fast'-THF relaxation.

It is noteworthy that in any case the Arrhenius extrapolation of the characteristic time of the 'slow'-THF process to high temperatures becomes unrealistic: there would be a temperature above which this time would display values smaller than those of the 'fast' process or even to those corresponding to typical phonon excitations. This is due to the small prefactor of the average characteristic time $\tau^s_\infty = 3.3 \times 10^{-18}$ s, which can definitely not be attributed to an inverse attempt frequency. Such finding is traditionally interpreted as due to contributions of entropic origin to the underlying relaxation process. In the Eyring formalism, the prefactor in the Arrhenius equation would be given by $\tau_\infty = \nu_{vib}^{-1} \exp[-\Delta S/(k_B T)]$, where ΔS is the activation entropy involved in the molecular motion. In this framework, $\Delta S/k_B \approx \ln(\bar{N}!)$, where $\bar{N}$ is the average number of elementary states involved; the non-vanishing value of σ^s_∞ would represent the distribution width around this average value. Considering $\nu_{vib} \approx 10^{13} s^{-1}$, a value of about 8 is obtained for $\bar{N}$. Now let us discuss about the nature of the entities involved in this collective process.

A key result provided by QENS spatial resolution is the evidence for localization of the relaxation mechanism underlying the 'slow'-THF process. We have deduced that THF hydrogen motions are spatially restricted within a volume of about 8.6 Å in size. This spatial extent would be in agreement with the above proposed scenario of confinement of the THF molecules within the nano-domains (most probably in a side-group rich environment) in the nano-phase segregated PDMAEMA –we remind that the size of the domains has been determined to be of about 12 Å. Moreover, we have discarded a significant presence of THF clusters in the mixture, at least for the present concentration (one THF molecule / PDMAEMA monomer). This would imply that THF molecules are practically screened from each other by the side-groups of the polymeric matrix. Thus, PDMAEMA side-groups have to be among the molecular units involved in the relaxational process leading to the 'slow'-THF process.

We propose the following scenario for the 'slow'-THF process: at very high temperatures, THF molecules should be able to relax independently from the environment, with motions occurring with characteristic times in the range of the picosecond. Upon cooling down, these motions start to couple with the surrounding environment, which is rich in polymeric side groups. Accordingly, the activation energy of the THF motion increases. This occurs until the relaxation within the nano-domain involves $\tilde{N} \approx 8$. At lower temperatures, THF molecules undergo such localized motions 'assisted' by their neighbors within the nano-domain, which provide a local relatively large mobility. As can be seen in Fig. 5.2(b), in this temperature region the faster relaxational β-process of the PDMAEMA component takes place. This has been characterized in our complementary QENS study as a localized motion of the side group involving rotations on discs of 3 Å radius for methylene hydrogens and 1.65 Å radius for methyl-group hydrogens. These motions of the side groups persist below the glass transition of the polymer, when the main-chain

motions freeze, providing the THF molecules the needed surrounding mobility to be able to relax.

The crossover in other systems with strong dynamic asymmetry, like e. g. water in polymer matrices, is observed because cooperativity effects on the structural relaxation of the fast component become progressively enhanced with decreasing temperature down to the region where the characteristic time of this relaxation reaches values of the order of microseconds. The THF motions involved in our mixture with PDMAEMA seem to not experience such a pronounced cooperativity. We may argue that in this mixture cooperativity effects arising from THF/THF interactions would be much weaker than in the bulk material or in large enough clusters of solvent within the polymeric matrix. We could speculate that the key ingredient for developing cooperativity effects is the direct interaction between molecular units of the same kind. This is favored if there is a significant number of nearest neighbors of the same nature around a given relaxing unit of the fast component. Such a situation is realized if the fast component forms clusters, as it is the case of water molecules interacting via H-bonds. In mixtures of polymeric units, chain connectivity would naturally provide also a source of collectivity. In our system, THF molecules seem to be screened from each other by the side-groups of the polymer. The high molecular mobility associated to these side-groups would induce a kind of 'plasticization' effect on THF motions. It is worth mentioning that the important role of local polymer relaxations on the solvent dynamics was also put forward in a study of PVME aqueous solutions [42].

Last, we mention that in the mixtures of THF and tristyrene investigated in Ref. [58] two dielectric relaxations with characteristic times longer than that of the previously commented δ process were also attributed to the THF component. For ϕ_{THF}=0.33%, the slowest one was found in a similar frequency/temperature regime as the 'slow'-THF process here reported. That process –called α'– was interpreted as the confined α-relaxation of THF molecules in the mixture, but it was characterized in a very narrow range (characteristic times between about 1 and 10^{-3} s.) due to its merging with the α-process. Thus, a crossover could not be identified. The relaxation with intermediate characteristic times between those of the so-called α' and δ is independent of THF-concentration and was identified by those authors as the β-process of the THF component. It was characterized as due to small-amplitude reorientations of the THF molecules. In our system we could not identify any THF motion of such characteristics from the QENS investigation, which is selectively sensitive to this component. In the same time/temperature region though, the dielectric response of the THF/PDMAEMA mixture presents the dynamical process that we have assigned to the β-relaxation of the polymer component (see Fig. 5.2(b)). This identification was proved by a complementary QENS study on the PDMAEMA dynamics in this mixture, through which we robustly characterized the dielectric relaxation assigned to the PDMAEMA β-process in terms of polymeric motions that can also be found in the dry polymer. We thus conclude that the origin of such intermediate relaxation in triphenyl and in PDMAEMA mixtures with THF has to be of different nature.

CHAPTER

6

STUDY ON THE EFFECT OF CONCENTRATION ON THE DYNAMICS OF PDMAEMA AND SOLVENT COMPONENTS IN THF AND WATER MIXTURES

The aim of this chapter is to elucidate how the different dynamical processes involved in PDMAEMA mixtures depend on solvent concentration. With this purpose, differential scanning calorimetry and dielectric spectroscopy measurements were carried out on PDMAEMA in mixture with THF and water at different concentrations. After giving the details about sample preparation and experimental conditions, the results obtained will be shown: first, the structural relaxation and the local relaxations of PDMAEMA in the mixture with THF, then the results on the THF component will be discussed. Finally, in the second part, the work on the dynamics in PDMAEMA aqueous solutions at different concentrations will be presented. There, dielectric spectroscopy is only sensitive to H_2O-component.

6.1 Samples and Experimental conditions

PDMAEMA (Polymer Source) was annealed for 7 h at T = 373 K under vacuum to exclude the presence of solvent molecules in pure polymer. Mixtures with THF (15, 20, 30, 40, 48 wt%) and with water (20, 30, 40 wt%) were prepared by mixing the dry polymer with the appropriate amount of solvent during a few days. Modulated DSC measurements were carried out with an average heating rate of 3 K/min and amplitude of modulation ±0.5 K with a period of t_p = 60 s. Broadband dielectric

spectroscopy measurements were carried out by using Novocontrol Alpha-S spectrometer to measure the complex dielectric function $\epsilon^*(\omega) = \epsilon^{'}(\omega) - i\epsilon^{''}(\omega)$, covering a frequency range of 10^{-2}-10^7 Hz. Measurements were carried out under isothermal conditions, every 5 K with a temperature stability better than 0.1 K.

6.2 Dynamics in PDMAEMA/THF mixtures

6.2.1 Experimental results

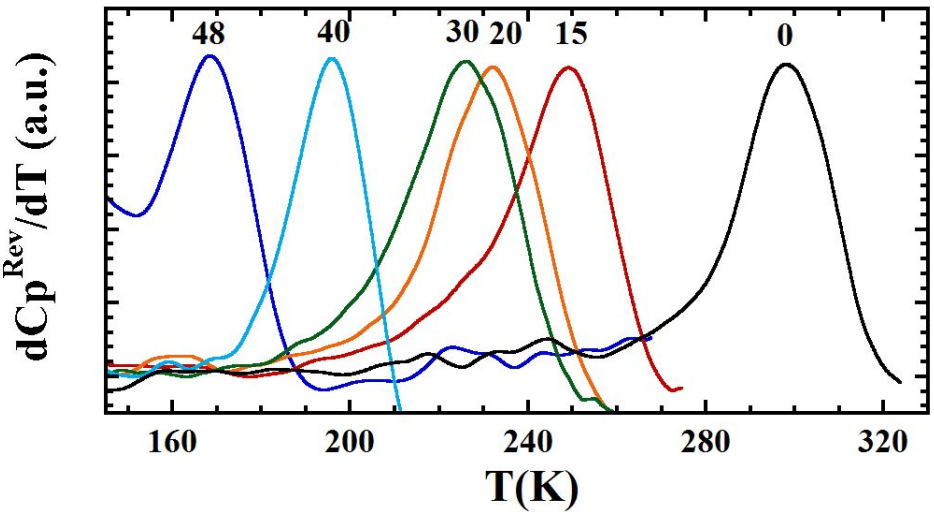

Figure 6.1: Normalized temperature derivative of the reversible specific heat of PDMAEMA (black) and THF mixtures: 15 wt% (red), 20 wt% (orange), 30 wt% (green), 40 wt% (azure), 48 wt% (blue).

Calorimetry measurements

In Fig. 6.1 the normalized temperature derivative of reversible part of the specific heat dC_p^{Rev}/dT of the mixtures is shown. In PDMAEMA/THF 48 wt%, a crystallization peak at around ∼130 K was found on cooling. Thus, the increase toward lower temperatures observed in the region below the glass transition temperature would suggest a partial melting. For lower concentrations, no sign of THF crystallization was detected during cooling. In Fig. 6.1, we clearly observe a shift of the glass transition temperature as function of THF concentration. Such a result suggests that the plasticization effect increases with the amount of solvent. However, this increase does not exhibit a monotonic behaviour. In Fig. 6.2 T_g obtained by DSC (from the maximum of the specific heat derivative) as function of the THF concentrations is shown. A strong decrease of the glass transition temperature (≈50 K) occurs already at the lowest concentration investigated (15 wt%). Increasing the THF amount, the shift of T_g appears much weaker up to approximately ≈30 wt%,

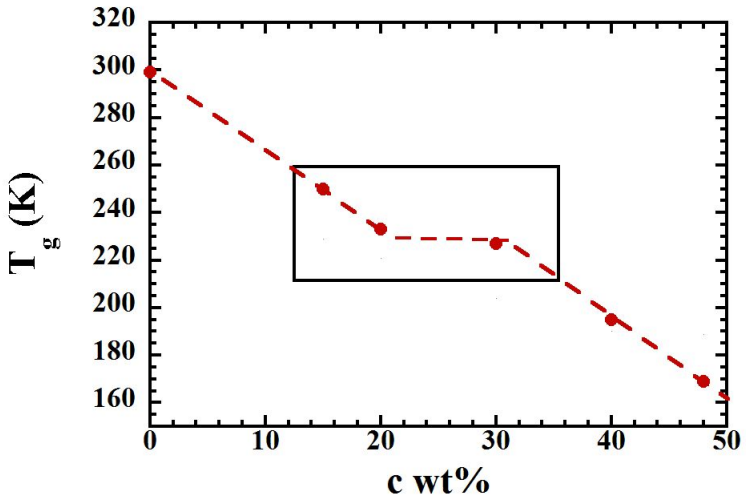

Figure 6.2: Temperature of the glass transition measured by DSC in function of the THF concentration. Points in the box are related to those concentrations exhibiting an homogeneous distribution of THF molecules in the sample

that is around 1 molecule of THF per monomer. Then the dependence on solvent concentration becomes stronger, likely also due to the increasing contributions of THF at high concentration.

Table 6.1: T_g values determined from DSC and DS and parameters obtained by VFT of the characteristic times of the α-relaxation of PDMAEMA in the dry state and at different THF concentrations by fixing the pre-factor with that obtained for the dry PDMAEMA ($\log(\tau_0(s)) = -11.7$)

c wt%	T_g^{DSC} (K)	$T_{g,onset}^{DSC}$ (K)	T_g^{DS} (K)	B (K)	T_0 (K)
0	299	285	287	1666 ± 6	230.8 ± 0.3
15	250	230	229	1946 ± 21	165 ± 1
20	233	215	221	2124 ± 38	152 ± 2
30	227	205	204	1881 ± 6	142 ± 0.3
40	195	175	190	1793 ± 17	135 ± 1
48	169	155	189	1821 ± 7	129.5 ± 0.4

Dielectric Spectroscopy measurements

In Chapter 4 it has been shown that for the 30 wt% concentration it is not possible to clearly resolve the high temperature process related to the structural relaxation of PDMAEMA from the large conductivity contributions to $\epsilon''(\omega)$. Therefore, the data analysis was carried out considering the derivative of $\epsilon'(\omega)$ with respect to $\log(\omega)$ in agreement with the study on the PDMAEMA in the dry state and in THF mixture 30 wt% previously discussed. As an example, the derivatives $\partial\epsilon'(\omega)/\partial\log(\omega)$ of representative concentrations at T=250 K are shown in Fig. 6.3. We notice, that the peaks are shifted in frequency in agreement with a change in T_g.

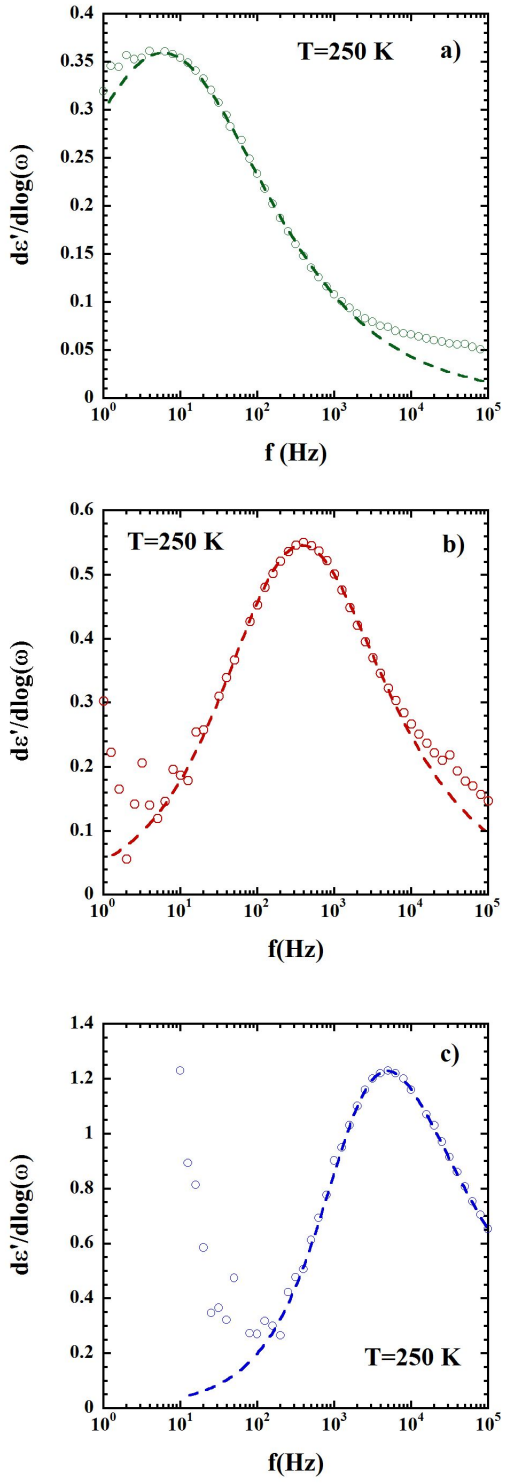

Figure 6.3: Derivative of $\epsilon^{'}(\omega)$ with respect to $\log(\omega)$ at T=250 K of a) PDMAEMA/THF 20 wt% b) PDMAEMA/THF 30 wt% and c) PDMAEMA/THF 40 wt%. Dotted lines show the fits with Eq. 4.2.

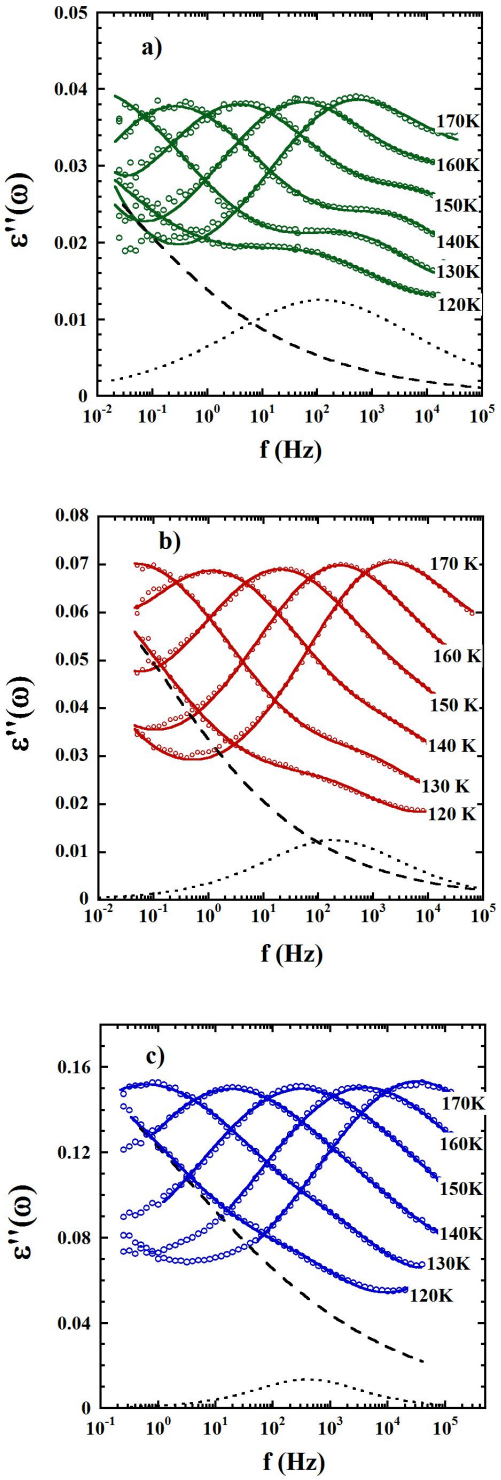

Figure 6.4: Imaginary part of the complex dielectric permittivity at different temperatures below the T_g: a) PDMAEMA/THF 20 wt% b) PDMAEMA/THF 30 wt% and c) PDMAEMA/THF 40 wt%. Continues lines show the fit curves, while black lines at the lowest temperatures represent the 'slow'-THF component (dashed lines) and the PDMAEMA β-relaxation component (dotted lines).

At low temperature, below T_g, three contributions were observed in the imaginary part of the dielectric response of PDMAEMA/THF 30 wt%. Their origin was deeply discussed by means of a comparative study of the DS results and neutron scattering spectroscopy investigation on both dry polymer and THF mixture (see Chapter 4 and 5). The processes at lower and higher frequencies have been related to the THF relaxations, while that at intermediate frequencies was assigned to the fast component of the β-relaxation of PDMAEMA. In Fig. 6.4 the dielectric permittivity at representative temperatures of PDMAEMA in mixtures with THF at 20, 30 and 40 wt% is shown in the frequency window $10^{-2} < \text{Hz} < 10^{6}$ to which this investigation has been restricted. There, the fastest process due to the fast THF internal motions is not visible. At low concentration two peaks –presumably those previously assigned to the 'slow'-THF process and the PDMAEMA β-relaxation– are well resolved. Supporting this identification, the intensity of the loss peak related to 'slow'-THF process increases with the THF concentration. At high concentration the polymer contribution is almost covered by the THF process.

6.2.2 PDMAEMA dynamics

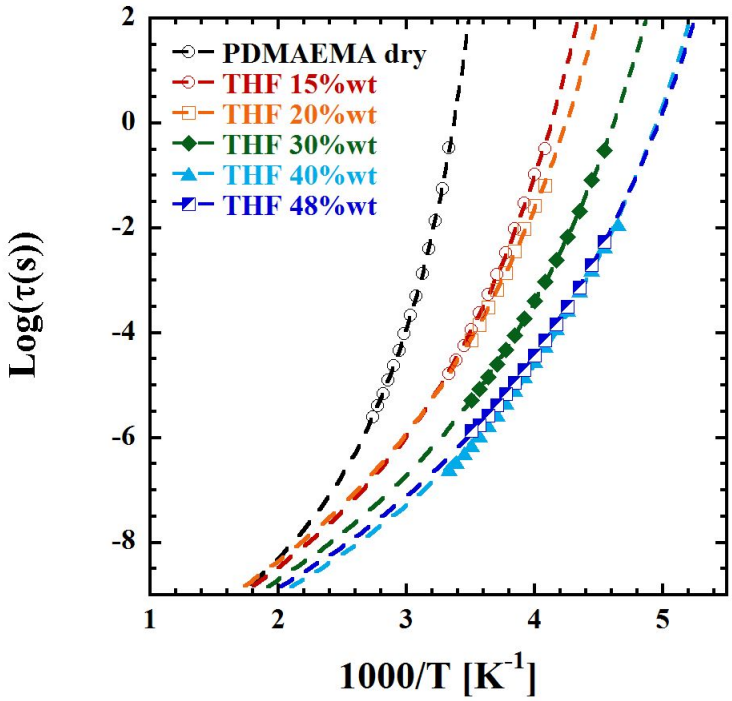

Figure 6.5: Inverse temperature dependence of the characteristic times of PDMAEMA α-relaxations in the dry state and at different THF concentrations obtained by DS. Dashed lines are fits with VFT expression.

α-relaxation

In agreement with the study on the polymer structural relaxation in PDMAEMA/THF 30 wt%, the derivative of $\epsilon^{'}(\omega)$ with respect to $\log(\omega)$ of the THF mixtures was fitted by Eq. 4.2. The obtained characteristic times τ_{max}, calculated according to Eq. 4.3, are shown in Fig. 6.5. All the samples show clearly a Vogel-Fulcher-Tammann (VFT) dependence on temperature, which is expected for a glass-forming material. We notice that the relaxation times of the highest concentration (48 wt%) are very similar to those obtained for PDMAEMA/THF 40 wt%. This could indicate a partial segregation of the THF molecules and, therefore, an inhomogeneous distribution of solvent molecules. In Chapter 4, the characteristic times of the α-relaxation of the dry PDMAEMA and the THF mixture (30 wt%) were analyzed. We obtained very similar VFT pre-factors for both samples. Therefore, assuming that such parameter does not depend on the THF amount, the curves in Fig. 6.5 were fitted by the VFT equation with the value of the pre-factor fixed with that obtained for the dry PDMAEMA ($\log(\tau_0(s)) = -11.7$). The obtained parameters are shown in Table 6.1. We may define the dielectric spectroscopy temperature of glass transition (T_g^{DS}) as the temperature at which the relaxation time determined by this technique is $\tau = 100$ s. The results obtained are given in Table 6.1 and shown with those deduced from DSC in Fig. 6.6. Starting from the glass transition temperatures observed by DSC, we have already mentioned that, after a strong decrease of T_g occurring even at the lowest THF concentration investigated, the dependence on the solvent amount appears rather weak up to $c_{wt}\% = 30$. This kind of saturation of the glass transition temperature suggests a homogeneous distribution of the solvent molecules. This would be related to the preference of THF to be linked with the polymer instead of forming solvent aggregates. On the contrary, for higher concentrations, the dependence becomes stronger suggesting some changes in the samples. However, it must to be taken into account that, while at low THF concentrations calorimetry is dominated by the polymer signal (that is the main component of the mixture), for higher solvent concentrations THF is also significantly contributing. Comparing the glass transition temperatures observed by DSC with those obtained by DS, we notice that $T_g^{DS} < T_g^{DSC}$ up to $c_{wt}\% = 30$. However, considering the onset temperature T_g^{DSC}, the values of the glass transition temperature T_g^{DS} and $T_{g,onset}^{DSC}$ nearly coincide for these concentrations. This could be attributed to the property of the dielectric relaxation of being highly sensitive to the onset of the molecular motions involved in the glass-transition, as it has been argued in Chapter 4. At higher THF concentrations, T_g^{DS} does not exhibit a change of dependence on the THF concentration, as it has been found in the T_g^{DSC} (Fig. 6.2), but it rather seems to be independent of the concentration. As commented above, this behaviour could be related to an inhomogeneous distribution of the THF given by a kind of partial segregation of the solvent molecules.
Figure 6.7 shows an Angell plot ($\log(\tau_{max})$ vs T_g^{DS}/T) of the results obtained at different concentrations. We observe that samples with THF show a "stronger" behaviour than the sample in the dry state. Data corresponding to the different THF mixtures almost collapse on the same curve suggesting that, after a sudden change, the fragility of the system hardly depends on the THF concentration.

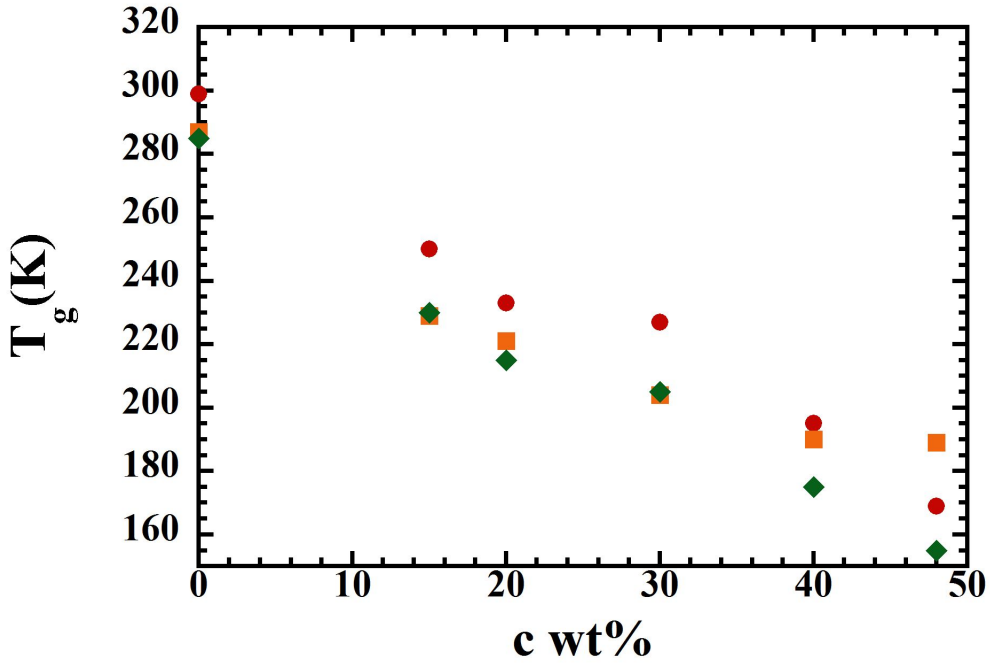

Figure 6.6: Comparison of the T_g obtained by DSC (orange squares) and DS (red circles) and the onset temperatures T_g^{DSC} (green diamonds) as function of THF concentration.

β-relaxations

Dielectric permittivity results reflecting local relaxations below the glass transition temperature were fitted by a sum of Cole-Cole (CC) functions, taking into account both the polymer and the THF contributions. It must be recalled that the study on PDMAEMA and PDMAEMA/THF 30 wt% carried out by DS and NS spectroscopy revealed the presence of a fast and a slow component of the polymer β-relaxation in the dry state. At that concentration it was found that the presence of the THF molecules did not significantly affect the fast motion but strongly reduce the population involved in the slow process. The obtained characteristic times related to the PDMAEMA local dynamics in mixtures with different THF concentrations are shown in Fig. 6.8. The temperature dependence of the polymer β-relaxation was studied by fitting the relaxation times with the Arrhenius law. The results are shown in Table. 6.2. We notice, at the lowest THF concentrations (15 and 20 wt%) as well, that the relaxation times present a rather lower activation energy than that of PDMAEMA in the dry state. This indicates that even the presence of few molecules of solvent could hinder the slow component of the β-relaxation of the dry polymer. Such scenario is also supported by the behaviour of the dielectric strength as function of the solvent amount (Figs. 6.9(a)–6.10). Indeed, we observe that $\Delta\epsilon$ of the polymer β-relaxation is rather smaller in presence of THF than in PDMAEMA in the dry state. Looking at the α_{CC} parameter of the CC function (Fig. 6.9(b)), we notice that the distribution of the relaxation times at the highest concentration clearly differs from those of the other mixtures. Nevertheless, at this concentration, it is not trivial to separate the polymer and the solvent components (see Fig. 6.4(c))

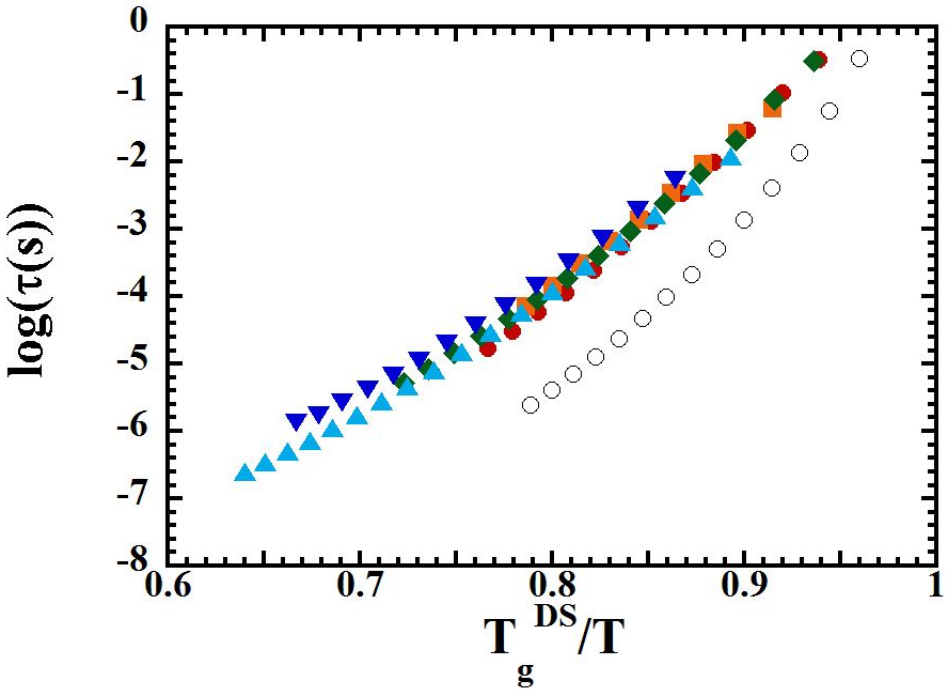

Figure 6.7: Relaxation times of the polymer α-relaxation as function of the temperature scaled on the calorimetric T_g (Angell's representation). Empty symbols refer to PDMAEMA in the dry state, while filled symbols represent the characteristic times in THF mixtures: PDMAEMA/THF 15 wt% (red circles), PDMAEMA/THF 20 wt% (oranges squares), PDMAEMA/THF 30 wt% (green diamonds), PDMAEMA/THF 40 wt% (light blue triangles) and PDMAEMA/THF 48 wt% (blue inverted triangles).

and, moreover, the presence of minor crystallization could strongly affect the deduced distribution of the characteristic times. Regarding the other mixtures, the α_{CC} parameter appears to be independent on the THF concentrations and takes an average value rather bigger than that of the polymer in the dry state. Such result is in agreement with the presence of only the fast component in the PDMAEMA dynamics in the mixtures. However, it must be mentioned that in the samples with less than 1 THF molecule per monomer the local composition could vary from place to place in the sample (some locations where the polymer would have a dry-like environment and other locations where there would be some THF molecules around). This would lead to the presence of parts where PDMAEMA is similar to that in the dry state. As a consequence, there we could imaging a polymer β-relaxation with both slow and fast components. Nevertheless, due to the THF contribution to our DS measurements, it is not possible to resolve the eventual loss peak given by such slow component.

Increasing the solvent amount, up to 40 wt%, the polymer dynamics becomes faster without significant change in the activation energy. On the contrary, increasing the concentration from 40 wt% to 48 wt%, the relaxation times increase and become comparable with those obtained for PDMAEMA/THF 30 wt%. This puzzling behaviour could be understood taking into account the partial segregation of

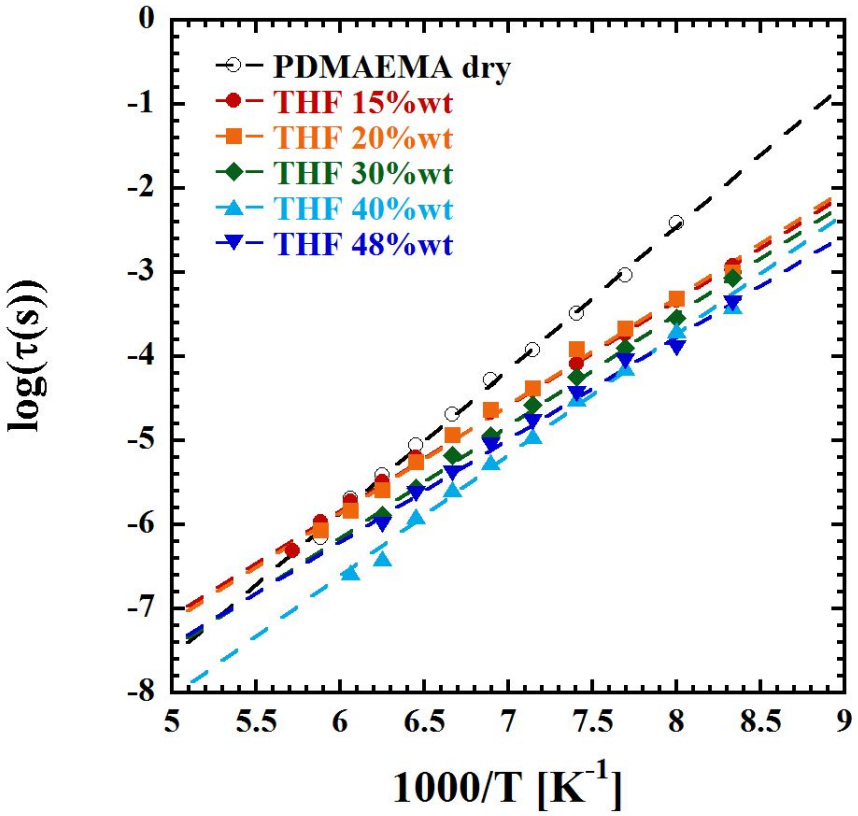

Figure 6.8: Inverse temperature dependence the relaxations times of PDMAEMA β-relaxation in the dry state (empty symbols) and in THF mixtures (filled symbols). Dashed lines are fits with the Arrhenius equation.

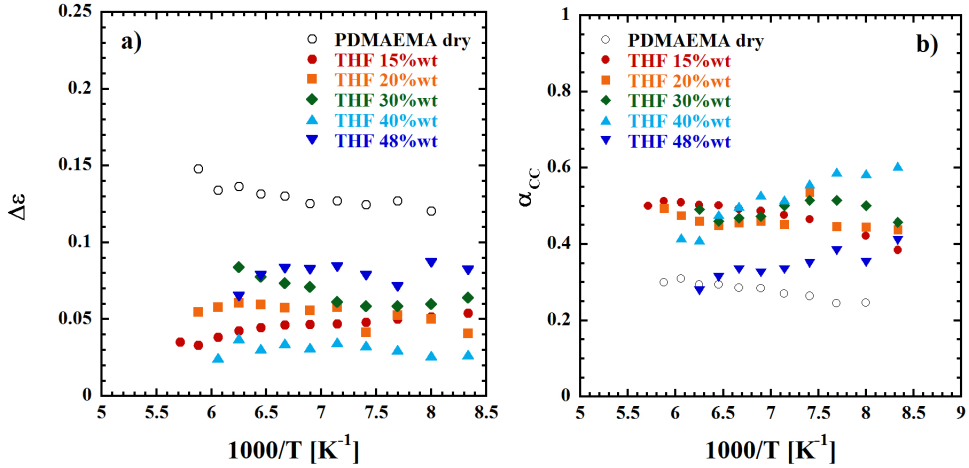

Figure 6.9: a) Dielectric strength $\Delta\epsilon$ and b) Cole-Cole shape parameter α_{CC} related to PDMAEMA β-relaxations obtained by the fitting procedure. Empty circles represent dry PDMAEMA, while filled symbols represent PDMAEMA results in THF mixtures.

THF molecules suggested for this concentration by the analysis of the α-relaxation and the DSC measurements. This could lead to an effective solvent concentration rather lower than expected and, therefore, to a behaviour of the relaxation times of the polymer β-relaxation similar to that exhibited in the samples with a lower solvent amount. Nevertheless, the uncertainties increase with the THF amount.

6.2.3 THF dynamics

In Fig. 6.11 the characteristic relaxation times of the THF process ('slow'-THF process) are shown revealing an Arrhenius dependence on temperature. Solvent dynamics results to be faster as we increase the solvent concentration. However, for the 48 wt% concentration (around 2 THF molecules per polymer monomer), the relaxation times become larger than those at smaller concentration (40 wt%). The results were fitted by the Arrhenius equation. In Fig. 6.11 it is clear that the activation energy of the process does not appreciably change with solvent concentration. Therefore, in the fitting procedure, the activation energy was fixed by using the results obtained previously on PDMAEMA/THF 30 wt% (E_a = 459 meV). The results so obtained for the pre-exponential factor are shown in Table. 6.2. The obtained values suggest, in the previously described Eyring framework (Chapter 5), that the average number of elementary states involved in the molecular motion increases with THF concentration. The width of the distribution of the activation energies was calculated by using Eq. 4.9 in Chapter 4. We observe that it is possible to identify two different populations (Fig. 6.12). At high THF concentrations the σ_{E_a} parameter has larger values than in the samples with a lower amount of THF. It must be noticed that the most homogeneous mixture seems to be that with 30 wt%, that is 1 molecule of THF per monomer. The stronger heterogeneity observed at higher concentrations can be related to the presence of two kinds of THF molecules. At low concentration, THF is distributed rather homogeneously

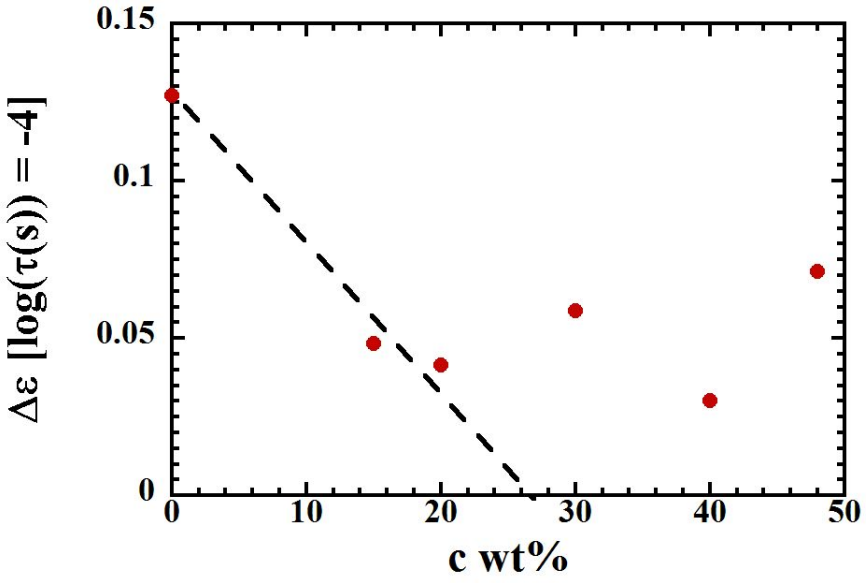

Figure 6.10: Dependence on THF concentration of the dielectric strength of the PDMAEMA β-relaxation evaluated at log(τ)=-4 s.

up to around one molecule of solvent for polymer monomer. Increasing the amount of THF, a partial segregation seems to occur as suggested by calorimetry and the analysis of the PDMAEMA dynamics in the mixtures. Therefore, we could assume that the THF molecules in 'excess' would have a weaker interaction with the polymer. This scenario would lead to differences in the solvent relaxations depending on the interactions with the environment. Moreover this could explain the behaviour of the dielectric strength as function of THF concentration shown in Fig. 6.13. We notice that it increases linearly with the solvent concentration amount up to around ∼40 wt%, then it takes a larger value than the extrapolated line. Such a behaviour appears in contrast with the presence of crystallization suggested at this concentration. However, invoking the presence of THF molecules that interact weakly with the polymer, we could assume that such excess in the dielectric strength would be related to those dipole moments which are less restricted by PDMAEMA. Such an effect is very relevant at 48 wt% while in the sample PDMAEMA/THF 40 wt% it appears that it does not strongly affect the dielectric strength behaviour. This is likely due to the presence of only few molecules weakly interacting with the polymer.

Table 6.2: Arrhenius parameters of the characteristic times of PDMAEMA β-relaxation and activation energy of the 'slow'-THF process in THF mixtures at different solvent concentrations (the activation energy was fixed by using the results obtained previously on PDMAEMA/THF 30 wt% ($E_a = 459$ meV)).

	PDMAEMA β-relaxation		'slow'-THF
c wt%	E_a(eV)	log[τ_0 (s)]	log[τ_0 (s)]
0	0.34	-16.1	
15	0.25	-13.3	-16.8
20	0.25	-13.5	-16.8
30	0.26	-14.1	-17.5
40	0.28	-15.2	-18.3
48	0.24	-13.5	-17.9

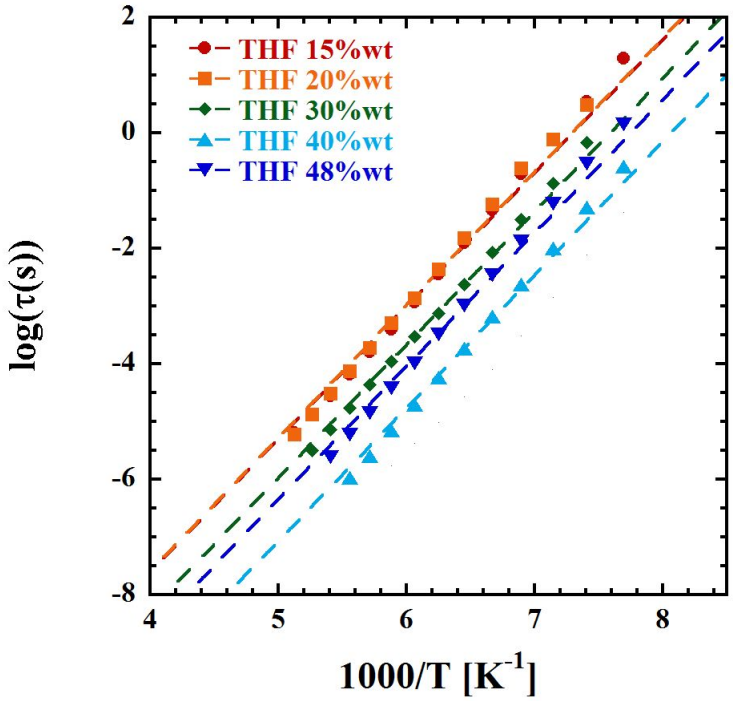

Figure 6.11: Inverse temperature dependence the relaxations times of the THF component in PDMAEMA/THF mixtures. Dashed lines are fits with the Arrhenius equation (as described in the text).

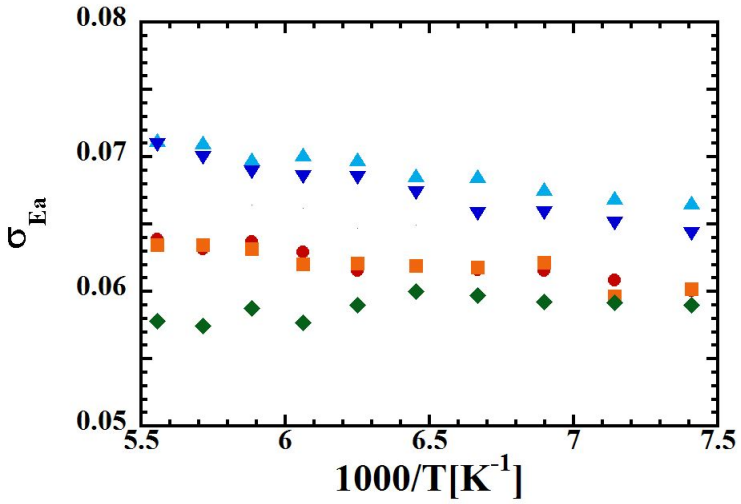

Figure 6.12: Width of the distribution of the activation energies related to the THF process in PDMAEMA/THF mixtures at different concentrations: PDMAEMA/THF 15 wt% (red circles), PDMAEMA/THF 20 wt% (orange squares), PDMAEMA/THF 30 wt% (green diamonds), PDMAEMA/THF 40 wt% (light blue triangles) and PDMAEMA/THF 48 wt% (blue inverted triangles).

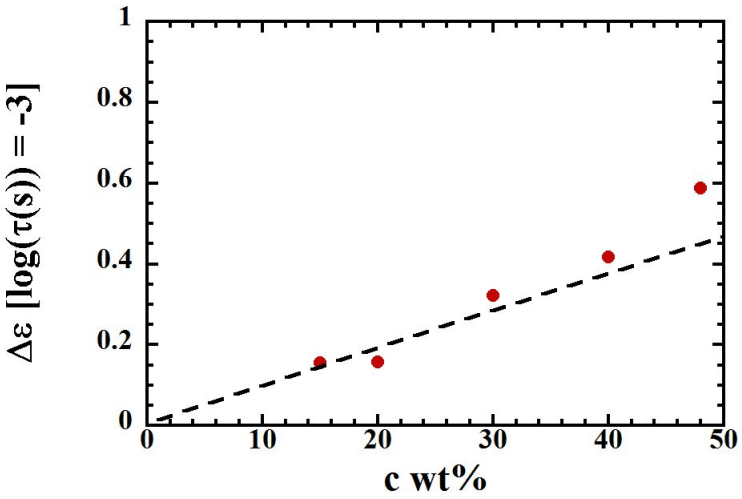

Figure 6.13: Dependence on THF concentration of the dielectric strength of the 'slow'-THF process evaluated at $\log(\tau(s))$=-3.

Summarizing the results obtained on the dynamics of PDMAEMA/THF mixtures, we found that:

i) Even a small amount of THF molecules strongly affect the dynamical features of the polymer. In fact, we observed a remarkable reduction of the T_g and a 'stronger' behaviour of the α-relaxation of PDMAEMA even at the lowest THF concentration (15 wt%). Moreover, a rather lower activation energy of the β-relaxation of the polymer was found in all the mixtures. This could indicate that, already at c=15 wt%, the slow component of PDMAEMA β-relaxation observed in the dry state is highly hindered.

ii) At the highest concentration (48 wt%), calorimetry and dielectric spectroscopy measurements suggest a segregation of THF molecules leading to a inhomogeneous distribution of solvent molecules in the mixtures.

iii) The mixture with the most homogeneous distribution of THF molecules seems to be that with c=30 wt% corresponding to one molecule of THF per monomer. This is suggested by the 'saturation' of the T_g as function of the solvent amount observed by DSC and by the smallest value obtained for the distribution of activation energies of the 'slow'-THF dynamics.

iv) At least in the temperature range investigated, there are no clear signs of a crossover from an Arrhenius to a non-Arrhenius dependence on temperature of the relaxation times of the 'slow'-THF dynamics.

6.3 Dynamics in PDMAEMA/H_2O mixtures

6.3.1 Experimental results

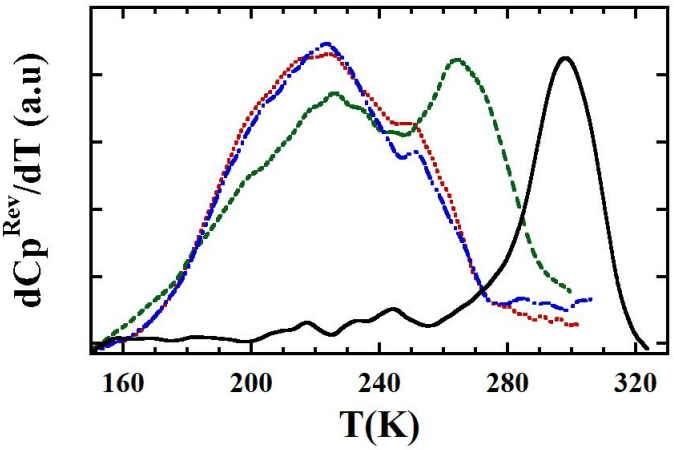

Figure 6.14: Normalized temperature derivative of the reversible specific heat of PDMAEMA/water mixtures: 20 wt% (dashed green line), 30 wt% (dotted red line), 40 wt% (dashed-dotted blue line) compared to the dry sample (solid black line).

DSC scans, showing the temperature derivative of the reversible specific heat, of PDMAEMA in the dry state and of the water mixtures are shown in Fig. 6.14.

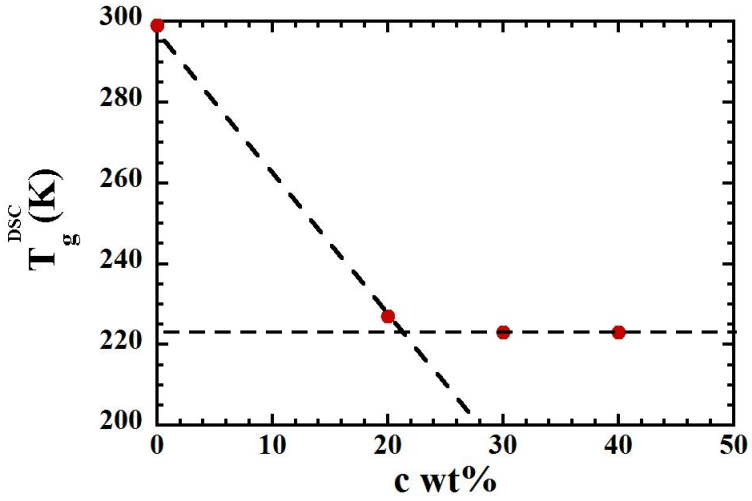

Figure 6.15: Glass transition temperature measured by DSC as function of water concentration.

First we notice that PDMAEMA/H_2O 20 %wt (green dashed line) is characterized by a bimodal behaviour indicating the presence of two different glass transition temperatures. The peak at higher temperature recalls that observed in the dry sample but considerably shifted, while the extremely broad glass transition at lower temperature is similar to that found in the other mixtures. However, even for the samples with the highest water amount (30 and 40 %wt) it is possible to identify a shoulder around ∼250 K on the flank of the peak suggesting a slight signature of bimodal behaviour. Such a behaviour could be related to a non-homogeneous hydration of the polymer during the sample preparation due to the more favourable water-water interaction. As a consequence, in the mixture with the lowest water concentration, a relevant part of the sample would be poorly hydrated giving rise to a well defined peak related to the polymer component. In Fig. 6.15 T_g of the low temperature contribution –i.e. the maximum of the peak observed in the derivative of the reversible part of the specific heat– as function of the water concentrations is shown. We note a strong decrease of the glass transition temperature even at the lowest concentration. However, increasing the water amount, T_g appears to be rather independent on the water concentration.

Fig. 6.16 shows the loss tangent (defined as $\tan(\delta) = \epsilon^{\text{“}}/\epsilon^{\text{‘}}$) of the dielectric response at T=160 K. Such representation has been chosen to minimize the influence of geometrical factors and, therefore, allow a better comparison between different samples. A very intense peak is observed for the high water concentrations, while polymer in water mixture at 20 %wt shows a much weaker relaxation and a larger broadening of the loss peak. Comparing the dielectric signals observed with that obtained for PDMAEMA in the dry state, we notice that the peaks are much more intense even at the lowest water concentration. Therefore, we can relate the contributions in the loss part to the strong water dipole moment. Unfortunately, due to the high conductivity contribution that dominates at higher temperatures, it is neither possible to observe the dielectric signature of the PDMAEMA structural relaxations.

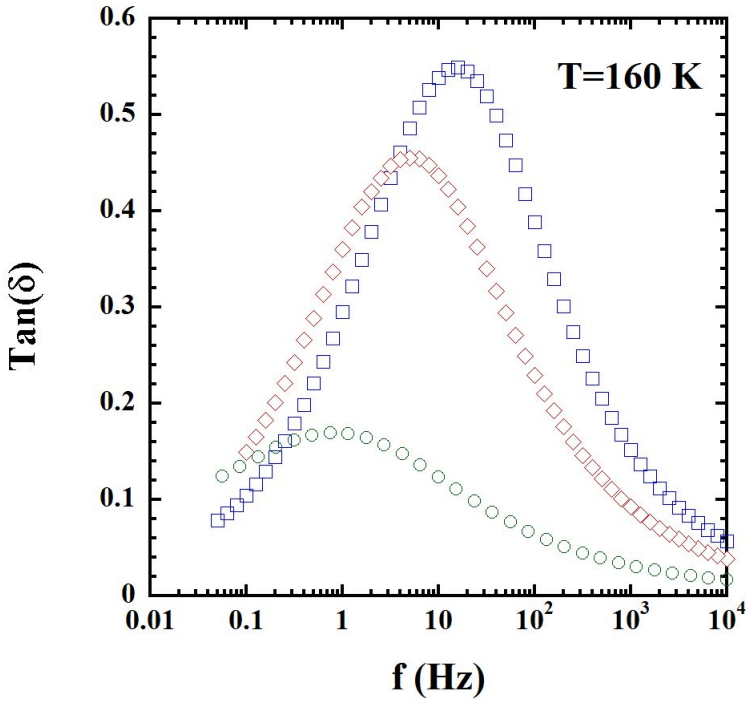

Figure 6.16: Tan(δ) of the complex dielectric permittivity of PDMAEMA in water mixtures at T=160 K. PDMAEMA/water 20 wt% (green circles), PDMAEMA/water 30 wt% (red diamonds), PDMAEMA/water 40 wt% (blue squares).

6.3.2 Water dynamics through dielectric relaxation

The dielectric permittivity of the three samples was fitted by a using a CC function. In the temperature range investigated, the conductivity is not appreciably contributing to the signal. The inverse temperature dependence of the relaxation times obtained for all the water concentrations is shown in Fig. 6.17. Water dynamics reveal two different behaviours depending on the temperature. At low temperature the processes exhibit an Arrhenius-like dependence. As the temperature increases, a systematic reduction of the relaxation times with respect to the line extrapolated from low temperature is observed. Such a deviation occurs at different temperatures depending on the water amount in the sample: while in the samples with 30 and 40 wt% of water the crossover takes place at almost the same temperature ($\approx$ 210 K), in the mixture with the lowest water amount such effect occurs at lower temperature ($\approx$ 190 K). Moreover, at low temperature, water dynamics in PDMAEMA/H_2O 30 %wt appears almost one order of magnitude faster than in PDMAEMA/H_2O 20 %wt, whereas the relaxation times obtained for PDMAEMA/H_2O 40 %wt are only slightly smaller than in 30 %wt water mixture.

The temperature dependence of the relaxation times of the three samples was analysed at low temperature by using the Arrhenius equation. In Table. 6.3 the values for E_a and $\log(\tau_0)$ obtained by this fitting are shown. We notice a slight

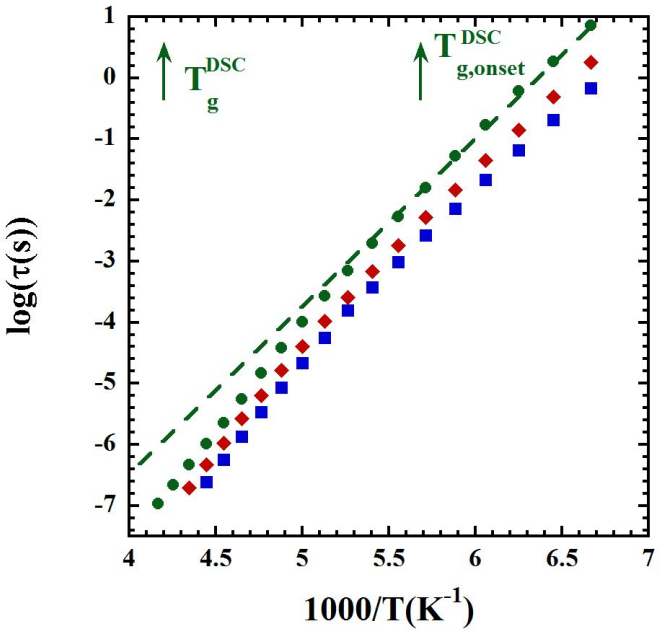

Figure 6.17: Inverse temperature dependence the relaxations times of the water component in PDMAEMA/water mixtures. Green circles refer to PDMAEMA/water 20 wt%, red diamonds to PDMAEMA/water 30 wt% and blue squares to PDMAEMA/water 40 wt%. Dashed line is a fit with the Arrhenius equation at low temperature(as described in the text). Arrows mark the position of the temperature of glass transition and its onset measured by DSC.

reduction of the activation energy as the concentration increases but, within the uncertainties, the values are in the range reported for the so-called 'universal' water process [25]. For all the samples, τ_0 takes values much smaller than that expected for the typical phonon frequency. This result suggests that some contributions of entropic origin to the underlying relaxation processes exist.

Table 6.3: Activation energy (E_a) and pre-exponential factor ($\log(\tau_0)$) obtained by Arrhenius equation fitting procedure

c wt%	$\log[\tau_0(\mathrm{s})]$	E_a (meV)
20	-17.9 ± 0.3	557 ± 8
30	-18.0 ± 0.1	544 ± 4
40	-17.7 ± 0.2	524 ± 5

In Fig. 6.18, the dielectric strength $\Delta\epsilon$ as function of water concentration is shown. We notice that it increases with the concentration at 20 wt%, then a stronger increase is observed. Such behaviour has been found in other aqueous solutions ([57, 33]). It has been suggested that at low concentration the reorientation of the water dipole moment is somehow restricted, indicating a strong interaction with the polymer. Increasing the water amount, water molecules tend to join together – as

it has been shown in Chapter 3, where the presence of clusters in PDMAEMA/H_2O 30 wt% sample is observed–. As a consequence, water molecules could orientate more easily, as water-water interactions are more advantageous than those with the PDMAEMA. Hence, the dielectric strength increases more than expected according to the extrapolation from low concentrations. Regarding the shape parameter of the CC function, the average values of the α_{CC} are shown in Fig. 6.19. The broad distribution of the relaxation times at low concentration suggests a rather inhomogeneous environment, while, increasing the water amount, the environment around the water molecule becomes more uniform. This is in accord with the dielectric strength behaviour as function of water concentrations and with the calorimetric measurements as well, where a strong bimodal behaviour at the lowest water concentration has been found. Moreover, such heterogeneity has been observed also in the water dynamics in polyamide (PA) aqueous solution at c=14 wt% [41], that is with a concentration slightly lower than that characterized by the broadest distribution of the relaxation times in this work.

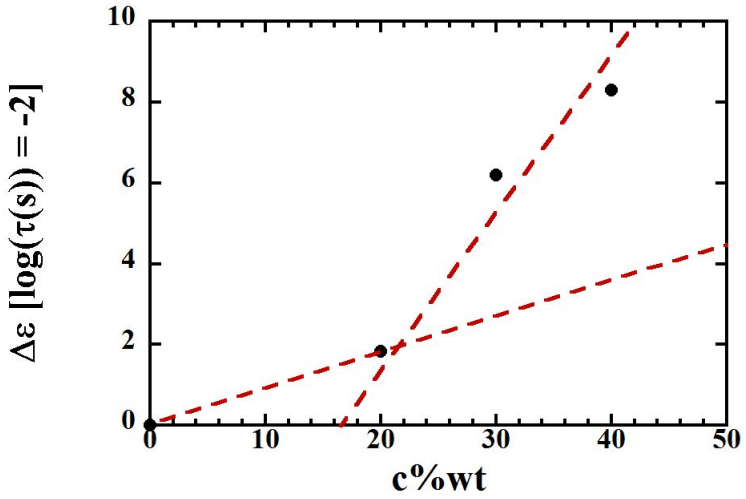

Figure 6.18: Dependency on solvent concentration of the dielectric strength of the water process evaluated at log(τ(s))=-2.

6.3.3 Confinement effects on water dynamics

At high temperature, the crossover in the temperature behaviour of the relaxation times could be due to a different Arrhenius dependence. However, this interpretation leads to a non-physical pre-exponential factor in all the samples ($\log(\tau_0(s)) \approx -24$). As it has been commented in the Introduction, this behaviour of the water relaxations has been observed in many other systems. To explain this behaviour, it has been proposed a transition on cooling from a liquid-like VFT behaviour at high temperature to a solid-like Arrhenius at low temperature. Some authors [31, 30] suggested a relation between such a crossover and the fragile-to-strong transition. However, other works[25], observed that the crossover occurs at the glass transition of the mixture, and so it would be related to a finite size effect. In Fig. 6.20 the characteristic relaxation times of water in PDMAEMA/H_2O 30 wt% sample are shown

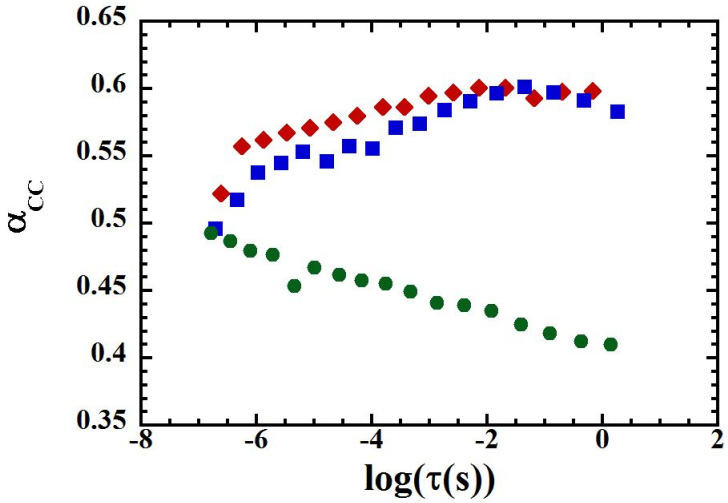

Figure 6.19: Cole-Cole α_{CC} parameter related to water dynamics obtained by the fitting procedure. Green circles refer to PDMAEMA/water 20 wt%, red diamonds to PDMAEMA/water 30 wt% and blue squares to PDMAEMA/water 40 wt%.

in comparison with the temperature derivative of the reversible specific heat (top). We observe that the temperature at which the crossover occurs almost coincides with the Tg measured by DSC. This behaviour is found also in the mixture with 40 wt% of water suggesting that, for these concentrations, the crossover is associated with the freezing of the mixture at the glass transition temperature. Such situation recalls that observed in other polymeric solutions [57, 33]. In those works it was suggested that below T_g the motions of the water molecules are restricted by the frozen polymeric matrix and, therefore, are similar to a β-relaxation of a simple glass. Above the glass transition temperature, the water reorientation is coupled with the α-relaxation of the polymer. Consequently, the crossover could be interpreted as a transition from a local-like dynamics to a cooperative-like dynamics.
At the lowest concentration investigated (PDMAEMA/H_2O 20 wt%), the glass transition takes place at almost the same temperature, as shown in Fig. 6.14. In this case the crossover temperature does not correspond to the T_g, but occurs at a lower temperature. This situation is similar to that found in PA/water mixtures with a comparable water concentration [41]. In those systems, the local mobility of the polymer –due there to a secondary relaxation– was invoked to be at the origin of the observed behaviour. The possible impact of localized motions of the polymeric matrix on the microscopic observation of the crossover in the dynamics of the water component was also emphasized in the study of the PVME/water system reported in Ref.[42]. It is worth noting that in the present case, the crossover temperature coincides with the onset of the glass transition (see Fig. 6.21). This fact could also be interpreted as a signature of the importance of the polymer mobility on the water dynamics.

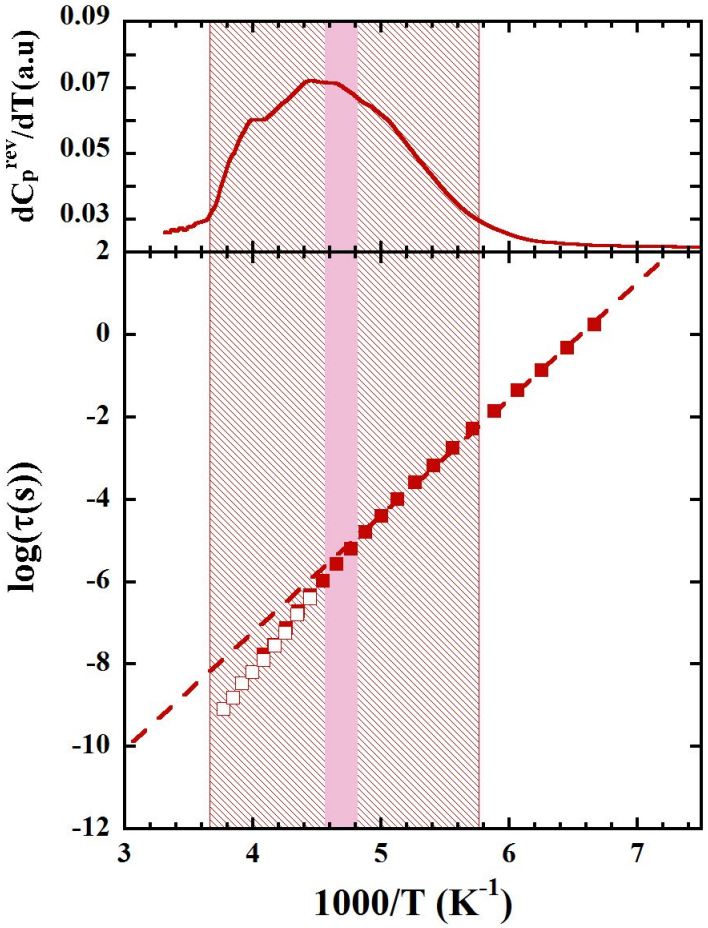

Figure 6.20: Top: Temperature derivative of the reversible specific heat of PDMAEMA/water 30 wt%. Bottom: inverse temperature dependence of the characteristic times of the water component in PDMAEMA/water 30 wt% obtained by DS. Filled symbols refer to broad-band measurements, while empty simbols to high-frequency dielectric measurements. Dashed line shows the Arrhenius fit at low temperature.

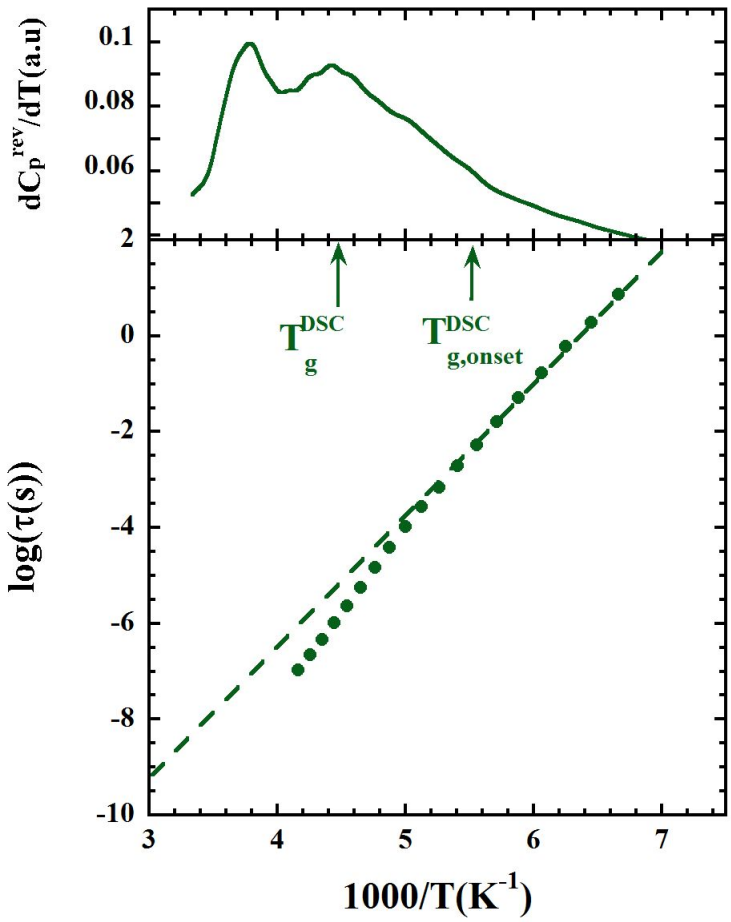

Figure 6.21: Top: Temperature derivative of the reversible specific heat of PDMAEMA/water 20 wt%. Bottom: inverse temperature dependence of the characteristic times of the water component in PDMAEMA/water 20 wt% obtained by DS. Dashed line shows the Arrhenius fit at low temperature.

On the other hand, we note that a transition from an Arrhenius to a non-Arrhenius dependence on temperature has also been found in the water dynamics confined in MCM-41[31]. This system does not exhibit any glass transition and, due to the nature of the host, there are not structural rearrangements. Therefore, only thermal energy could contribute to the crossover. As mentioned above, in the mixture with lowest water concentration water molecules are strongly interacting with the polymer. For this reason, and due to the very low amount of water, we can assume that water clusters in PDMAEMA/H_2O 20 wt% are rather smaller than those in the mixtures at higher concentrations and therefore less stable. In this framework, the thermal energy contribution would be sufficient to disturb the water clusters allowing the crossover to a cooperative-like motion of the water molecules. Both scenarios for the origin of the crossover –emphasizing either polymer dynamics or thermal energy– would a priori be plausible to explain the observed phenomenology.

CHAPTER

7

CONCLUSIONS

This Ph.D. thesis has been focused on the role of solvent/polymer interactions on the structure and dynamics of highly concentrated polymer solutions. In particular, the comparative study of mixtures with solvents interacting differently with the polymer has allowed to highlight the relevance of the H-bonds interactions. For this purpose, the chosen systems have been PDMAEMA in mixtures with either THF and water. The joint use of NS (quasi-elastic and inelastic) and DS has demonstrated to be a powerful tool to investigate the dynamics in the mixtures, while the combination of X-ray and neutron diffraction has given relevant information about the structural properties of the systems. Furthermore, calorimetry has also been very useful for the interpretation of the results. First PDMAEMA in the dry state and in mixture with THF and water at a representative concentration (c=30 wt%) have been deeply investigated. Afterwards the dynamical properties of the mixtures as function of the solvent concentration have been studied by DS and DSC, since contrary to DS it is always sensitive to both components of the mixtures.

Structural Properties

• The structure of dry PDMAEMA has been characterized by using X-ray diffraction (SAXS and WAXS) and neutron diffraction (DNS). Four peaks have been identified in the diffraction patterns. Through a comparison with studies on similar polymers –i.e. polymers having a bulky side group– these contributions have been associated to different correlations between molecular groups of PDMAEMA. The peak at around ~ 2.2 Å^{-1} has been associated to intra-chain correlations. The main peak, at ~ 1.2 Å^{-1}, has been related to the correlations between atoms located at the side groups of different monomers. At around ~ 0.8 Å^{-1} a non-well resolved peak has been found. In similar polymers such Q-range is characterized by correlations involving the backbone atoms. Finally, at around ~ 0.5 Å^{-1} a 'pre-peak' has been found. Its presence has been associated to a kind of nano-phase segregation between

side groups and backbones leading to the existence of nano-domains rich in each of the polymeric subspecies. This peak would then reflect inter-domain correlations including inter-mainchain distances.

• In PDMAEMA/THF 30 wt% the presence of THF molecules has been found to mainly affect the distances between different side groups. The pre-peak is only slightly affected suggesting that the nano-domains structure associated to this peak is essentially the same as that found in the dry polymer. Finally in this mixture the solvent molecules seem to be homogeneously distributed within the sample since there is no sign of THF clusters in the results.

• X-ray and NS diffraction experiments on PDMAEMA/H_2O 30 wt% have shown the presence of water clusters. Such aggregates lead to a non-uniform hydration of the polymer as suggested by the strong heterogeneity in the Q-range from 0.6 to 1.0 Å^{-1}. In addition, the distances between the nano-domains are larger than those found in the polymer in the dry state and in the PDMAEMA/THF mixture. Finally, the temperature dependence of the contributions observed in the Q-range $\sim$1–2 Å^{-1} is similar to that reported for water confined in other systems, suggesting a change in the water-water interactions and an extra finite size effect upon the vitrification of the polymeric matrix.

Dynamical Properties

PDMAEMA dynamics

We have addressed the question how the presence of plasticizers –THF and H_2O– affects PDMAEMA dynamics at different levels by combining DSC, dielectric spectroscopy and neutron scattering techniques. Unfortunately, DS fails in giving information about the polymer component in the aqueous mixtures due to the overwhelming signal of water. Despite this fact, interesting conclusions can be drawn also for these systems. Differential scanning calorimetry and dielectric spectroscopy measurements on PDMAEMA in mixtures with THF and water at different concentrations allowed to investigate the dynamical processes involved in the systems as function of the solvent amount.

• The α-relaxation of the polymer is drastically affected by the presence of solvents. DSC shows strong shifts of the glass-transition temperature. Regarding the THF mixtures, the shift increases as function of the solvent amount and a 'stronger' behaviour of the α-relaxation of the polymer in mixtures has been observed even at the lowest solvent concentration (15 wt%). In the aqueous mixtures a bimodal behaviour has been observed by DSC, suggesting an inhomogeneous distribution of the water molecules. Moreover, DSC measurements have revealed a much more pronounced broadening of the glass transition in the hydrated regions.

• On the other extreme, INS measurements on PDMAEMA in the dry state and in mixtures at a representative concentration (c=30 wt%) revealed that the methyl-group dynamics are unaffected by the presence of solvent.

•The synergetic analysis of DS and QENS results on dry PDMAEMA and its mixture with THF has allowed identifying two kinds of side-group molecular motions –a slow and a fast one– contributing to the β-process in the dry state. Based on the spatial information provided by QENS, a model for the geometry of the motions involved in the fast process has been proposed. Upon addition of solvent, this process remains essentially unaltered, while the population involved in the slower one is reduced. This reduction is complete, within the experimental uncertainties, in the THF mixtures, but only partial in the aqueous systems. In addition, a rather lower activation energy of the β-relaxation of PDMAEMA has been found by DS measurements in all the THF mixtures. This result suggests that, already at c=15 wt%, the slow component of PDMAEMA β-relaxation observed in the dry state is highly hindered.

• Both, the more pronounced broadening of the glass-transition region and the weaker influence on the local side-group motions of the polymer produced by the presence of water, with respect to THF, could be attributed to the existence of clusters of water molecules heterogeneously distributed in the polymeric matrix and consequently some polymer segments are not much affected by water. This would be the main difference introduced by the capability of H-bond formation of water molecules in contrast to the case of THF molecules.

THF dynamics

The combination of dielectric spectroscopy and neutron scattering on a labelled sample has allowed characterizing the dynamics of THF molecules in mixture with PDMAEMA at $c^{THF} = 30\ wt\%$. Moreover, the dynamical properties of the solvent as function of the concentration have been investigated by DS and DSC experiments.

• The partial crystallization on cooling observed by DSC measurements on the sample with the highest THF concentration (c=48 wt%) evidences the presence of a segregation of THF molecules leading to a rather inhomogeneous distribution of solvent molecules in the mixtures. Such behaviour is confirmed by the dielectric spectroscopy investigation on both polymer and THF dynamics at such concentration.

• The mixture with c=30 wt%, corresponding to one molecule of THF per monomer, is characterized by the most homogeneous distribution of solvent among the concentrations investigated. This is mainly suggested by the 'saturation' observed of the T_g as function of the THF amount observed by DSC.

• Two independent processes have been identified. The 'fast' one has been qualified as due to an internal motion of the THF ring leading to hydrogen displacements of about 3 Å. The activation energies of this motion are rather broadly distributed around an average value of 104 meV (10.03 kJ/mol). The 'slow' process is characterized by an Arrhenius-like temperature dependence of the characteristic time which persists in the whole range investigated, up to very high temperatures, where the times reach values in the range of some nanoseconds. The QENS results evidence the confined nature of this process, determining a size of about 8 Å for the region within which THF hydrogen motions are restricted. This process has been

tentatively assigned to the α-relaxation of THF molecules confined by the slower or even rigid polymeric matrix.

• In all the THF mixtures and in the temperature range investigated, no signature of a crossover toward a cooperative character of the 'slow'-THF dynamics could be identified and no indications for a calorimetric glass transition could be resolved.

• The interpretation of the results on THF dynamics has been based on the information about the structural properties of the PDMAEMA/THF 30 wt% mixture extracted from scattering experiments. As commented above, the THF molecules are well dispersed among the nano-domains of the polymer matrix and thus rather isolated from each other. As a consequence, they experience an environment rich in polymeric side groups. Such a dispersion, together with a locally highly mobile environment provided by the side groups, would prevent cooperativity effects between THF molecules to develop for the structural relaxation of the solvent, frustrating thereby the emergence of Vogel-Fulcher-like behavior even at very high temperatures. We thus interpret the 'slow'-THF process as a process involving collectivity with other few molecular units –mainly polymeric side-groups– within the nano-domains of the polymeric PDMAEMA matrix.

Water dynamics

Water dynamics as function of the solvent amount has been mainly characterized by DS, due to the large dipole moment of water molecules. In all the mixtures just one process has been detected.

• On heating, a crossover from an Arrhenius to a non-Arrhenius dependence in the temperature dependence of the characteristic times of the process has been found in all the mixtures. At low temperature, in the Arrhenius regime, the activation energy does not appreciably depend on the water concentration and assumes values similar to those reported for analogous process found in water confined in other systems.

• In the samples with 30 and 40 wt% of water, the crossover takes place where the glass transition is observed. Such situation recalls that found in other studies on water dynamics in polymeric solutions. According to the interpretation given in those works, it has been proposed that a coupling of the water relaxation with the α-relaxation of the polymer destabilizes the water clusters (observed by X-ray an neutron diffraction) allowing a transition from a local-like dynamics to a cooperative-like dynamics on heating.

• In the mixture with the lowest water amount (c=20 wt%) some different characteristics have been found. The broader distribution of relaxation times of the water process suggests a rather inhomogeneous environment. The low values of the dielectric strength indicate a strong interaction of the water molecules with PDMAEMA at this concentration. The relaxation times of the process in the Arrhenius regime are about one order of magnitude larger than those of water in the 30 and 40 wt% mixtures. Finally, the crossover occurs at a temperature lower than the glass transition temperature. In this framework, the following scenario has been suggested: at low concentrations, due to the stronger interactions with the polymer,

the water clusters would be smaller and the thermal contribution could be sufficient to disturb the water aggregates and, therefore, to allow the observed crossover from the Arrhenius to the non-Arrhenius temperature dependence. Nevertheless, an alternative origin of the observation of the crossover based on the onset of some polymeric molecular motions cannot be discarted.

ACKNOWLEDGEMENT

En primer lugar quiero dar las más sinceras gracias al Prof. Colmenero y a mis directores de tesis Prof. Arbe y Prof. Alegría por haberme dado la oportunidad de conseguir el doctorado en el Centro de Física de Materiales: con su constante guía he podido vivir plenamente esta experiencia humana y cientfica. Gracias por todo lo que, con pasión, han sabido transmitirme, y por la sensibilidad con la que me han apoyado en los momentos más difciles.

Agradezco sinceramente a todas las personas del Polymer and Soft Matter Group: a Silvia y Luis por sus preciados consejos cuando me sentía perdido; a Daniele per le strategie sperimentali e tattiche nel post-partita del Giovedí; a Silvina por los consejos científicos durante las frecuentes 'pausas-cigarro'; a mis compañeros de despacho, por la magia que han sabido crear; y a todos los que he tenido la suerte de conocer en este viaje.

Ringrazio la mia famiglia che é sempre stata presente nella distanza. Grazie per i pacchi che hanno riempito la mia cucina d'Italia e per i loro sforzi nell'imparare ad usare Skype.

Gracias a Raisa por haber aguantado mis cambios de humor, por creer en mí y por haberme dado la fuerza y la calma necesarias para superar los obstáculos del primer mundo.

Grazie Amilcare, Pierluigi, Feffe e Matteo per aver reso piú facile i miei primi passi a Donostia e per tutte le splendide birrate all' Alboka.

Grazie Patrizia per gli esperimenti ai fornelli, gli amari e le serate in Calle Esterlines: grazie per tutti i ricordi che abbiamo creato.

Ringrazio a Giuseppe per le tue avventure kafkiane e ai ragazzi del Nanogune per le risate tra Malandrino e Hamabost. Eskerrik asko Xabiri sozietateko afariengatik.

Thanks to Gerardo, Eric, Nosir, Petra, Michele, Leonardo, Manu, Juliana, Eneritz and Michele for all the precious moments that we shared.

Un particolare ringraziamiento va ai miei amici perugini Fede, Mattia, Ale, Luca, Ele, l'Aquo, Giamma, Scavizzi, il Foca, il Pat, Buro e il Bebba per non avermi fatto mancare l'affetto né dimenticare le mie radici.

Gracias, Mila Esker, Thanks, Grazie...

BIBLIOGRAPHY

[1] Martin Moeller and Krzysztof Matyjaszewski. *Polymer Science: A Comprehensive Reference, 10 Volume Set*. Newnes, 2012.

[2] Pablo G Debenedetti and Frank H Stillinger. Supercooled liquids and the glass transition. *Nature*, 410(6825):259–267, 2001.

[3] Arthur K Doolittle. Studies in newtonian flow. ii. the dependence of the viscosity of liquids on free-space. *Journal of Applied Physics*, 22(12):1471–1475, 1951.

[4] Morrel H Cohen and David Turnbull. Molecular transport in liquids and glasses. *The Journal of Chemical Physics*, 31(5):1164–1169, 1959.

[5] Morrel H Cohen and GS Grest. Liquid-glass transition, a free-volume approach. *Physical Review B*, 20(3):1077, 1979.

[6] Gerold Adam and Julian H Gibbs. On the temperature dependence of cooperative relaxation properties in glass-forming liquids. *The journal of chemical physics*, 43(1):139–146, 1965.

[7] C Austen Angell. Formation of glasses from liquids and biopolymers. *Science*, 267(5206):1924–1935, 1995.

[8] Dieter Richter, Michael Monkenbusch, Arantxa Arbe, and Juan Colmenero. Neutron spin echo in polymer systems. *Neutron Spin Echo in Polymer Systems*, pages 1–221, 2005.

[9] W Götze, JP Hansen, D Levesque, and J Zinn-Justin. Liquids, freezing and the glass transition, 1991.

[10] W Gotze and L Sjogren. Relaxation processes in supercooled liquids. *Reports on progress in Physics*, 55(3):241, 1992.

[11] Wolfgang Götze. Recent tests of the mode-coupling theory for glassy dynamics. *Journal of Physics: condensed matter*, 11(10A):A1, 1999.

[12] Shankar P Das. Mode-coupling theory and the glass transition in supercooled liquids. *Reviews of modern physics*, 76(3):785, 2004.

[13] David R Reichman and Patrick Charbonneau. Mode-coupling theory. *Journal of Statistical Mechanics: Theory and Experiment*, 2005(05):P05013, 2005.

[14] KL Ngai and M Paluch. Classification of secondary relaxation in glass-formers based on dynamic properties. *The Journal of chemical physics*, 120(2):857–873, 2004.

[15] Gyan P Johari and Martin Goldstein. Viscous liquids and the glass transition. ii. secondary relaxations in glasses of rigid molecules. *The Journal of Chemical Physics*, 53(6):2372–2388, 1970.

[16] VG Karpov, I Klinger, and FN Ignat'Ev. Theory of the low-temperature anomalies in the thermal properties of amorphous structures. *Zh. Eksp. Teor. Fiz*, 84:775, 1983.

[17] U Buchenau, Yu M Galperin, VL Gurevich, DA Parshin, MA Ramos, and HR Schober. Interaction of soft modes and sound waves in glasses. *Physical Review B*, 46(5):2798, 1992.

[18] SR Elliott. A unified model for the low-energy vibrational behaviour of amorphous solids. *EPL (Europhysics Letters)*, 19(3):201, 1992.

[19] VK Malinovsky. Excitation relaxation processes in amorphous and vitreous materials. *Journal of Non-Crystalline Solids*, 90(1):37–44, 1987.

[20] Walter Schirmacher, Gregor Diezemann, and Carl Ganter. Harmonic vibrational excitations in disordered solids and the boson peak. *Physical review letters*, 81(1):136, 1998.

[21] W Götze and MR Mayr. Evolution of vibrational excitations in glassy systems. *Physical Review E*, 61(1):587, 2000.

[22] H Eugene Stanley. Unsolved mysteries of water in its liquid and glass states. *MRS bulletin*, 24(05):22–30, 1999.

[23] Marie-Claire Bellissent-Funel. Water near hydrophilic surfaces. *Journal of molecular liquids*, 96:287–304, 2002.

[24] https://news.slac.stanford.edu/image/no-mans-land.

[25] Silvina Cerveny, Ángel Alegría, and Juan Colmenero. Universal features of water dynamics in solutions of hydrophilic polymers, biopolymers, and small glass-forming materials. *Physical Review E*, 77(3):031803, 2008.

[26] Seiichi Sudo, Sosuke Tsubotani, Mayumi Shimomura, Naoki Shinyashiki, and Shin Yagihara. Dielectric study of the α and β processes in supercooled ethylene glycol oligomer–water mixtures. *The Journal of chemical physics*, 121(15):7332–7340, 2004.

[27] Silvina Cerveny, Gustavo A Schwartz, Rikard Bergman, and Jan Swenson. Glass transition and relaxation processes in supercooled water. *Physical review letters*, 93(24):245702, 2004.

[28] Jan Swenson, Helén Jansson, and Rikard Bergman. Relaxation processes in supercooled confined water and implications for protein dynamics. *Physical review letters*, 96(24):247802, 2006.

[29] J Swenson, GA Schwartz, R Bergman, and WS Howells. Dynamics of propylene glycol and its oligomers confined in clay. *The European Physical Journal E: Soft Matter and Biological Physics*, 12(1):179–183, 2003.

[30] A Faraone, Li Liu, C-Y Mou, C-W Yen, and S-H Chen. Fragile-to-strong liquid transition in deeply supercooled confined water. *The Journal of chemical physics*, 121(22):10843–10846, 2004.

[31] S-H Chen, Li Liu, Emiliano Fratini, Piero Baglioni, Antonio Faraone, and Eugene Mamontov. Observation of fragile-to-strong dynamic crossover in protein hydration water. *Proceedings of the National Academy of Sciences*, 103(24):9012–9016, 2006.

[32] S Cerveny, GA Schwartz, A Alegria, Rikard Bergman, and Jan Swenson. Water dynamics in n-propylene glycol aqueous solutions. *The Journal of chemical physics*, 124(19):194501, 2006.

[33] S Cerveny, J Colmenero, and A Alegria. Dielectric investigation of the low-temperature water dynamics in the poly (vinyl methyl ether)/h2o system. *Macromolecules*, 38(16):7056–7063, 2005.

[34] Nilashis Nandi, Kankan Bhattacharyya, and Biman Bagchi. Dielectric relaxation and solvation dynamics of water in complex chemical and biological systems. *Chemical Reviews*, 100(6):2013–2046, 2000.

[35] S Takashima, C Gabriel, RJ Sheppard, and EH Grant. Dielectric behavior of dna solution at radio and microwave frequencies (at 20 degrees c). *Biophysical journal*, 46(1):29, 1984.

[36] Tian-Xiang Xiang and Bradley D Anderson. Distribution and effect of water content on molecular mobility in poly (vinylpyrrolidone) glasses: A molecular dynamics simulation. *Pharmaceutical research*, 22(8):1205–1214, 2005.

[37] Shuichi Takahara, Masatsugu Nakano, Shigeharu Kittaka, Yasushige Kuroda, Toshinori Mori, Hideaki Hamano, and Toshio Yamaguchi. Neutron scattering study on dynamics of water molecules in mcm-41. *The Journal of Physical Chemistry B*, 103(28):5814–5819, 1999.

[38] Shigeharu Kittaka, Shinji Ishimaru, Miki Kuranishi, Tomoko Matsuda, and Toshio Yamaguchi. Enthalpy and interfacial free energy changes of water capillary condensed in mesoporous silica, mcm-41 and sba-15. *Physical Chemistry Chemical Physics*, 8(27):3223–3231, 2006.

[39] Jan Swenson, Helén Jansson, Johan Hedström, and Rikard Bergman. Properties of hydration water and its role in protein dynamics. *Journal of Physics: Condensed Matter*, 19(20):205109, 2007.

[40] Rémi Busselez, Arantxa Arbe, Silvina Cerveny, Sara Capponi, Juan Colmenero, and Bernhard Frick. Component dynamics in polyvinylpyrrolidone concentrated aqueous solutions. *The Journal of chemical physics*, 137(8):084902, 2012.

[41] M Laurati, P Sotta, DR Long, L-A Fillot, A Arbe, A Alegrıa, JP Embs, T Unruh, GJ Schneider, and J Colmenero. Dynamics of water absorbed in polyamides. *Macromolecules*, 45(3):1676–1687, 2012.

[42] Sara Capponi, Arantxa Arbe, Silvina Cerveny, R Busselez, B Frick, JP Embs, and J Colmenero. Quasielastic neutron scattering study of hydrogen motions in an aqueous poly (vinyl methyl ether) solution. *The Journal of chemical physics*, 134(20):204906, 2011.

[43] I Cendoya, A Alegria, JM Alberdi, J Colmenero, H Grimm, D Richter, and B Frick. Effect of blending on the pvme dynamics. a dielectric, nmr, and qens investigation. *Macromolecules*, 32(12):4065–4078, 1999.

[44] Reiner Zorn, Michael Monkenbusch, Dieter Richter, Angel Alegría, Juan Colmenero, and Bela Farago. Plasticizer effect on the dynamics of polyvinylchloride studied by dielectric spectroscopy and quasielastic neutron scattering. *The Journal of chemical physics*, 125(15):154904, 2006.

[45] Marco Lagi, Piero Baglioni, and Sow-Hsin Chen. Logarithmic decay in single-particle relaxation of hydrated lysozyme powder. *Physical review letters*, 103(10):108102, 2009.

[46] Wolfgang Doster and Marcus Settles. Protein–water displacement distributions. *Biochimica et Biophysica Acta (BBA)-Proteins and Proteomics*, 1749(2):173–186, 2005.

[47] Wolfgang Doster, Stephen Cusack, and Winfried Petry. Dynamical transition of myoglobin revealed by inelastic neutron scattering. 1989.

[48] Angel Alegría, Olatz Mitxelena, and Juan Colmenero. On the molecular motions originating from the dielectric γ-relaxation of bisphenol-a polycarbonate. *Macromolecules*, 39(7):2691–2699, 2006.

[49] S Bistac and J Schultz. Solvent retention in solution-cast films of pmma: study by dielectric spectroscopy. *Progress in organic coatings*, 31(4):347–350, 1997.

[50] M Tyagi, A Arbe, A Alegria, J Colmenero, and B Frick. Dynamic confinement effects in polymer blends. a quasielastic neutron scattering study of the slow component in the blend poly (vinyl acetate)/poly (ethylene oxide). *Macromolecules*, 40(13):4568–4577, 2007.

[51] A-C Genix, A Arbe, F Alvarez, J Colmenero, L Willner, and D Richter. Dynamics of poly (ethylene oxide) in a blend with poly (methyl methacrylate):

A quasielastic neutron scattering and molecular dynamics simulations study. *Physical Review E*, 72(3):031808, 2005.

[52] M Diehl, W Doster, W Petry, and H Schober. Water-coupled low-frequency modes of myoglobin and lysozyme observed by inelastic neutron scattering. *Biophysical journal*, 73(5):2726–2732, 1997.

[53] J Fitter. The temperature dependence of internal molecular motions in hydrated and dry α-amylase: the role of hydration water in the dynamical transition of proteins. *Biophysical journal*, 76(2):1034–1042, 1999.

[54] A Paciaroni, A Orecchini, S Cinelli, G Onori, RE Lechner, and J Pieper. Protein dynamics on the picosecond timescale as affected by the environment: a quasielastic neutron scattering study. *Chemical physics*, 292(2):397–404, 2003.

[55] Yasumasa Joti, Akio Kitao, and Nobuhiro Go. Protein boson peak originated from hydration-related multiple minima energy landscape. *Journal of the American Chemical Society*, 127(24):8705–8709, 2005.

[56] Osamu Yamamuro, Kiyoshi Takeda, Itaru Tsukushi, and Takasuke Matsuo. Boson peaks in hydrogen-bonded molecular glasses. *Physica B: Condensed Matter*, 311(1):84–89, 2002.

[57] Silvina Cerveny, Ángel Alegría, and Juan Colmenero. Broadband dielectric investigation on poly (vinyl pyrrolidone) and its water mixtures. *The Journal of chemical physics*, 128(4):044901, 2008.

[58] T Blochowicz, SA Lusceac, P Gutfreund, S Schramm, and B Stuhn. Two glass transitions and secondary relaxations of methyltetrahydrofuran in a binary mixture. *The Journal of Physical Chemistry B*, 115(7):1623–1637, 2011.

[59] Dieter Bingemann, Nadine Wirth, Jürgen Gmeiner, and Ernst A Rössler. Decoupled dynamics and quasi-logarithmic relaxation in the polymer-plasticizer system poly (methyl methacrylate)/tri-m-cresyl phosphate studied with 2d nmr. *Macromolecules*, 40(15):5379–5388, 2007.

[60] Hongwei Wang, Lei Wang, Pengchao Zhang, Lin Yuan, Qian Yu, and Hong Chen. High antibacterial efficiency of pdmaema modified silicon nanowire arrays. *Colloids and Surfaces B: Biointerfaces*, 83(2):355–359, 2011.

[61] Song Lin, Fusheng Du, Yang Wang, Shouping Ji, Dehai Liang, Lei Yu, and Zichen Li. An acid-labile block copolymer of pdmaema and peg as potential carrier for intelligent gene delivery systems. *Biomacromolecules*, 9(1):109–115, 2007.

[62] Ernst Wagner and Julia Kloeckner. Gene delivery using polymer therapeutics. *Polymer Therapeutics I*, pages 135–173, 2006.

[63] Kurt Skold and David Long Price. *Methods of Experimental Physics: Neutron Scattering*. Academic Press, 1986.

[64] Stephen W Lovesey. Theory of neutron scattering from condensed matter. 1984.

[65] Julia S Higgins and Henri Benoît. *Polymers and neutron scattering*. Clarendon press Oxford, 1994.

[66] Gordon Leslie Squires. *Introduction to the theory of thermal neutron scattering*. Cambridge university press, 2012.

[67] Marc Bée. Quasielastic neutron scattering. 1988.

[68] Juan Colmenero and Arantxa Arbe. Recent progress on polymer dynamics by neutron scattering: From simple polymers to complex materials. *Journal of Polymer Science Part B: Polymer Physics*, 51(2):87–113, 2013.

[69] A Arbe, A Alegria, J Colmenero, S Hoffmann, L Willner, and D Richter. Segmental dynamics in poly (vinylethylene)/polyisoprene miscible blends revisited. a neutron scattering and broad-band dielectric spectroscopy investigation. *Macromolecules*, 32(22):7572–7581, 1999.

[70] RG Kirste, WA Kruse, and K Ibel. Determination of the conformation of polymers in the amorphous solid state and in concentrated solution by neutron diffraction. *Polymer*, 16(2):120–124, 1975.

[71] H Benoit, J Cotton, D Decker, B Farnoux, J Higgins, G Jannink, R Ober, and C Picot. Nature (london) phys. *Sci*, 245:13, 1973.

[72] P Schleger, B Farago, C Lartigue, A Kollmar, and D Richter. Clear evidence of reptation in polyethylene from neutron spin-echo spectroscopy. *Physical review letters*, 81(1):124, 1998.

[73] M Brodeck, F Alvarez, A Arbe, F Juranyi, T Unruh, O Holderer, J Colmenero, and D Richter. Study of the dynamics of poly (ethylene oxide) by combining molecular dynamic simulations and neutron scattering experiments. *The Journal of chemical physics*, 130(9):094908, 2009.

[74] Jean-Marc Zanotti, Luis J Smith, David L Price, and Marie-Louise Saboungi. A unified approach to the dynamics of a polymer melt. *Journal of Physics: Condensed Matter*, 18(36):S2391, 2006.

[75] R Pérez Aparicio, A Arbe, J Colmenero, B Frick, L Willner, D Richter, and LJ Fetters. Quasielastic neutron scattering study on the effect of blending on the dynamics of head-to-head poly (propylene) and poly (ethylene-propylene). *Macromolecules*, 39(3):1060–1072, 2006.

[76] Victoria García Sakai, Chunxia Chen, Janna K Maranas, and Zema Chowdhuri. Effect of blending with poly (ethylene oxide) on the dynamics of poly (methyl methacrylate): a quasi-elastic neutron scattering approach. *Macromolecules*, 37(26):9975–9983, 2004.

[77] Juan Colmenero, Angel J Moreno, and Angel Alegría. Neutron scattering investigations on methyl group dynamics in polymers. *Progress in polymer science*, 30(12):1147–1184, 2005.

[78] S Arrese-Igor, A Arbe, A Alegrıa, J Colmenero, and B Frick. Phenylene ring dynamics in bisphenol-a-polysulfone by neutron scattering. *The Journal of chemical physics*, 120(1):423–436, 2004.

[79] G Floudas, F Kremer, and A Schonhals. Broadband dielectric spectroscopy. *Berlin: Springer*, 2002.

[80] Friedrich Kremer and Andreas Schnhals, editors. *Broadband Dielectric Spectroscopy*. Springer, 2003 edition, 12 2002.

[81] M Prager and A Heidemann. Rotational tunneling and neutron spectroscopy: A compilation. *Chemical reviews*, 97(8):2933–2966, 1997.

[82] A Chahid, A Alegria, and J Colmenero. Methyl group dynamics in poly (vinyl methyl ether). a rotation rate distribution model. *Macromolecules*, 27(12):3282–3288, 1994.

[83] Juan José Del Val and Juan Colmenero. Study of interchain structural correlations in glassy polymers by x-ray diffraction. *Journal of non-crystalline solids*, 232:377–382, 1998.

[84] H-G Kilian and K Boueke. Röntgenographische strukturanalyse von amorphem polystyrol. vi. *Journal of Polymer Science*, 58(166):311–333, 1962.

[85] G Floudas, T Pakula, M Stamm, and EW Fischer. Density fluctuations in bisphenol a polycarbonate and tetramethyl bisphenol a polycarbonate as studied by x-ray diffraction. *Macromolecules*, 26(7):1671–1675, 1993.

[86] B Frick, D Richter, and Cl Ritter. Structural changes near the glass transition–neutron diffraction on a simple polymer. *EPL (Europhysics Letters)*, 9(6):557, 1989.

[87] A Arbe, A-C Genix, J Colmenero, D Richter, and P Fouquet. Anomalous relaxation of self-assembled alkyl nanodomains in high-order poly (n-alkyl methacrylates). *Soft Matter*, 4(9):1792–1795, 2008.

[88] Mario Beiner and Heiko Huth. Nanophase separation and hindered glass transition in side-chain polymers. *Nature materials*, 2(9):595–599, 2003.

[89] A-C Genix and F Lauprêtre. Subglass and glass transitions of poly (di-n-alkylitaconate) s with various side-chain lengths: dielectric relaxation investigation. *Macromolecules*, 38(7):2786–2794, 2005.

[90] Christine Gerstl, Martin Brodeck, GJ Schneider, Y Su, J Allgaier, A Arbe, J Colmenero, and D Richter. Short and intermediate range order in poly (alkylene oxide) s. a neutron diffraction and molecular dynamics simulation study. *Macromolecules*, 45(17):7293–7303, 2012.

[91] I Iradi, F Alvarez, J Colmenero, and A Arbe. Structure factors in polystyrene: a neutron scattering and md-simulation study. *Physica B: Condensed Matter*, 350(1):E881–E884, 2004.

[92] Rémi Busselez, Arantxa Arbe, Fernando Alvarez, Juan Colmenero, and Bernhard Frick. Study of the structure and dynamics of poly (vinyl pyrrolidone) by molecular dynamics simulations validated by quasielastic neutron scattering and x-ray diffraction experiments. *The Journal of chemical physics*, 134(5):054904, 2011.

[93] M Wind, Robert Graf, S Renker, Hans Wolfgang Spiess, and W Steffen. Structure of amorphous poly-(ethylmethacrylate): A wide-angle x-ray scattering study. *The Journal of chemical physics*, 122(1):014906, 2005.

[94] S Hiller, O Pascui, H Budde, O Kabisch, D Reichert, and M Beiner. Nanophase separation in side chain polymers: new evidence from structure and dynamics. *New Journal of Physics*, 6(1):10, 2004.

[95] A-C Genix, A Arbe, F Alvarez, J Colmenero, W Schweika, and D Richter. Local structure of syndiotactic poly (methyl methacrylate). a combined study by neutron diffraction with polarization analysis and atomistic molecular dynamics simulations. *Macromolecules*, 39(11):3947–3958, 2006.

[96] M Tyagi, A Arbe, F Alvarez, J Colmenero, and MA González. Short-range order and collective dynamics of poly (vinyl acetate): A combined study by neutron scattering and molecular dynamics simulations. *The Journal of chemical physics*, 129(22):224903, 2008.

[97] Measurements were performed on SANS-II intrument at Paul Sherrer Institut (Villigen, Switzerland).

[98] Nicole Floquet, Jean Paul Coulomb, Nathalie Dufau, Gilles Andre, and Remi Kahn. Confined water in mesoporous mcm-41 and nanoporous alpo4-5: structure and dynamics. *Adsorption*, 11(1):139–144, 2005.

[99] R Mancinelli. The effect of confinement on water structure. *Journal of Physics: Condensed Matter*, 22(40):404213, 2010.

[100] J Colmenero, R Mukhopadhyay, A Alegria, and B Frick. Quantum rotational tunneling of methyl groups in polymers. *Physical review letters*, 80(11):2350, 1998.

[101] T. Peterlin-Neumaier and T. Springer. *J. of Polym. Sci.: Polym. Phys. Ed.*, 14:1351, 1976.

[102] Arantxa Arbe, A-C Genix, Silvia Arrese-Igor, J Colmenero, and Dieter Richter. Dynamics in poly (n-alkyl methacrylates): a neutron scattering, calorimetric, and dielectric study. *Macromolecules*, 43(6):3107–3119, 2010.

[103] BK Annis, DJ Lohse, and Frans Trouw. Observation of boson peaks by inelastic neutron scattering in polyolefins. *The Journal of chemical physics*, 111(4):1699–1704, 1999.

[104] Mark A Adams, Barbara J Gabrys, Wojciech M Zajac, and Dennis G Peiffer. High-resolution incoherent inelastic neutron scattering spectra of polyisobutylene and polyisoprene. *Macromolecules*, 38(1):160–166, 2005.

[105] B Frick, D Richter, and S Trevino. Inelastic fast relaxation in a weakly fragile polymer glass near¡ i¿ t¡/i¿¡ sub¿ g¡/sub¿. *Physica A: Statistical Mechanics and its Applications*, 201(1):88–94, 1993.

[106] G Allen, CJ Wright, and JS Higgins. Effect of polymer microstructure on methyl group torsional vibrations. *Polymer*, 15(5):319–322, 1974.

[107] AJ Moreno, A Alegria, J Colmenero, and B Frick. Isotope effect on the rotational tunneling transitions of methyl groups in glassy polymers. *Physical Review B*, 59(9):5983, 1999.

[108] AJ Moreno, A Alegría, J Colmenero, and B Frick. Methyl group dynamics in poly (methyl methacrylate): from quantum tunneling to classical hopping. *Macromolecules*, 34(14):4886–4896, 2001.

[109] A-C Genix, Arantxa Arbe, Juan Colmenero, Joachim Wuttke, and Dieter Richter. Neutron scattering and x-ray investigation of the structure and dynamics of poly (ethyl methacrylate). *Macromolecules*, 45(5):2522–2536, 2012.

[110] A Arbe, J Colmenero, F Alvarez, M Monkenbusch, D Richter, B Farago, and B Frick. Non-gaussian nature of the α relaxation of glass-forming polyisoprene. *Physical review letters*, 89(24):245701, 2002.

[111] B Farago, A Arbe, J Colmenero, R Faust, U Buchenau, and D Richter. Intermediate length scale dynamics of polyisobutylene. *Physical Review E*, 65(5):051803, 2002.

[112] J Colmenero, A Alegria, A Arbe, and B Frick. Correlation between non-debye behavior and q behavior of the α relaxation in glass-forming polymeric systems. *Physical review letters*, 69(3):478, 1992.

[113] J Colmenero, A Arbe, A Alegria, M Monkenbusch, and D Richter. On the origin of the non-exponential behaviour of the-relaxation in glass-forming polymers: Incoherent neutron scattering and dielectric relaxation results. *Journal of Physics: Condensed Matter*, 11(10A):A363, 1999.

[114] J Colmenero, A Arbe, and A Alegría. The dynamics of the α- and β-relaxations in glass-forming polymers studied by quasielastic neutron scattering and dielectric spectroscopy. *J. Non-Cryst. Solids*, 172-174:126–137, 1994.

[115] M. Tyagi, A. Arbe, F. Alvarez, J. Colmenero, and M. A. Gonzalez. *J. Chem. Phys.*, 129:224903, 2008.

[116] C. Gerstl, G. J. Schneider, A. Fuxman, M. Zamponi, B. Frick, T. Seydel, M. Koza, A.-C. Genix, J. Allgaier, D. Richter, J. Colmenero, and A. Arbe. Quasielastic Neutron Scattering Study on the Dynamics of Poly(alkylene oxide)s. *Macromolecules*, 45(10):4394–4405, May 2012.

[117] Víctor M Rayón and Jose A Sordo. Pseudorotation motion in tetrahydrofuran: An ab initio study. *The Journal of chemical physics*, 122(20):204303, 2005.